

Variable Star and Exoplanet Section of Czech Astronomical Society and Masaryk University

Proceedings of the 50th Conference on Variable Stars Research

Masaryk University (Department of Theoretical Physics and Astrophysics), Brno, Czech Republic

30th November - 2nd December 2018

Editor-in-chief **Radek Kocián**



Participants of the conference

TABLE OF CONTENTS

The Basic Informatics approach applied to the Modeling and Observations of the QS Virginis System	4
<i>V. BAHYL, M. GAJTANSKA, TINH PHAM VAN</i>	
Variability of the Spin Periods of Intermediate Polars: Recent Results	8
<i>V. BREUS, I.L. ANDRONOV, P. DUBOVSKY, K. PETRIK, S. ZOLA</i>	
A new multi-periodic delta Scuti variable in the field of NS Cep	10
<i>V. DIENSTBIER, M. WOLF & M. SKARKA</i>	
The peculiar outburst activity of the symbiotic binary AG Draconis	15
<i>R. GÁLIS, J. MERC, L. LEEDJÄRV, M. VRAŠŤÁK & S. KARPOV</i>	
Activity of flare star GJ 3236	21
<i>J. KÁRA</i>	
The activity of the symbiotic binary Z Andromedae and its latest outburst	23
<i>J. MERC, R. GÁLIS, M. WOLF, L. LEEDJÄRV, F. TEYSSIER</i>	
Improvement of Simplified Models of Variability of Stars: A review	28
<i>IVAN L. ANDRONOV</i>	
The Informatics in the Doppler Tomography Modeling of the Envelopes of the Close Binaries Systems	37
<i>V. BAHYL, M. GAJTANSKA, P. HANISKO, PHAM VAN TINH</i>	
Modeling variability of Be stars	43
<i>P. KURFÜRST & J. KRŤIČKA</i>	
Using neural networks in searching for variable stars	50
<i>P. CAGÁŠ</i>	
Modeling the effects of interaction between supernova ejecta and dense circumstellar material	57
<i>P. KURFÜRST, J. KRŤIČKA & M. ZEJDA</i>	
FLEXIBLE VARIABLE STAR EXTRACTOR: new software for detection of variable stars	61
<i>V. BREUS</i>	
MAVKA: Software for statistically optimal determination of extrema	65
<i>KATERYNA D. ANDRYCH, IVAN L. ANDRONOV</i>	
New tool with GUI for fitting O-C diagrams	71
<i>P. GAJDOŠ & Š. PARIMUCHA</i>	
Exoplanetary reseach in Czech Republic	78
<i>M. SKARKA, P. KABÁTH, P. CAGÁŠ</i>	
Binaries at Charles University	83
<i>M. WOLF</i>	
Double eclipsing systems: from observer's perspective	89
<i>P. ZASCHE</i>	
The Next 50 Years of Variable Star and Exoplanet Section	93
<i>O. PEJCHA</i>	

INTRODUCTION

The Variable Star and Exoplanet Section of the Czech Astronomical Society organized traditional autumn conference on research and news in the field of variable stars. This year the conference celebrated of 50th anniversary, that's why conference held again at historic place of observing variable stars; Masaryk University in Brno. In addition to 31 contributions that were presented on site in Czech, Slovak and English language from participants from eight countries, we had an opportunity to hear lectures given by invited speakers from USA via Internet. More than 90 participants visited and participated the conference. The most of presented contributions can be viewed on our YouTube channel. I would like to thank all conference participants and all speakers for their contributions.

I also would like to thank the Director of Department of Theoretical Physics and Astrophysics of Masaryk University, prof. Rikard von Unge, Ph.D. for providing venues for conference and to his colleagues from Department for helpful organisation (Assoc. Prof. RNDr. Miloslav Zejda, Ph.D.).

Katerina Honkova

president of Variable Star and Exoplanet Section of Czech Astronomical Society

Praha, April 2019

NOTES

The scientific content of the proceedings contributions was not reviewed by the OEJV editorial board.

The Basic Informatics approach applied to the Modeling and Observations of the QS Virginis System

V. BAHYL¹, M. GAJTANSKA², TINH PHAM VAN³

- (1) Júlia observatory, Zvolenská Slatina, SZA, Slovak Republic, basoft@zv.psg.sk
- (2) KFEAM, DF TU vo Zvolene, Masarykova 24, 960 53 Zvolen, Slovak Republic
- (3) Fac. of Inf. Technol., Nong Lam Univ. Thu Duc Distric, Ho Chi Minh City, Vietnam

Abstract: The paper presents our observations of the short period binary QS Virginis in the integral light. We have observed successfully in four nights. We have obtained two complete light curves. Our observations had been influenced with the rather low position of the variable over the horizon. We have realized the model of the system too with the usage of the MB3 software. We have detected one flare too.

Introduction

We prefer the measurements in which we can obtain the full light curve of the variable in our effort focused on the close binaries observations. We concentrate us on the low observed variables. Even if there are well defined types of variables or types of variability we feel that there are or there may be many phenomena worth to be observed and studied in such rare or low observed variables. More if we have the complete light curve from the one night observations we can determine the model or the period with the higher precision. So we have decided to devote our observational time to the QS Virginis system.

Observations and analysis

The QS Virginis system is positioned on the coordinates:

$$\alpha = 13^{\text{h}} 49^{\text{m}} 52^{\text{s}}, \delta = -13^{\circ} 13' 37''.$$

The system is rather low under the equator! The magnitude changes from 14.27 mag to 17.76 mag in the primary minimum.

The basic parameters of the period of this variable are:

$$M_0 = 48689.18 \text{ d, Per} = 0.1507576 \text{ d.}$$

We have observed in the integral light only as in the goals of our observations there were not included the colour indices studies. We have not supposed “drastic” changes of them.

We have successfully observed in the subsequent nights in the year 2018. There has been very big problem for us – the rather low position of the variable over the horizon. According to our experience and opinion the object lower than 30 degrees relative to the horizon is not suite to observe with the exception of the excessive necessity of course.

In our observatory “Júlia” we have used our Schmidt – Cassegrain telescope Celestron 9.25” equipped with the MI camera G2-1600. The exposition time we have done to 30 seconds. The interval between the expositions was 30 seconds too.

Table1: Observation nights of QS Virginis.

Month	Day	From	To	No. of files
March	22	21-19-30	22-18-31	60
April	8	19-19-03		270
	9		00-31-32	32
	22	19-49-01		239
	23		00-30-48	15
May	6	19-58-48	20-58-57	120
	12	20-03-13	21-05-23	63

The observational field is on the Fig. 1. The selection of the comparison and check stars is on the same figure too.

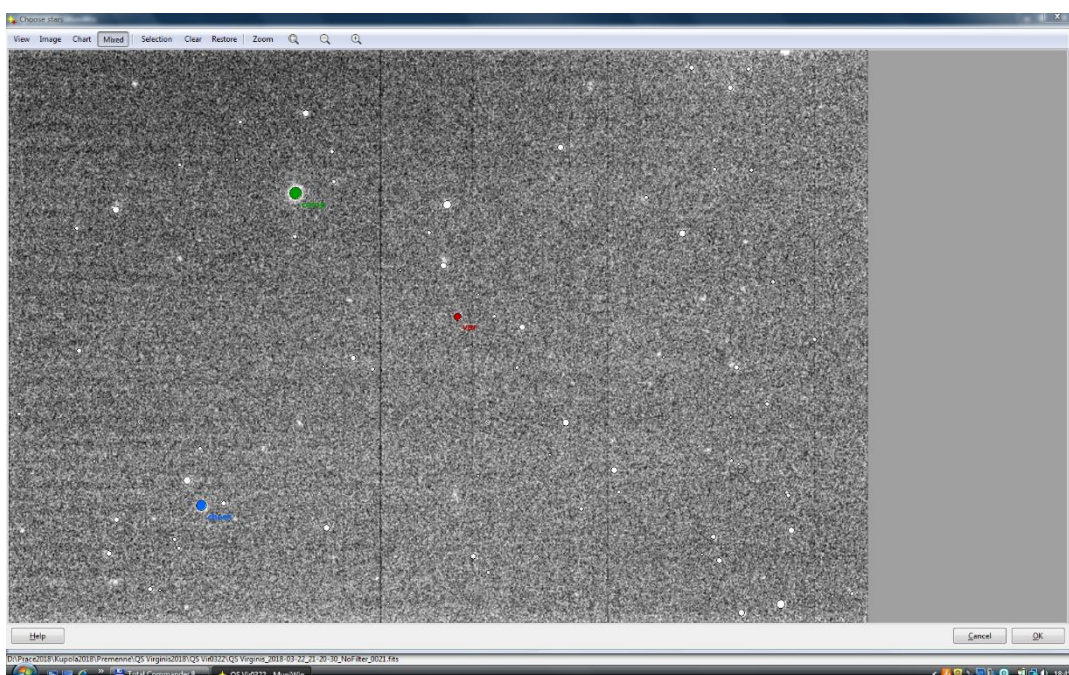


Figure 1: There is here the selection of the stars in the SQ Virginis field.
Variable = red; comparison = green; check star = blue.

The best results we have from the night April 22, 2018 as there is given on the Fig. 2. But we can see here two phenomena. First in the range of phase (0.6; 0.8) there is clearly visible the influence of the low position of the system above the horizon. Second in the phase 1.8 we allow us to interpret the measurements not as a mistake but as the real flare! Of course, this conclusion we will (or we would like to) support with our observations in the season 2019. Rather unconventionally we have used here the phases from 0.4 to 2.2 with the aim to show fully without the mix of data from phases given according the classical formula.

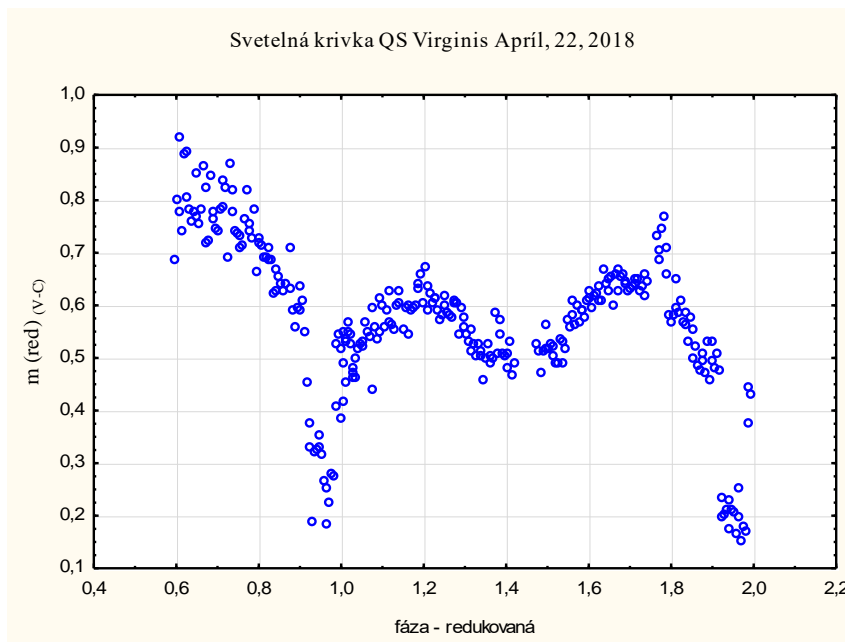


Figure 2: The Light curve of the QS Virginis from April, 22 2018.

We would like to present the changes in the time of minima with the Fig. 3.

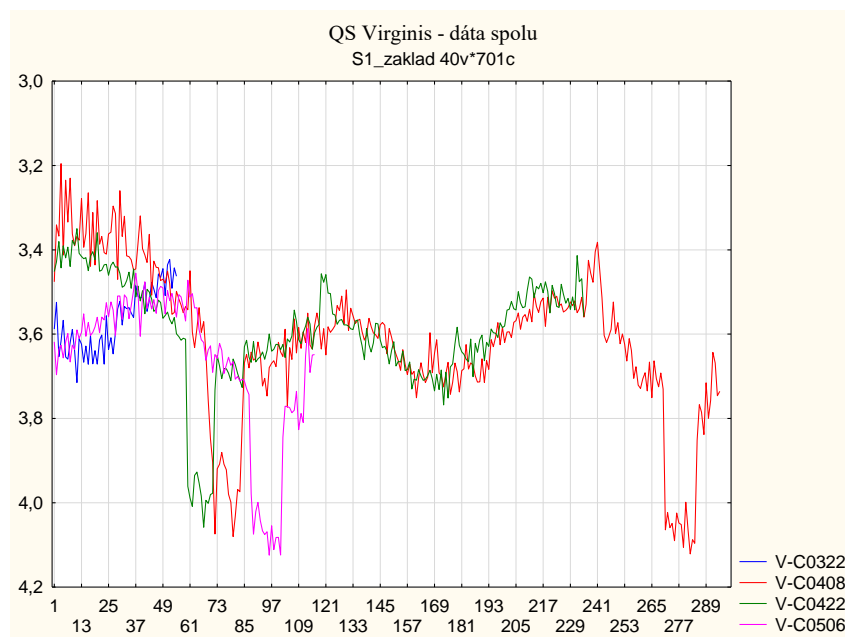


Figure 3: The positions of the primary minima relative to the secondary ones.

According to our opinion the changes in the positions of the primary minima relative to the positions of the secondary minima are enough in their value to be interpreted not as the mistakes but as the real changes. The true interpretation of this phenomenon is the next challenge for us.

Model

As we have at our disposal the BM3 software package we try to realize the model of the QS Virginis system too. The CALEB (Catalogue and Atlas of Eclipsing Binaries) is the integral part of the BM3 package. From this we have guessed that the QS Virginis is contact system so we have started our modelling effort from this point. Our results are in the Fig. 4.

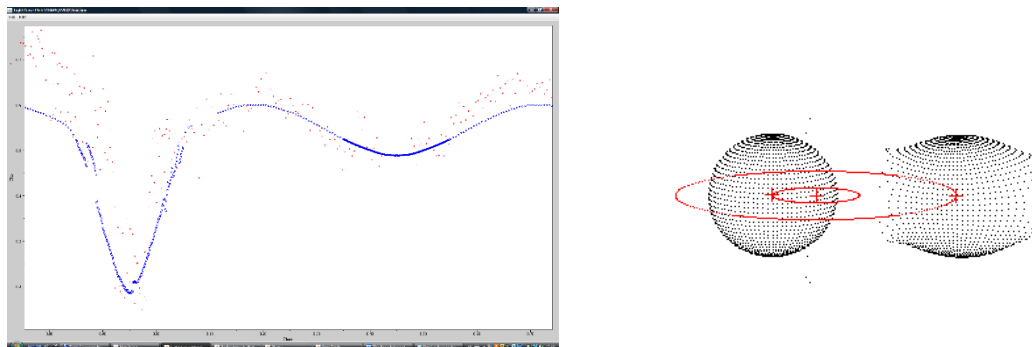


Figure 4: The QS Virginis light curve model (left) and the components shape model (right).

Conclusions

We allow us to conclude from our observations and modeling that the QS Virginis is suite system to be observed more and more. Next we conclude that the BM3 system is suite for the models of the component shapes from the observations of the light curves as a whole.

The short periodic close binaries are very dynamical systems so we can not to be quiet if we have obtained the set of the primary minima or several light curves. These systems should be observed period after period and many years. This is the way to new and deep results and the way to higher improvement our knowledge in the field of fundaments of these systems.

Of course the high professional astronomers cannot waste their time in the observations which are now accessible to the telescopes of the amateur or non- professional astronomers. Here there is the place where there is possible to obtain highly professional results with the enthusiasm and with the selfless work of the “non-professional” persons.

Acknowledgement

We would like to express our thanks to the Slovak Union of Astronomers for the obtained support.

References

- Brandstreet, D. H., 2017, **BM3**, Eastern University, PA, www.euastronomy.com
- Motl, D., 2010, MuniWin V2.0.10, <http://c-munipack.sourceforge.net>
- Raab, H., 2011, Astrometrica V4.6.6.394, <http://www.astrometrica.at>
- Scientific Image Processing System (SIPS), 2016, Moravské Přístroje a.s. V3.3 32 bit (x86)
- StatSoft, Inc, 2011, STATISTICA (data analysis software system), V10, www.statsoft.com
- Známé zákrytové dvojhvězdy, 2018, ČAS, http://var2.astro.cz/brno/eclipsing_binaries.php

Variability of the Spin Periods of Intermediate Polars: Recent Results

V. BREUS¹, I.L. ANDRONOV¹, P. DUBOVSKY², K. PETRIK³, S. ZOLA^{4,5}

(1) Department "Mathematics, Physics and Astronomy", Odessa National Maritime University, Mechnikova, 34, 65029 Odessa, Ukraine, bvv_2004@ua.fm

(2) Vihorlat Astronomical Observatory, Humenne, Slovakia

(3) Astronomical Observatory and Planetarium, Hlohovec, Slovakia

(4) Astronomical Observatory of the Jagiellonian University, Krakow, Poland

(5) Mt. Suhora Observatory, Pedagogical University, Krakow, Poland

Abstract: We present brief results of long-term monitoring of a group of intermediate polars. Some objects show period variations, at the same time other objects do not. Continuous photometric monitoring is needed to avoid cycle miscounting. We determined the values of characteristic time of period variations for different intermediate polars.

Introduction

Intermediate polars, often called DQ Her star, are close binary systems. Gravity of the primary component (a magnetic white dwarf) leads to the gravitational capture of the part of the matter of the secondary component, filling its Roche lobe, near the inner Lagrangian point. Due to high angular momentum of plasma leaving the Lagrangian point, the stream cannot be accreted directly by a compact star but it forms accretion disk around the white dwarf. The magnetic field is strong enough to destroy the inner part of the accretion disk and matter is being accreted along the magnetic field lines, leading to the formation of one or two accretion columns near the magnetic poles. The matter forms a shock wave, heats up, and eventually settles down on the surface of the white dwarf. The accretion columns in such systems are often the brightest sources of polarized radiation in a wide spectral range from X-ray to radio (cf. Patterson, 1994, Warner 2003).

Usually intermediate polars show two kinds of optical variability which are caused by different physical processes. The orbital period is usually 3-7 hours. The spin variability is caused by the rotation of the white dwarf with one or two accretion columns with the period range from few to dozens of minutes. So, the light curve is a superposition of 2 different periodic variations and some aperiodic processes like flickering, outbursts, changes from high to low luminosity state etc. To determine parameters of the 2-period model, we have used the software MCV (Andronov & Baklanov, 2004).

In this paper, we present brief results of long-term monitoring of different intermediate polars.

Spin period variability

In the case of V1323 Her, one may see no orbital variability, O-C is linear and it means that the spin period should be corrected. The final ephemeris was $T_{\max} = 2454604.04449(14) + 0.017596986(3).E$. The orbit inclination of the system is low (Andronov et al., 2011).

In case of V709 Cas we may see no spin variability because the object is faint, spin period is very short and time resolution is not sufficient, but this system shows stable variability with a period of $P = 0.d016449979(5)$ which was interpreted as a vibration of the accretion stream in the magnetic field (Hric et al., 2014).

Using data taken during 10 years of photometric monitoring of the magnetic cataclysmic variable V2306 Cygni, we first discovered the spin period variability which shows a spin-up of the white dwarf with a characteristic time of $(53 \pm 5)104$ years, which is typical for this kind of objects (the paper is preparing for publication). Also using O-C analysis we derived and improved the value of the orbital period of the system to be 4.371523 ± 0.000009 hours which is more accurate than our previous result (Breus et al, 2015). Photometric data used in this research were obtained mainly with the 60-cm Zeiss-Cassegrain telescope at the Observatory and Planetarium in Hlohovec, Slovakia and 50-cm Cassegrain telescope at the Fort Skala Astronomical Observatory of the Jagiellonian University in Krakow, Poland.

FO Aqr shows complicated O-C changes. Historical data show the spin-down of the white dwarf, which changed to a spin-up. After the 6-year gap in observations we started our monitoring. We suggested a spin-down again

during recent years (see Breus et al., 2012) but using the data obtained during latest years in Kolonica and in Hlohovec, we see that the most probable fit to the O-C during 2008 – 2018 is linear with a cycle miscount around 2 cycles per year. There are noticeable small amplitude periodic changes relatively to the linear fit which may be caused either by the evolution of the system or by the presence of the third body orbiting the close binary system. Previous studies of intermediate polars argue for smooth period variations rather than period jumps, but this case is extraordinary. The significant change of the period was rapid, during few years. These results are not final and we will continue the research of this system.

Two models of possible O-C changes calculated for the intermediate polar V405 Aur were previously suggested: third order polynomial fit that corresponds to the spin-up of the white dwarf and periodic model of (O-C) changes that corresponds to the presence of the third body orbiting the inner binary system (Breus & Andronov, 2013). Recent data obtained in 2016-2018 in Hlohovec shows that the spin-up changed to spin-down few years ago like it was previously reported for FO Aqr. The third body was not confirmed.

Conclusions

Period variations are often observed in intermediate polars and are typically detectable at a time scale of decades. Some objects do not show a statistically significant period change (e.g. V1323 Her), some show a period decrease e.g. MU Cam (Kim et al., 2005a, Petrik et al., 2015), EX Hya (Andronov & Breus, 2013), V405 Aur (Breus & Andronov, 2013), BG CMi (Kim et al., 2005b), some show more complicated spin period variations like FO Aqr (Breus et al., 2012).

From theoretical expectations, the spin periods of the white dwarf should be equal to some equilibrium value, which is equal to period of "Kepler" rotation of the inner accretion disk at a distance of the magnetosphere radius. Period variations may be caused by different physical processes and should be monitored (Andronov et al., 2017). O-C analysis on the time scale of decades usually allows us to obtain the value of characteristic time of period variations with high precision.

References

- Andronov I.L. et al., 2011, JKAS, 44, 89, [2011JKAS...44...89K](#)
- Andronov I.L. et al., 2017, ASPC, 511, 43, [2017ASPC..511...43A](#)
- Andronov I. L., Baklanov A. V., 2004, Astron. School Rep., 5, 264, [2004AstSR...5..264A](#)
- Andronov I. L., Breus V. V., 2013, Astrophysics. 56, 4, 518-530, [2013Ap.....56..518A](#)
- Breus, V. V., Andronov I. L., Hegedus T., Dubovsky P. A., Kudzej I., 2012, AASP, 2, 9, [2012AASP...2....9B](#)
- Breus, V. V., Andronov I. L., 2013, OAP, 26, 35, [2013OAP....26...35B](#)
- Breus V., Andronov I.L., et al., 2013, JPhSt, 17, 3902, [2013JPhSt.17.3901B](#)
- Breus V., Petrik K., Zola S., Baransky A., Hegedus T., 2015, AASP, 5, 17, [2015AASP....5...17B](#)
- Hric L., Breus V., Katysheva N. A., Shugarov S.Yu., Dubovský P., 2014, AN, 335, 362, [2014AN....335..362H](#)
- Kim Y., Andronov I.L. et al., 2005a, JASS, 22, 197, [2005JASS...22..197K](#)
- Kim Y., Andronov I.L. et al., 2005b, A&A, 441, 663, [2005A%26A...441..663K](#)
- Patterson J., 1994, PASP, 106, 209, [1994PASP..106..209P](#)
- Petrik K, Breus V., Andronov I.L. et al., 2015, ASPC, 496, 252, [2015ASPC..496..252P](#) //MU, 2306, 1323
- Warner B., 2003, "Cataclysmic Variable Stars", Cambridge University Press, 592pp., [2003cvs..book....W](#)

A new multi-periodic delta Scuti variable in the field of NS Cep

V. DIENSTBIER^{1,4}, M. WOLF² & M. SKARKA^{3,4}

- (1) Slovanské gymnázium, Jiřího z Poděbrad 13, 771 11, Olomouc, Czech Republic, vojtech.dienstbier@gmail.com
- (2) Astronomical Institute, Faculty of Mathematics and Physics, Charles University in Prague, V Holešovičkách 2, 180 00 Praha 8, Czech Republic, wolf@cesnet.cz
- (3) Department of Theoretical Physics and Astrophysics, Masaryk University, Kotlářská 2, 611 37 Brno, Czech Republic, maska@physics.muni.cz
- (4) Astronomical Institute, Czech Academy of Sciences, Fričova 298, CZ-251 65 Ondřejov, Czech Republic

Abstract: Discovery of a new variable star TYC 4246-883-1 in Cepheus constellation is reported. The star has mean brightness of about 11 mag in Johnson V. It appears to be a delta Scuti type pulsator with a dominant frequency of $f=19.6174$ c/d and amplitude changing from 0.025 to 0.065 mag. The strong amplitude variation suggests the existence of multiple pulsation modes, which we have not detected directly yet.

Discovery

During an unfiltered photometric observation of eclipsing binary NS Cep in the night 11/12 August 2018, subtle brightness variation of a nearby star TYC 4246-883-1 (RA 20:42:58.33s, DEC +60:38:06.3, J2000) was detected. No record of this star was found in the General Catalogue of Variable Stars (GCVS, Samus et al., 2018) or in the International Variable Star Index (VSX, Watson, Henden & Price, 2006). Two more observations were performed to confirm variability. The variability type was estimated as delta Scuti, based on the amplitude of light variations of 0.06 mag with period of about 0.048 d. The star received designation CzeV1361 in the Catalogue of new variable stars discovered by Czech observers (CzeV, Brát, 2006)¹.

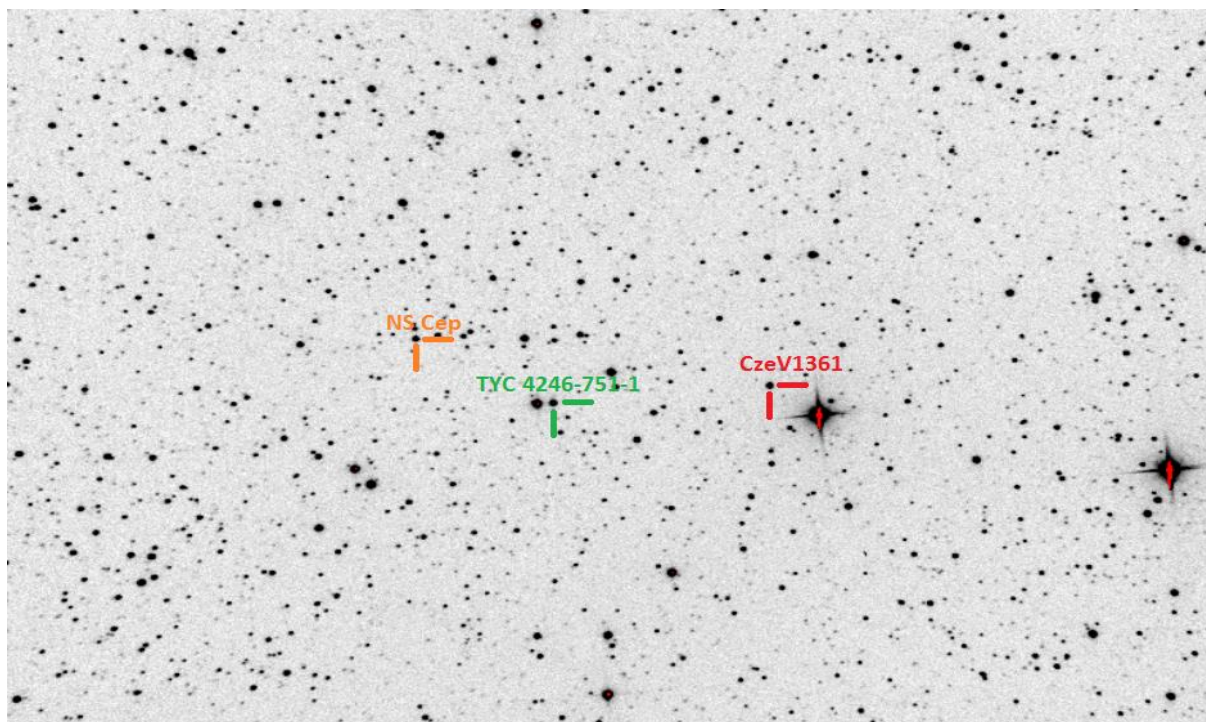


Figure 1: Vicinity of CzeV1361 as seen by the used Newtonian telescope (NWT 150/750 equipped with G2-1600 CCD camera) with correct orientation. The Field of View (FOV) is 62.8x41.9 arcmin. Dark and Flat field frames have been applied.

¹ <http://var2.astro.cz/czev.php>

Data acquisition and reduction

The data from the initial three observing nights were acquired with NWT 150/750 + G2-3200 CCD camera installed on HEQ5 mount at the Úpice observatory during the Astronomical summer school 2018. Exposures of 60 s with binning 2x2 were used to get high enough S/N ratio for NS Cep ($V=12.2 - 12.6$ mag). Differential aperture photometry, as well as dark frame and flat field corrections were performed using the C-MUNIPACK package (Motl, 2009).

TYC 4246-751-1 was chosen to be a comparison star as it has a similar B-V index and is a bit brighter (see Table 1). It does not show any observable variability in data from ASAS-SN (Shappee et al., 2014; Kochanek et al., 2017) in time span of 980 days. The ASAS-SN measurements scattering is approximately 0.015 mag, so possibility of smaller variations has to be taken into consideration.

Table 1: Identification of the variable and comparison stars, their position and brightnesses. Values are taken from the Tycho-2 catalogue (Høg et al., 2000).

Identification	RA (hh:mm:ss.ss)	DEC (\pm dd:mm:ss.s)	B (mag)	V (mag)	B-V (mag)
CzeV1361 Cep (TYC 4246-883-1)	20:42:58.33	+60:38:06.3	11.47	11.05	0.42
TYC 4246-751-1	20:44:29.88	+60:38:36.7	11.20	10.80	0.40

Since multiple pulsation periods are quite common in delta Scuti stars, more data were required for period analysis. The first idea was to use the survey data (ASAS-SN, NSVS - Northern Sky Variability Survey, Woźniak et al., 2004), but it turned out that they were not usable because of low cadence and unsatisfactory quality. Another option was to acquire more data using the telescope of Variable Star and Exoplanet Section of the Czech Astronomical Society (NWT 150/750 + G2-1600, HEQ5) located at the Valašské Meziříčí observatory (ValMez), Czech Republic. The additional unfiltered photometry was performed in seven more nights. This gives us about 2000 data points of unfiltered measurements with time span of 98 days. The full observation log is shown in Table 2. During the ninth night the amplitude of variation was less than 0.03 mag, which means amplitude change of about 50 %.

Measurements in Johnson B and V filters from D65 telescope at Ondřejov Observatory show that the variations are wavelength dependent, which is typical for the pulsating stars (Fig. 3).

Table 2: List of measurements (C - Clear, B - Johnson blue, V - Johnson visual). Data from the unfiltered ninth and tenth nights have not been used for the presented period analysis.

#	Observatory	Date (MJD)	Time interval (JD)	Data points	Maxima	Observed epoch
C1	Úpice	58342	0.4989 – 0.6058	165	1	0
C2	Úpice	58346	0.3417 – 0.5031	195	3	75-78
C3	Úpice	58347	0.3759 – 0.6051	271	5	95-100
C4	ValMez	58422	0.2789 – 0.5383	339	5	1565 – 1570
C5	ValMez	58423	0.2972 – 0.5017	182	2	1584 – 1585
C6	ValMez	58429	0.2835 – 0.4415	186	2	1703 – 1704
C7	ValMez	58434	0.2317 – 0.3282	108	2	1799 – 1800
C8	ValMez	58439	0.2384 – 0.3843	115	2	1898 – 1899
B1	Ondřejov	58439	0.2422 – 0.2954	76	1	1898
V1	Ondřejov	58439	0.2440 – 0.2950	74	1	1898
(C9)	ValMez	(58451)	(0.2289 – 0.4127)	(217)	(4)	(2132 – 2136)
(C10)	ValMez	(58452)	(0.1688 – 0.3496)	(250)	(4)	(2151 – 2154)
B2	Ondřejov	58452	0.2481 – 0.3199	107	2	2152 – 2153
V2	Ondřejov	58452	0.2481 – 0.3199	107	2	2152 – 2153

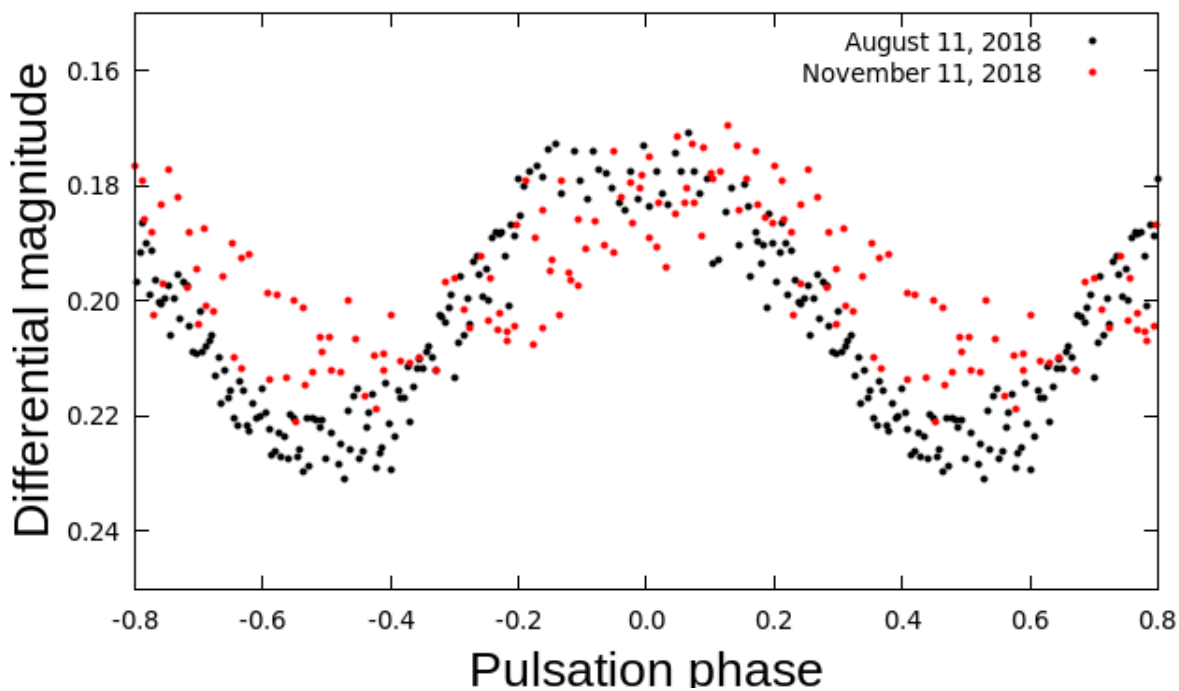


Figure 2: Two unfiltered observations with significant amplitude change. Data phased according to ephemerides from eq. 1

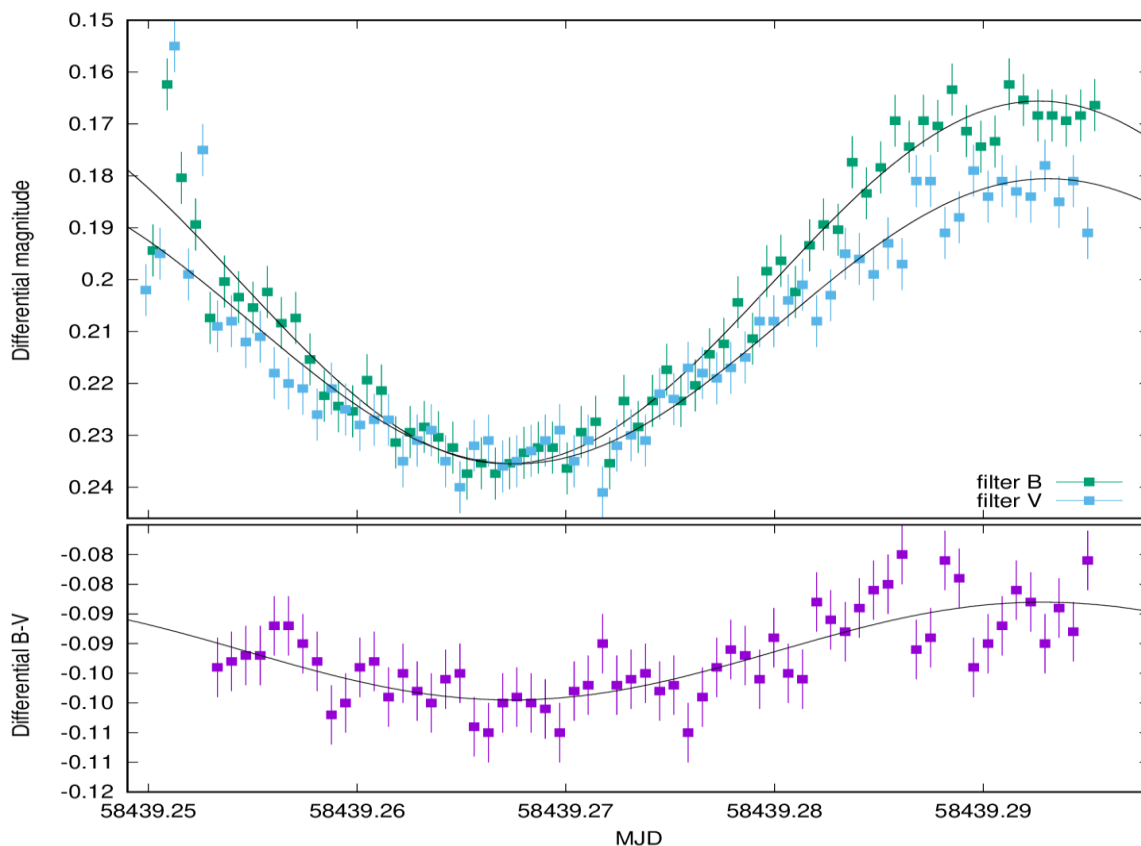


Figure 3: The first colour observation. Measurements in the B filter were shifted by -0.1046 mag, so the values of minima match. This clearly shows the wavelength dependency of the variation. The data were fitted with a sine function with the derived frequency.

Period analysis

A period analysis was performed using PerSea software (Maciejewski, 2001). This software employs the method for fast and statistically optimal period search in uneven sampled observations by Schwarzenberg-Czerny (1996). We also used Period04 software (Lenz & Breger, 2005) which uses discrete Fourier transform (DFT). Both methods give the same result for the strongest frequency: $f=19.6174$ c/d. The times of maxima, based on the dominant frequency, can be expressed as

$$T_{\max} = 2458342.5927(4) + 0.050975(2) d . E \tag{1}$$

Conformity of the results is especially important, because of known problems of DFT based methods (aliasing, S/N sensitivity,...) amplified by data features (low S/N, frequency close to 20 c/d, 24 hour sampling interval) result in extremely noisy Fourier spectra (Fig. 7).

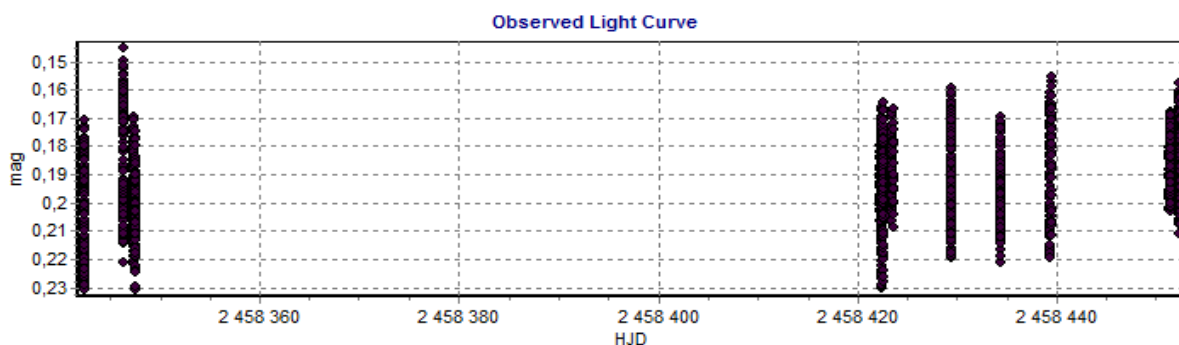


Figure 4: Acquired unfiltered measurements plotted in PerSea. As all measurements contain at least one whole period, this shows the amplitude variation quite clearly.

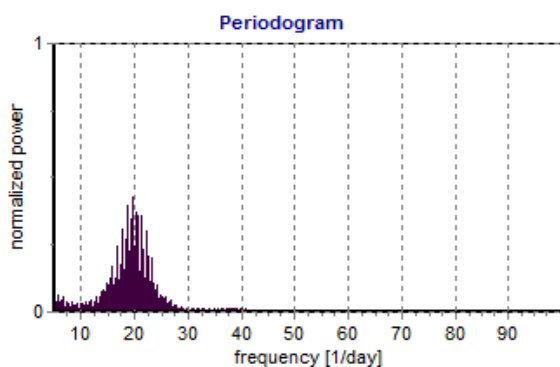


Figure 5: PerSea periodogram.

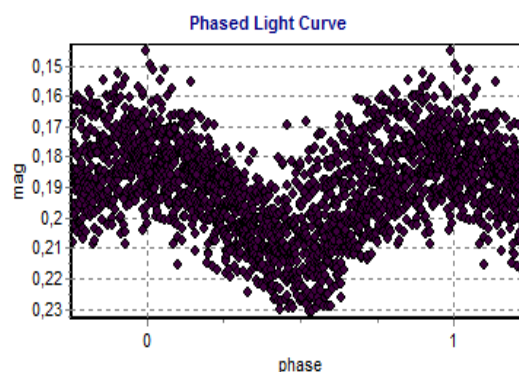


Figure 6: Data phased according to ephemerides from eq. 1

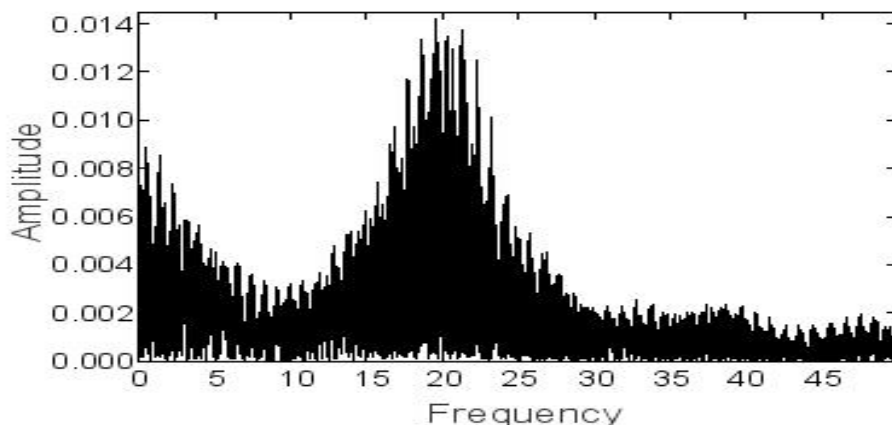


Figure 7: Fourier spectra by Period04.

Discussion and Conclusion

We reported discovery of variability of TYC 4246-883-1 and determined its type as a low amplitude delta Scuti. This claim is supported by the amplitude variation and wavelength dependency of the light curves. The brightness usually changes from $m_{\min, v} = 11.04$ mag to $m_{\max, v} = 10.99$ mag. The dominant pulsation frequency was found to be $f_1 = 19.6174$ c/d. No other frequency could be identified, but the muliperiodicity is demonstrated by a high amplitude variation.

Significantly more data and long term monitoring are required for a sufficiently better period analysis. We should consider using other methods than DFT, e.g. Bayesian inference. Spectroscopic observations would provide important insights in the characteristics of the star, mainly its temperature, and consequently help us better locate its position in the H-R diagram.

Acknowledgement

This research has made use of the SIMBAD database, operated at CDS, Strasbourg, France, ASAS-SN data and the VSX database, operated by the AAVSO. We also thank to Variable Star and Exoplanet Section of the Czech Astronomical Society, especially Kateřina Hoňková, Ladislav Šmelcer, Petr Mrňák and Radek Dřevěný, for allowing us to use the VSES telescope and their assistance during observations. MS acknowledges the Postdoc@MUNI project CZ.02.2.69/0.0/0.0/16_027/0008360.

References

- Samus et al., 2018, AR 61, 1, [2017ARep...61...80S](#)
- Henden, Price & Watson 2006, Society for Astronomical Sciences., p.47, [2006SASS...25...47W](#)
- Brat, L., 2006, OEJV, 23, 55, [2006OEJV...23...55B](#)
- Høg et al., 2000, A&AS 355, L27-L30, [2000A&A...355L..27H](#)
- Lenz, P. & Breger, M., 2005, CoAst, 146, 53, [2005CoAst.146...53L](#)
- Wenger et al., 2000, A&AS, 143, 9, [2000A&AS..143...9W](#)
- Motl, D., 2009, C-MuniPack <http://c-munipack.sourceforge.net/>
- Schwarzenberg-Czerny, A. 1996, *ApJ* **460** L107, [1996ApJ...460L.107S](#)
- Shappee *et al.* 2014, *ApJ* **788** 48, [2014ApJ...788...48S](#)
- Kochanek *et al.* 2017, *PASP* **129** 104502, [2017PASP..129j4502K](#)
- Woźniak et al., 2004, *AJ* **127** 2436, [2004AJ....127.2436W](#)

The peculiar outburst activity of the symbiotic binary AG Draconis

R. GÁLIS¹, J. MERC^{1,2}, L. LEEDJÄRV³, M. VRAŠŤÁK⁴ & S. KARPOV^{5,6,7}

- (1) Institute of Physics, Faculty of Science, P. J. Šafárik University in Košice, Park Angelinum 9, 040 01 Košice, Slovakia, rudolf.galis@upjs.sk
- (2) Astronomical Institute, Faculty of Mathematics and Physics, Charles University, V Holešovičkách 2, 180 00 Prague, Czech Republic
- (3) Tartu Observatory, Faculty of Science and Technology, University of Tartu, Observatooriumi 1, Tõravere, 61602 Tartumaa, Estonia
- (4) Variable Star and Exoplanet Section of Czech Astronomical Society, LSO (private observatory), 03401 Liptovská Štiavnica, Slovakia
- (5) CEICO, Institute of Physics, Czech Academy of Sciences, Na Slovance 1999/2, 182 21 Prague, Czech Republic
- (6) Special Astrophysical Observatory, Russian Academy of Sciences, Nizhniy Arkhyz 369167, Russia
- (7) Institute of Physics, Kazan Federal University, 16a Kremlyovskaya St., Kazan 420008, Russia

Abstract: AG Draconis is a strongly interacting binary system which manifests characteristic symbiotic activity of alternating quiescent and active stages. The latter ones consist of the series of individual outbursts repeating at about a one-year interval. After seven years of flat quiescence following the 2006–2008 major outbursts, in the late spring of 2015, the symbiotic system AG Dra started to become brighter again toward what appeared to be a new minor outburst. The current outburst activity of AG Dra was confirmed by the following three outbursts in April 2016, May 2017 and April 2018. The photometric and spectroscopic observations suggest that all these outbursts are of the *hot* type. Such behaviour is considerably peculiar in almost 130-year history of observing of this object, because the major outbursts at the beginning of active stages are typically *cool* ones. In the present work, the current peculiar activity of the symbiotic binary AG Dra is described in detail.

Introduction

AG Dra is one of the best studied symbiotic systems. Its cool component is a metal-poor cool giant of spectral type K3 and higher luminosity than that of standard class III (Smith et al., 1996). The hot component of AG Dra is probably a white dwarf (WD) sustaining a high temperature of $(1-1.5) \times 10^5$ K and luminosity of $(1-5) \times 10^3 L_{\odot}$ due to the thermonuclear burning of accreted matter on its surface (Mikołajewska et al., 1995; Sion et al., 2012). The giant is under-filling its Roche lobe and the accretion most likely takes place from the stellar wind of the cool giant. Both components are in a circumbinary nebula, partially ionised by the WD.

The period analysis of long-term photometric and spectroscopic observations confirmed the presence of two periods in AG Dra (Hric et al., 2014). The longer one (≈ 551 d) is related to the orbital motion and the shorter one (≈ 355 d) could be due to pulsation of the cool component in this symbiotic system (Gális et al., 1999; Friedjung et al., 2003). The orbital period is mainly manifested during the quiescent stages of AG Dra at shorter wavelengths (*U* band), while the pulsation period is present during quiescent as well as the active stages at longer wavelengths (*B* and *V* bands).

The period analysis of active stages confirmed the presence of a period of around 360 d, which is the median of the time interval between outbursts. It is worth noting that these time intervals vary from 300–400 d without an apparent long-term trend. Most of the longer periods (e.g. 1330, 1580, 2350, 5500 d) are more likely related to the complex morphology of the light curve (LC) during the active stages than to the real variability present in this symbiotic system (Hric et al., 2014).

The LC of AG Dra, available since 1890 (Robinson, 1969), manifests characteristic symbiotic activity with alternating quiescent and active stages (Fig. 1). The latter ones occur in intervals of 9–15 yr and consist of several outbursts repeating at about one-year interval with a brightening of about 1–1.4 mag in the *V*/visual band and up to 2.3 and 3.6 mag in the *B* and *U* bands, respectively. During the period 1890–2018, AG Dra underwent six (or seven?) stages of activity: A (1932–1939), B (1949–1955), C (1963–1966), D (1980–1986), E+F (1993–2008) and G (2015–). In total, we recognized 36 outbursts in this period.

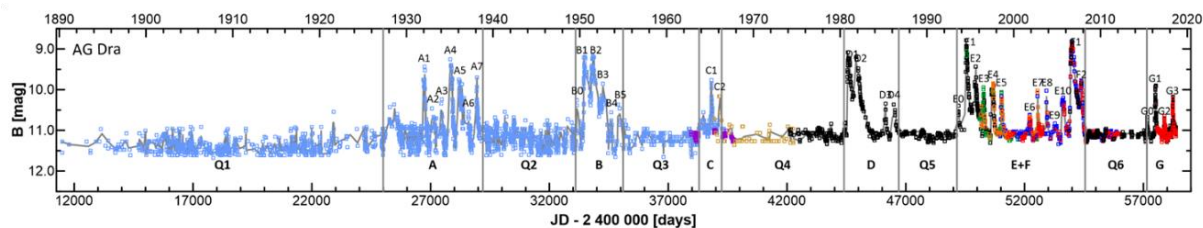


Figure 1: The historical LC of AG Dra, which manifests 129 yr of the photometric history of this symbiotic system, was constructed based on photographic (1890–1966; Robinson, 1969) and B band observations (1966–2018; Hric et al. 2014; this work). The LC is divided into active (A–G) and quiescence (Q1–Q6) stages by vertical lines. Particular outbursts are assigned as A1–A7, B1–B5, C1, C2, D1–D5, E0–E10, F1, F2 and G0–G3. The thin curves show spline fits to the data points.

UV and X-ray observations showed that there are two types of outbursts: *cool* and *hot* ones (González-Riestra et al., 1999). Major outbursts at the beginning of active stages (e.g. 1981–1983, 1994–1996 and 2006–2008) are usually *cool*, during which the expanding pseudo-atmosphere of the WD cools down and the He II Zanstra temperature drops. In smaller scale *hot* outbursts, the He II Zanstra temperature increases or remains unchanged. In the previous work, we demonstrated that the outbursts of AG Dra can also be clearly distinguished according to the behaviour of the prominent emission lines in optical spectra (Leedjärv et al., 2016).

The nature of these periodical outbursts has been a matter of long-term debate. One of the promising explanations of at least some individual outbursts of AG Dra might be the combination nova model proposed for Z And by Sokolowski et al. (2006). In this model, thermonuclear reactions are ignited when accretion rate onto the WD exceeds some critical value, and luminosity of the hot component increases significantly. One of the subsequent tasks would be to study whether the recent outbursts of AG Dra will fit into such a picture.

Observations

In this study, we analysed the photometric and spectroscopic observations that cover the ongoing active stage of AG Dra. The new photometric measurements were obtained during 167 nights at the Liptovská Štiavnica Observatory using the Newtonian telescope 355/1600 equipped with CCD G2-1600 and the set of Johnson–Cousins U , B , V , R_C and I_C filters. The AG Dra system was also observed for 358 nights using the 9-channel wide-field optical monitoring system with sub-second temporal resolution, Mini-MegaTORTORA, in operation at the Special Astrophysical Observatory of Russian Academy of Sciences in Caucasus. We also utilised the observations from *AAVSO International Database* (Kafka, 2018) acquired for 721 nights. To compare the behaviour of the latest outbursts of AG Dra with previous ones, we also used all photometric observations of this symbiotic system that had already been analysed and discussed in our previous study (Hric et al., 2014).

The spectroscopic observations of AG Dra were acquired by *ARAS Group*² observers mostly in the framework of two observing campaigns which we initiated and coordinated in 2017 and 2018. Although the spectra were obtained with small telescopes (25–35 cm, $R \approx 1800$ –11000), they provided us valuable information about the recent activity of AG Dra. In total, we used 278 spectra covering the time interval from JD 2 456 765 (April 17, 2014) to JD 2 458 447 (November 24, 2018). Moreover, we analysed the new intermediate-dispersion spectra of AG Dra obtained at the Tartu Observatory in Estonia (4 spectra, 1.5-m telescope, $R \approx 6000$ and 7000) and at the Observatory of the Astronomical Institute of ASCR in Ondřejov (16 spectra, 2.0-m telescope, $R \approx 13000$).

Our analysis was focused on the prominent emission lines in the wavelength regions under study: the hydrogen Balmer lines $H\alpha$ (λ 6563) and $H\beta$ (λ 4861), the neutral helium He I (λ 6678) line, the ionised helium He II (λ 4686) line, and the Raman-scattered O VI line at λ 6825. Equivalent widths (EWs), fluxes in lines, peak intensities relative to the continuum and the positions of these lines were measured.

Recent outburst activity of AG Dra

After seven years of quiescence following the 2006–2008 major outbursts, the symbiotic system AG Dra started to become brighter again toward what appeared to be a new minor outburst in the late spring of 2015 (Fig. 2). The outburst activity of AG Dra was definitely confirmed by the following three outbursts in April 2016, May 2017 and April 2018 (Gális et al., 2018). In the next sections, the photometric and spectroscopic behaviour of the symbiotic system AG Dra during ongoing outburst activity stage are described in detail.

² http://www.astrosurf.com/aras/Aras_DataBase/Symbiotics.htm

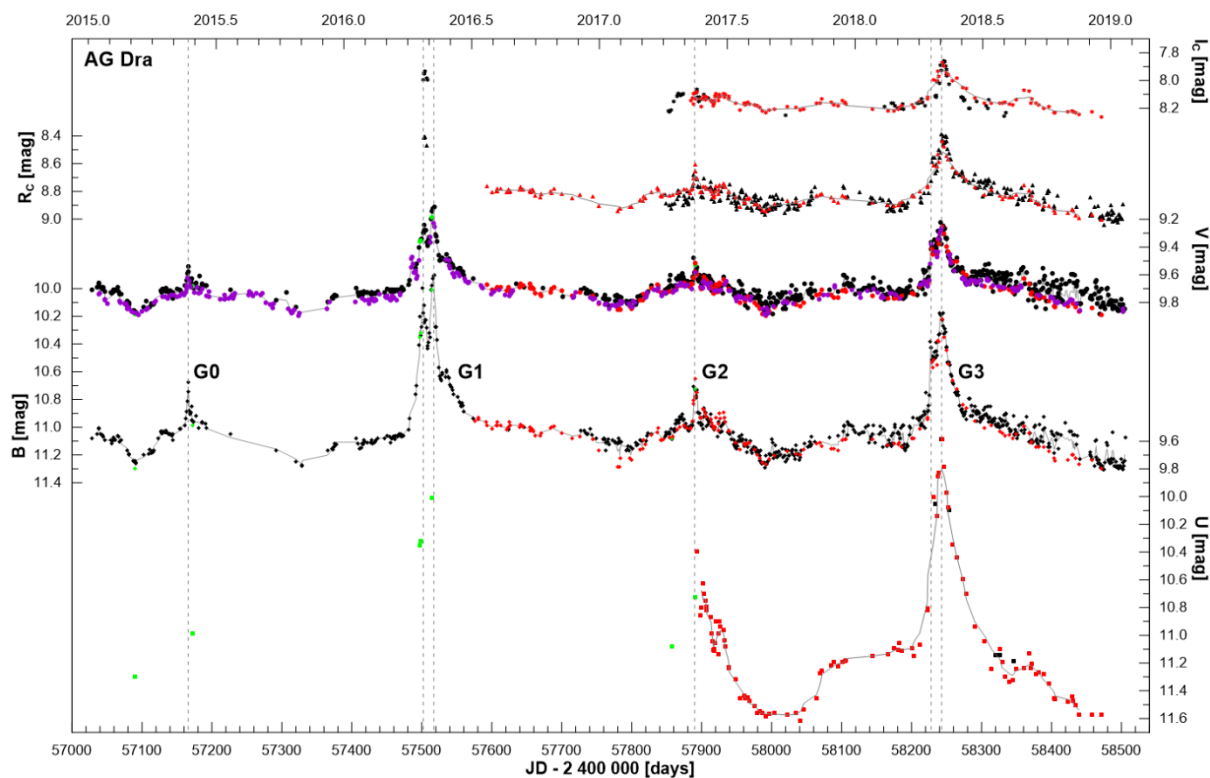


Figure 2: The LCs of the symbiotic system AG Dra during the recent active stage (2015–2018) constructed on the basis of the U , B , V , R_c and I_c band observations. The new photometric measurements are depicted by red and purple symbols for observations obtained at the Liptovská Štiavnica Observatory and the Special Astrophysical Observatory in Russian Caucasus, respectively. The green and black symbols represent observations acquired from Munari et al. (2015, 2016, 2017) and AAVSO (Kafka, 2018), respectively. The thin curves show spline fits to the data points. The dashed vertical lines indicate the times of individual brightness maxima of AG Dra during the ongoing active stage.

Photometric behaviour

The first, less prominent outburst (G0) was observed in May 2015. The maximum brightness was achieved around JD 2 457 166 (10.7 and 9.6 mag in the B and V bands, respectively). It turned out that it was minor outburst of AG Dra, a precursor of its activity as it was observed in some of the previous active stages. The major outbursts were preceded by the pre-outbursts with brightness around 10.4 and 9.4 mag in B and V band, respectively, in the case of the active stages B, E and probably C.

During the second, more prominent outburst (G1), the brightness around JD 2 457 517 (May 8, 2016) reached the maximum of 9.9 and 9.1 mag in the B and V bands, respectively. Actually, the outburst had double-peak structure with the first minor brightening occurring 15 days (JD 2 457 502) before the main one.

As in the case of previous outburst (G0), its amplitude ranks this brightening to the minor outbursts of AG Dra. Such photometric behaviour of the active stage is very unusual in the historical LC of AG Dra. More often, the pre-outbursts of AG Dra are followed by major outbursts, during which the brightness can reach around 8.8 and 8.4 mag in the B and V bands, respectively. A major outburst was not observed only during activity stage in 1963–1966, which was the shortest one in the almost 130-year photometric history of this interacting symbiotic system.

In May 2017, the third brightening (G2) during the recent activity of AG Dra was detected. It was a very sharp and short-lasting outburst of the *hot* type. Maximal brightness of the symbiotic system reached at JD 2 457 890 (10.7, 9.5 and 8.6 mag in the B , V and R_c bands, respectively) was similar to the case of G0. In the filter I_c , the outburst G2 was not detected at all. Very low amplitude of this brightening would be related not only to specific physical conditions during this outburst but also to orbital motion since the symbiotic system AG Dra was in the photometric minimum according to the orbital ephemeris given by Gális et al. (1999).

According to our statistical analysis of photometric observations, we determined that time intervals between outbursts of the symbiotic system AG Dra vary from 300 to 400 d (without an apparent long-term trend), with a median around 360 d. Therefore, we expected the next outburst in the interval from April 21, 2018 (JD 2 458 230) to May 31, 2018 (JD 2 458 270).

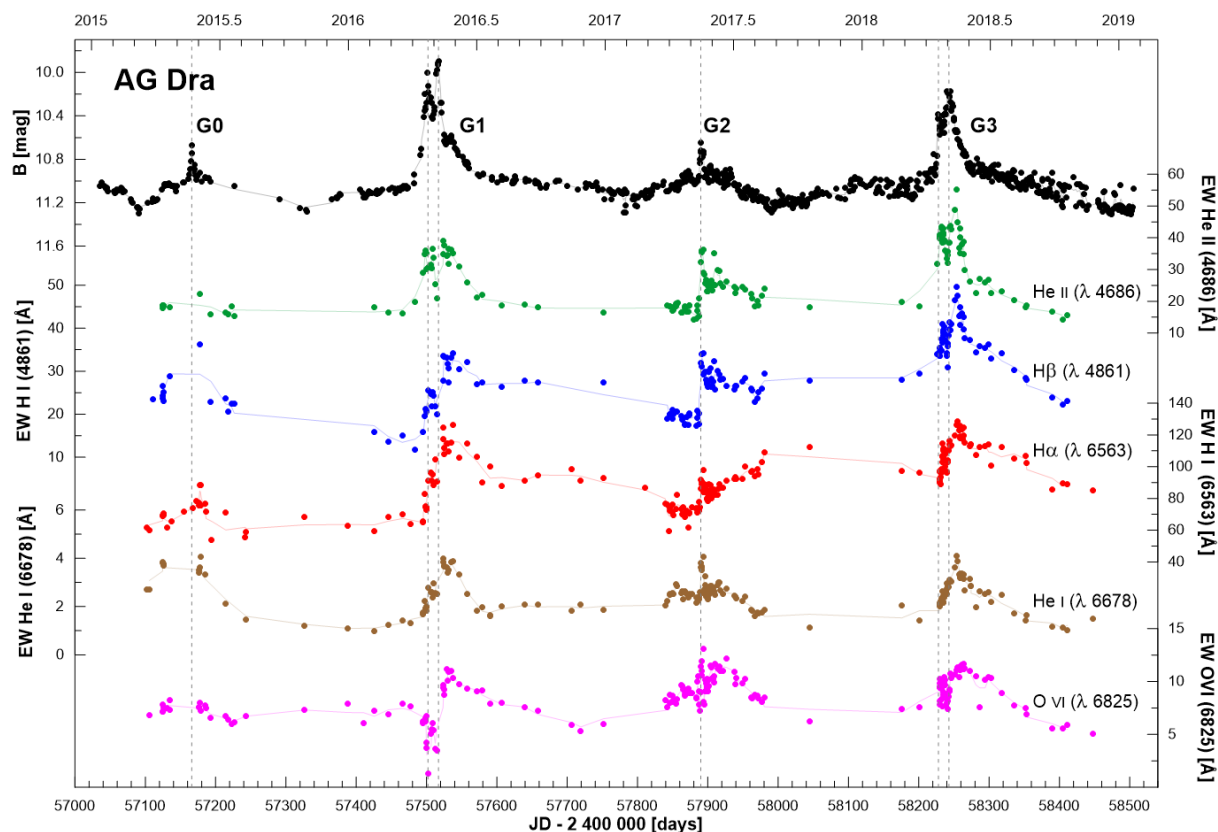


Figure 3: The light curve of AG Dra during the recent active stage in the B band together with the curves of studied emission line EWs. The thin curves show spline fits to the data points. The dashed vertical lines indicate the times of individual brightness maxima of AG Dra during the ongoing active stage.

Actually, the AG Dra system had already begun a rise in brightness, reaching 10.82, 10.95, 9.67, 8.77 and 8.13 mag in the U , B , V , R_C and I_C bands, respectively, on April 14, 2018. The outburst was confirmed on April 20, 2018 when the brightness of AG Dra increased to 10.53 and 9.42 mag in the B and V filters, respectively. We alerted the astronomical community (Gális et al., 2018) and initialised the observational campaigns to study photometric and spectroscopic behaviour of the recent outburst of AG Dra.

The maximum of the fourth outburst of the ongoing activity stage was reached 353 days after previous one, on May 4, 2018 (JD 2 458 243), with brightness of 9.6, 10.2, 9.2, 8.4 and 7.9 mag in the U , B , V , R_C and I_C bands, respectively. As in the case of the G1 outburst, the latest one had double-peak structure with the first minor brightening occurring around 25 days (JD 2 458 228) before the main one.

At the end of July 2018, the brightness of AG Dra almost returned to values typical for quiescence (11.4, 11.1 and 9.8 mag in U , B and V bands, respectively), so the fourth outburst has finished (Merc et al., 2018). The photometric behaviour suggests that all four recent outbursts of AG Dra belong to the minor, *hot* type. Such classification is also supported by the increase of the EWs of studied emission lines detected during all these events.

Spectroscopic behaviour

We analysed variability of selected emission lines in the optical spectrum of AG Dra during almost 14 years (1997–2011) using own intermediate-dispersion spectroscopic observations (Leedjävrv et al., 2016). It is worth noting that these emission lines originate in the circumbinary nebula, which is generated by the stellar wind of the cool giant. Moreover, the nebula is partially ionized by short-wave radiation of the WD, resulting in its complex structure and variability. We studied the variability of EWs of the selected emission lines: $H\alpha$ (λ 6563), $H\beta$ (λ 4861), He I (λ 6678), He II (λ 4686) and the Raman-scattered O VI line at λ 6825.

One of the most interesting features of this variability is the significant increase of the EWs of all the five emission lines considered, but in particular that of $H\alpha$ and Raman-scattered O VI (λ 6825), during some minor outbursts of this symbiotic system (e.g. E10). On the other hand, the major, *cool* outbursts of AG Dra (e.g. in July 2006) are not specifically distinct in the EWs of hydrogen and helium lines, but the weakening of the Raman-scattered O VI (λ 6825) line is very well seen.

A simple interpretation of this behaviour could be that during the *cool* outburst, the temperature of the hot component of the symbiotic system decreased considerably, so that the high excitation Raman-scattered O VI (λ 6825) line faded significantly and almost disappeared, however leaving the lower excitation emission lines of hydrogen and helium mainly unaffected.

Direct comparison of the spectra of AG Dra obtained during the quiescence stage Q6 (JD 2 456 906) and the pre-outburst G0 (JD 2 457 176) reveals significant increase of the EWs of all studied emission (Fig. 3). Such spectroscopic behaviour is typical for the *hot* outbursts of this symbiotic system. Moreover, the absorption component observed in the profiles of the emission lines He I (λ 6678), H α and H β completely disappeared during this outburst, which again testifies to its *hot* character.

The EWs of emission lines H α , H β , He I (λ 6678) and He II (λ 4686) manifest an even more prominent increase during the minor outburst G1. Such behaviour would suggest that this brightening belongs also to the *hot* outbursts of AG Dra. On the other hand, the EWs of the Raman-scattered O VI (λ 6825) line dropped to deep minimum during this outburst, which was observed only during the major, *cool* outbursts. By that manner, the outburst G1 manifested the spectroscopic behaviour of both *hot* and *cool* outbursts of AG Dra (Merc et al., 2017). The open question remains whether it is a new type of outburst or some kind of transition between (or combination of) the *hot* and *cool* outbursts?

Although the third outburst G2 during the recent active stage of AG Dra was similar to the pre-outburst G0 in its brightness, we detected the same prominent increase of all the emission line EWs as in the case of brightening G1. Only exception was the H α line: its EWs were comparable to ones during the G0 pre-outburst. Other interesting feature of this outburst was the weakening of hydrogen emission lines just before the G2 outburst. Overall spectroscopic behaviour ranks this brightening as the *hot* outburst of AG Dra.

The last outburst of the symbiotic system detected in April 2018 was also of the *hot* type. The maxima of the EWs were either comparable to the values reached during previous outbursts (in the case of H α , He I (λ 6678) and Raman-scattered O VI (λ 6825) lines) or demonstrated the highest values detected during the ongoing active stage of AG Dra (H β and He II (λ 4686) lines).

Conclusions

Periodical outbursts and their relation to periodicities in the symbiotic system AG Dra have been a matter of long-term debate. As mentioned in the introduction, González-Riestra et al. (1999) have distinguished between *cool* and *hot* outbursts of AG Dra according to the spectroscopic behaviour of this interacting binary observed in the far ultraviolet. In our previous study (Leedj arv et al., 2016), we showed that *cool* and *hot* outbursts of AG Dra can be clearly distinguished by the behaviour of the emission lines in the optical spectrum of this symbiotic system.

To sum it up, photometric as well as spectroscopic behaviour suggests that the last four outbursts of AG Dra belong to the minor, *hot* type. Such classification is also supported by the results of our analysis of the hot component's temperature during the ongoing active stage of this symbiotic system (more details are given in Merc et al., 2019). On the other hand, some specific effects observed during the outburst G1 (e.g. the almost disappearance of the Raman-scattered O VI lines) are more typical for the *cool* outbursts, despite the fact that the WD's temperature reached the historical maximum during this event.

The future evolution of AG Dra is an open question. Can we expect (finally) a major, *cool* or (again) minor, *hot* outburst? Another possibility is, that the symbiotic system will return to quiescence as we have already detected such behaviour during the weak activity stage 1963–1966. According to our detailed period analysis of photometric and spectroscopic observations we know that the median of the time interval between outbursts is around 360 days. It is worth noting that these time intervals vary from 300–400 d without an apparent long-term trend. Nevertheless, we are able to predict the time of next outburst of AG Dra during the spring of 2019. We can expect it in the interval from JD 2 458 581 (April 7, 2019) to JD 2 458 625 (May 21, 2019).

In any case, AG Dra clearly demonstrates the importance of long-term monitoring of symbiotic stars in order to disentangle the nature and mechanisms of their active stages and outbursts.

Acknowledgement

We acknowledge with thanks the variable star observations from the *AAVSO International Database* and *ARAS Database* contributed by observers worldwide and used in this research. This work was supported by the Slovak Research and Development Agency project APVV 15-0458, the Estonian Ministry of Education and Research institutional research funding IUT 40-1, the Russian Foundation for Basic Research project No. 17-52-45048 and European structural and investment funds and the Czech Ministry of Education, Youth and Sports project

CoGraDS – CZ.02.1.01/0.0/0.0/15_003/0000437. Mini-MegaTORTORA belongs to Kazan Federal University and the work is performed according to the Russian Government Program of Competitive Growth of Kazan Federal University.

References

- Friedjung M., Gális R., Hric L., Petřík K., 2003, A&A, 400, 595, [2003A&A...400..595F](#)
- Gális R., Hric L., Friedjung M., Petřík K., 1999, A&A, 348, 533, [1999A&A...348..533G](#)
- Gális, R., Merc, J., Vrašťák, M., Teyssier, F., Lester, T., Boyd, D., Sims, W., Leedjarv, L., 2018, The Astronomer's Telegram, 11559, 1, [2018ATel11559....1G](#)
- González-Riestra R., Viotti R., Iijima T., Greiner J., 1999, A&A, 347, 478, [1999A&A...347..478G](#)
- Hric L., Gális R., Leedjärv L., Burmeister M., Kundra E., 2014, MNRAS, 443, 1103, [2014MNRAS.443.1103H](#)
- Leedjärv, L., Gális, R., Hric, L., Merc, J., Burmeister, M., 2016, MNRAS, 456, 2558, [2016MNRAS.456.2558L](#)
- Kafka, S., 2018, Observations from the AAVSO International Database, <https://www.aavso.org>
- Merc, J., Gális, R., & Leedjärv, L., 2017, Contributions of the Astronomical Observatory Skalnaté Pleso, 47, 192, [2017CoSka..47..192M](#)
- Merc, J., Gális, R., & Teyssier, F. 2019, Contributions of the Astronomical Observatory Skalnaté Pleso, in press
- Merc, J., Gális, R., Vrašťák, M., & Leedjärv, L., 2018, Research Notes of the American Astronomical Society, 2, 142 [2018RNAAS...2c.142M](#)
- Mikołajewska J., Kenyon S. J., Mikołajewski M., Garcia M. R., Polidan R. S., 1995, AJ, 109, 1289, [1995AJ....109.1289M](#)
- Munari, U., Righetti, G. L., Sollecchia, U., Castellani F., 2015, The Astronomer's Telegram, 7582, 1, [2015ATel.7582....1M](#)
- Munari, U., Righetti, G. L., 2016, The Astronomer's Telegram, 8975, 1, [2016ATel.8975....1M](#)
- Munari, U., Righetti, G. L., Valisa, P., Buzzi, L., Moretti, S., 2017, The Astronomer's Telegram, 10390, 1, [2017ATel10390....1M](#)
- Robinson L., 1969, Peremennye Zvezdy, 16, 507, [1969PZ.....16..507R](#)
- Sion E. M., Moreno J., Godon P., Sabra B., Mikołajewska J., 2012, AJ, 144, 171, [2012AJ....144..171S](#)
- Smith, V. V., Cunha, K., Jorissen, A., & Boffin, H. M. J., 1996, A&A, 315, 179, [1996A&A...315..179S](#)
- Sokoloski, J. L., Kenyon, S. J., Espey, B. R., 2006, ApJ, 636, 100, [2006ApJ...636.1002S](#)

Activity of flare star GJ 3236

J. KÁRA¹

(1) Astronomical Institute, Charles University, V Holešovičkách 2, 180 00 Praha 8, Czech Republic,
kara@sirrah.troja.mff.cuni.cz

Abstract: We present a report on monitoring of stellar activity of low-mass red dwarf eclipsing binary GJ 3236 based on photometric data obtained during years 2012–2018 on various observing sites using various photometric filters. A total number of 296 flares were detected among the photometric data and will be used for statistical analysis.

Introduction

Red dwarfs are stars with masses less than 0.6 solar mass and of late spectral type. They are the most abundant group of stars in the Galaxy, but due to their low luminosity, only about 20 eclipsing binaries consisting of two red dwarfs are known. Properties of these systems can be determined with high accuracy up to 1 % by modelling photometric and spectroscopic data.

Stellar flares are enormous releases of energy connected with the magnetic activity of stars, namely with the reconnection of magnetic loops in stellar atmospheres. This event manifests itself in the photometric observations as a rapid brightening followed by a slower decrease of brightness. Mechanism of flares can be studied on solar flares, which can be observed with high spatial resolution.

We present a monitoring of stellar activity of red-dwarf eclipsing binary GJ 3236. This star was listed in a catalogue of flare stars located in the solar vicinity by Gershberg et al. (1999). It was classified as a spectroscopic binary by Pourbaix et al. (2004) and first detection of eclipses was reported by Irwin et al. (2009), who also derived its properties based on spectroscopic and photometric observations. The binary was studied also by Parimucha et al. (2016), who observed 7 flares. Most recent study of flare activity was performed by Šmelcer et al. (2017) based on 59 observed flares.

Observations

Photometric data were obtained at five different observing sites in different photometric filters. All observing sites are listed in the Table 1 accompanied by the time period of observations, used telescopes and used photometric filters. Observations in Ondřejov observatory during years 2012–2015 were obtained using photometric filter R and for subsequent observations photometric filter V was used, because flares proved to be more prominent in light curves obtained using V filter.

Table 1: List of observatories where photometric data were obtained.

Observatory	Observers	Time period	Telescope	Filters*
Ondřejov	H. Kučáková, K. Hoňková, J. Kára, J. Vraštil, K. Hornoch, M. Wolf	2012–2018	65-cm	R, V
Valašské Meziříčí	L. Šmelcer	2014–2018	25-cm, 35-cm, 28-cm	R, V, C
Trhové Sviny	F. Bílek	2015–2017	20-cm	C
Kolonica Saddle	P. Dubovský	2015–2016	36-cm	R, V, I
Piszkéstető	M. Skarka	2016–2017	1-m	B

*Filter C corresponds to configuration with no optical filter.

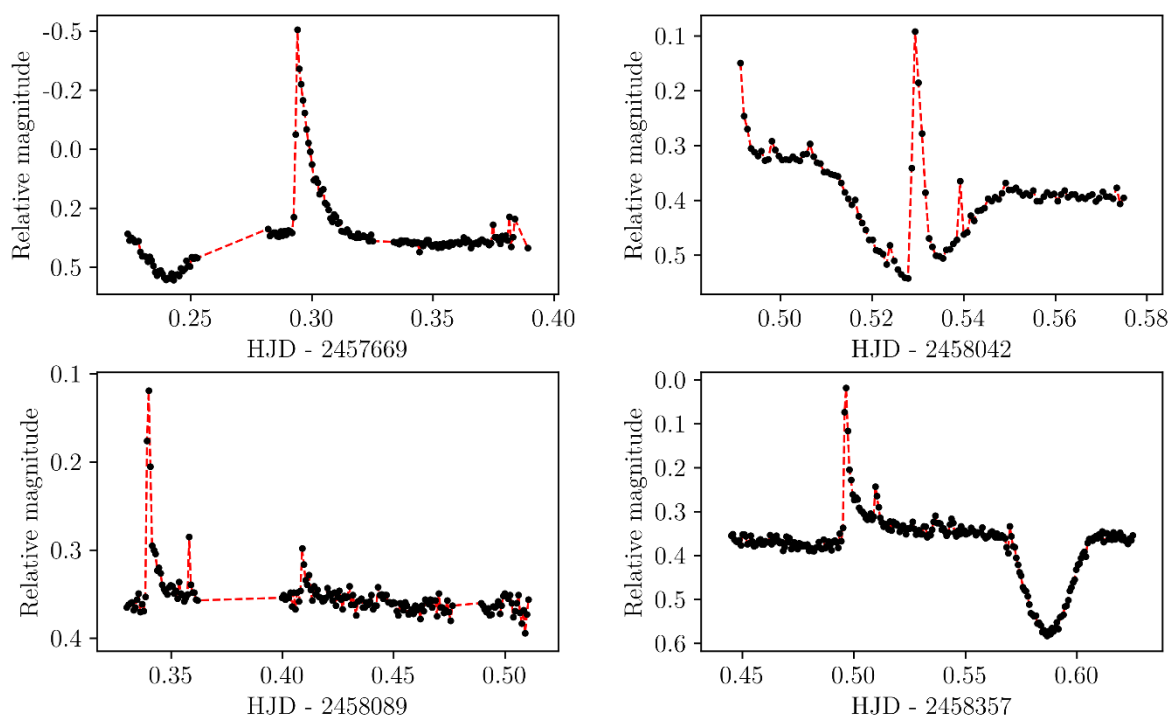


Figure 1: Examples of V light curves of GJ 3236 containing flares obtained at the Ondřejov observatory in years 2016–2018.

Data analysis

Among all available photometric data 296 flares were detected. Figure 1 shows examples of V light curves containing flares which were obtained at the Ondřejov observatory in years 2016–2018. For 234 flares, which occurred outside of eclipses, an estimation of portions of released energy for given photometric filters is possible to be made. The set of flares will be used for a statistical analysis of a flare occurrence in time, a distribution of flares in phase, energy distributions of flares for different photometric filters and relations between released energy, duration and amplitude of flares. A paper covering findings of this study in detail is in preparation.

Acknowledgement

This study would not be possible to make without the observational data, which were obtained by Hana Kučáková, Kateřina Hoňková, Jan Vraštil, Kamil Hornoch, Marek Wolf (Ondřejov), Ladislav Šmelcer (Valašské Meziříčí), František Bílek (Trhové Sviny), Marek Skarka (Pizskéstető), and Pavol Dubovský (Kolonica Saddle). I would like to thank all observers and Štefan Parimucha (UPJŠ) for providing me the observations obtained at the Kolonica Saddle observatory.

References

- Gershberg, R. E. et al., 1999, *A&AS*, 139:555–558, [1999A&AS..139..555G](#)
- Irwin, J. et al. 2009, *ApJ*, 701, 1436, [2009ApJ...701.1436I](#)
- Parimucha, Š., Dubovský, P., Vaňko, M., & Čokina, M. 2016, *Ap&SS*, 361, 302, [2016Ap&SS.361..302P](#)
- Pourbaix, D. et al., 2004, *A&A*, 424:727–732, [2004A&A...424..727P](#)
- Šmelcer, L., Wolf, M., Kučáková, H., et al. 2017, *MNRAS*, 466, 2542, [2017MNRAS.466.2542S](#)

The activity of the symbiotic binary Z Andromedae and its latest outburst

J. MERC^{1,2}, R. GÁLIS², M. WOLF¹, L. LEEDJÄRV³, F. TEYSSIER⁴

(1) Astronomical Institute, Faculty of Mathematics and Physics, Charles University
V Holešovičkách 2, 180 00 Prague, Czech Republic

(2) Institute of Physics, Faculty of Science, P. J. Šafárik University
Park Angelinum 9, 040 01 Košice, Slovak Republic

(3) Tartu Observatory, Faculty of Science and Technology, University of Tartu
Observatooriumi 1, Tõravere, 61602 Tartumaa, Estonia

(4) Astronomical Ring for Amateur Spectroscopy Group

Abstract: Z Andromedae is a prototype of classical symbiotic variable stars. It is characterized by alternating of quiescent and active stages, the later ones are accompanied by changes in both photometry and spectral characteristics of this object. The current activity of Z And began in 2000, and the last outburst was recorded at the turn of years 2017 and 2018. An important source of information about the behaviour of this symbiotic binary during the ongoing active stage is photometric and spectroscopic observations obtained with small telescopes by amateur astronomers. In this paper, we present the results of analysis of these observations, with an emphasis on the significant similarity of the last outburst of Z And with the previous ones, during which jets from this symbiotic system were observed. The presented results point to the importance of long-term monitoring of symbiotic binaries.

Introduction

Symbiotic stars are strongly interacting systems, in which physical mechanisms related to transfer and accretion of matter cause observable activity. During their active stages, which may last from a few days to decades, they manifest increases of brightness (about 2–5 mag) and significant changes in their spectra. Usually, these systems consist of a cool giant of spectral type K–M and hot compact star, mostly a white dwarf. The mass transfer most likely takes place by the stellar wind of the cool giant, which is also the source of a dense circumbinary envelope. Symbiotic systems are detached binaries with orbital periods of hundreds to thousands of days.

Z Andromedae is a prototype of classical symbiotic binaries. The binary consists of a late-type M4.5 III giant (Skopal, 2008) and a white dwarf with a strong magnetic field, $B_S \geq 10^5 \text{G}$ (Sokoloski & Bildsten, 1999) accreting from the giant's wind. The orbital period of the binary system is 758 days (Mikołajewska & Kenyon, 1996). Sokoloski et al. (2006) proposed a combination of dwarf nova-like accretion disk instability and nova-like nuclear shell burning as an explanation for its outbursts. Distance estimates of Z And range from 0.6 to 2.19 kpc (average value 1.2 ± 0.5 kpc; Sokoloski et al., 2006). Recently, the parallax of (0.512 ± 0.030) mas was published for Z And in the Gaia DR2 (Gaia Collaboration et al., 2018) from which Bailer-Jones et al. (2018) derived the point distance of 1.84 kpc with uncertainty of (1.75–1.95) kpc representing 68% confidence interval.

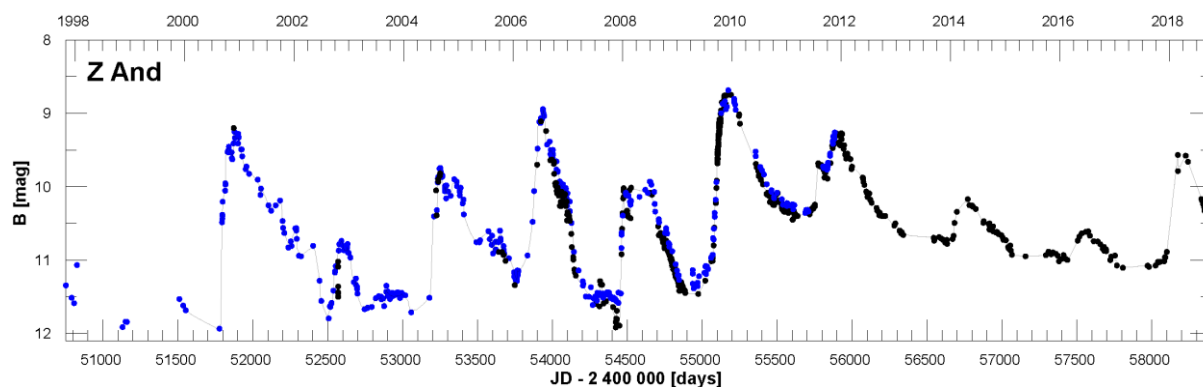


Figure 1: The light curve of Z And in the B filter over the period 1997–2018. Data from AAVSO and Skopal et al. (2002, 2004, 2007, 2012) are depicted in black and blue, respectively.

Z And is also one of a few known symbiotic stars producing collimated outflows or jets (Brocksopp et al., 2004; Leedj arv, 2004). The jets were detected in the radio images obtained during the 2000–2002 outburst (Brocksopp et al., 2004). The jet signatures were also recognised in the optical spectra of Z And acquired during the maxima of outbursts in 2006 (Skopal & Pribulla, 2006; Burmeister & Leedj arv, 2007; Tomov et al., 2007; Skopal et al., 2009) and 2009–2010 (Skopal et al., 2018).

During more than a hundred years of monitoring, Z And manifested several active stages with brightness variations ranging from a few tenths of a magnitude to about three magnitudes (Formigini & Leibowitz, 1994; Skopal, 2008). The symbiotic system is in the active stage since the year 2000 (fig. 1). In this paper, we present the results of analysis of the spectroscopic observations obtained during the latest outburst of Z And which occurred at the beginning of the year 2018.

Observations and analysis

We have used medium resolution spectra of symbiotic star Z And obtained by the ARAS (Astronomical Ring for Amateur Spectroscopy) Group observers to study the activity and overall behaviour of Z And during the ongoing active stage. ARAS³ is an initiative dedicated to promotion of amateur astronomical spectroscopy and professional/amateur collaborations. The observations of the group focus mainly on novae and symbiotic binaries. The network consists of independent amateur astronomers with small telescopes (20 to 60 cm) and spectrographs of different resolution (500 to 15000) covering the range from 3500 to nearly 8000  .

In the present study, we have analysed 61 spectra obtained by 6 observers from the overall number of 127 spectra (including low-resolution spectra that were not used) available in the ARAS database. In addition, we have used the spectra acquired on Tartu Observatory (Burmeister & Leedj arv, 2007) and Ondřejov Observatory (Skopal et al. 2009, 2018) to compare the latest outburst of Z And with the previous ones.

Our analysis was focused on the prominent emission lines in optical spectra of Z And: the neutral He I lines at λ 4471   and 6678  , ionized He II line at λ 4686  , the hydrogen lines H β at λ 4861   and H α at λ 6563  . We measured equivalent widths (EWs) of these lines using the software *PlotSpectra* and computed the fluxes in lines using the photometric observations of Z And obtained from AAVSO International Database (Kafka, 2018) and from papers by Skopal et al. (2002, 2004, 2007, 2012).

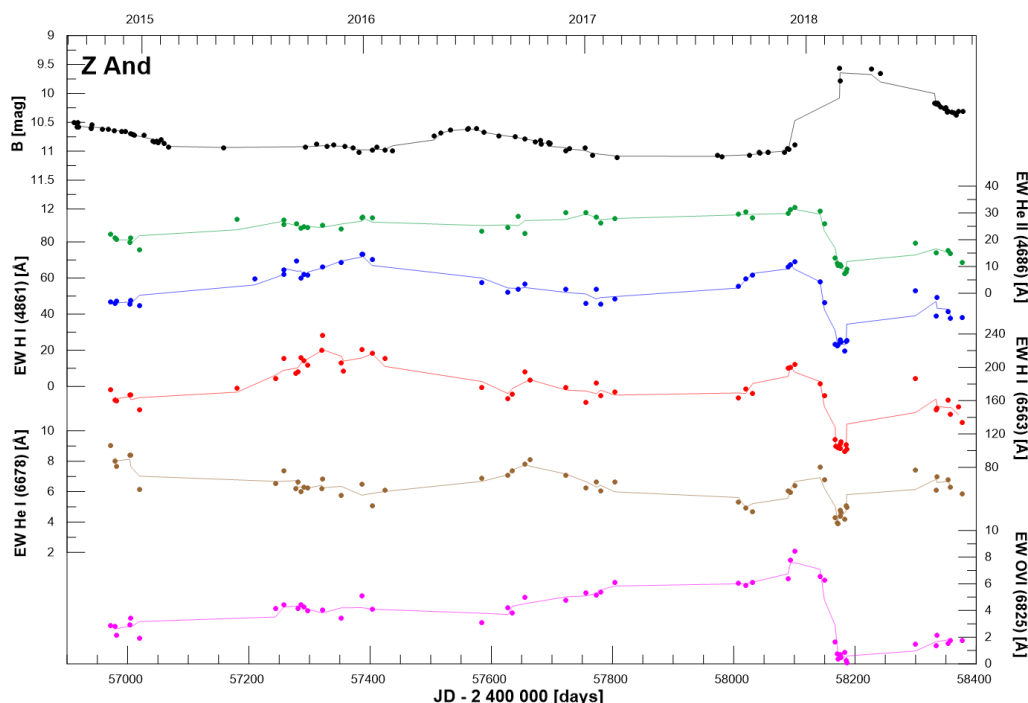


Figure 2: The EWs of prominent emission lines in spectra of Z And together with the AAVSO light curve in the B filter. The solid lines represent a spline fits to the data points.

³ http://www.astrosurf.com/aras/Aras_DataBase/DataBase.htm

Recent outburst activity of Z And

Since September 2000, the symbiotic system has manifested a typical Z And-type outburst activity with multiple outbursts of which the major ones occurred in December 2000, July 2006, December 2009 and December 2011. The recent outburst was observed at the beginning of the year 2018, and since then the brightness slowly declines (fig. 1). Photometrically, it was the most prominent outburst since 2012 with the maximal magnitudes of 9.6 and 9.0 in the *B* and *V* filters, respectively.

At the same period, the EWs of studied emission lines in optical spectra of Z And showed significant decline anticorrelated with brightness changes (fig. 2). In the case of AG Dra, such behaviour is typical for its *cool* outbursts and is related to the decrease of ionization source's temperature (Leedj rvi et al., 2016). Moreover, the Raman-scattered O VI lines completely disappeared during the outburst. Other high ionisation lines such as [Fe VII] also disappeared during the outburst, but these lines reappeared at the time when O VI lines remained undetectable. The O VI lines are discussed in more details in separate section.

Similar behaviour of the emission lines in optical spectra of Z And was observed during some of its previous outbursts. In 2006, the symbiotic system underwent the strong outburst accompanied by the ejection of bipolar jets (Burmeister & Leedj rvi, 2007; Tomov et al., 2007; Skopal et al., 2009). During that outburst, the He II line also practically disappeared. Despite the similarity of these two outbursts (in 2006 and 2018), no sign of the jet components around the H α and H β lines was observed during the recent one (fig. 3). Their transient character is also supported by other observations: the jet components were detected during the outburst in 2008 and 2009–2010, but not during those in 2012 or 2014 (Skopal et al., 2018).

Temperature evolution of the white dwarf

The behaviour of prominent emission lines in optical spectra of Z And suggests that the latest outburst of this symbiotic system could be of a *cool* type. We investigated the temperature evolution of the white dwarf in Z And using the method proposed by Iijima (1981) and modified by Sokolowski et al. (2006). Using some simplifications, which are discussed in detail in our recent paper (Merc et al., 2018), we can consider the He II/H β ratio as a proxy to the temperature of the hot component in symbiotic binaries:

$$T_{hot}(10^4 K) \approx 14.16 \sqrt{\frac{EW_{4686}}{EW_{H\beta}}} + 5.13$$

Even though the applied simplifications allow to obtain only the upper limit of the temperature (Merc et al., 2018), this method can still be used to study the temperature changes of the hot component of symbiotic systems. Applying this method to Z And, we confirmed the decrease of the white dwarf's temperature during and after the last outburst of this symbiotic system (Fig. 4). During the period 2014–2018, the average value of the ratio was 0.44 which is corresponding to the white dwarf's temperature around 145 000 K. In the course of the outburst 2018, its value dropped to about 0.29 (about 129 000 K).

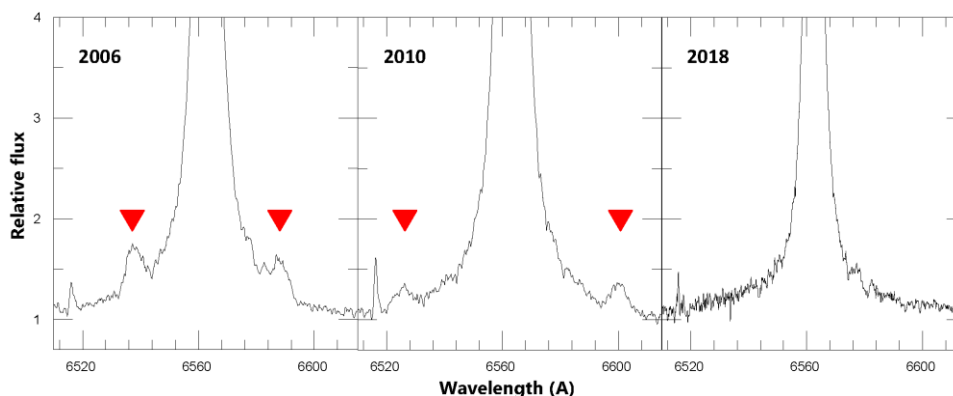


Figure 3: The jet components (marked by the red triangles) around the H α emission line occurred during the outbursts of Z And in 2006 and 2010. No sign of the jet components was observed during the recent outburst in 2018. The spectra from 2006 and 2010 were obtained on Ondřejov Observatory, the spectrum from 2018 is from the ARAS database.

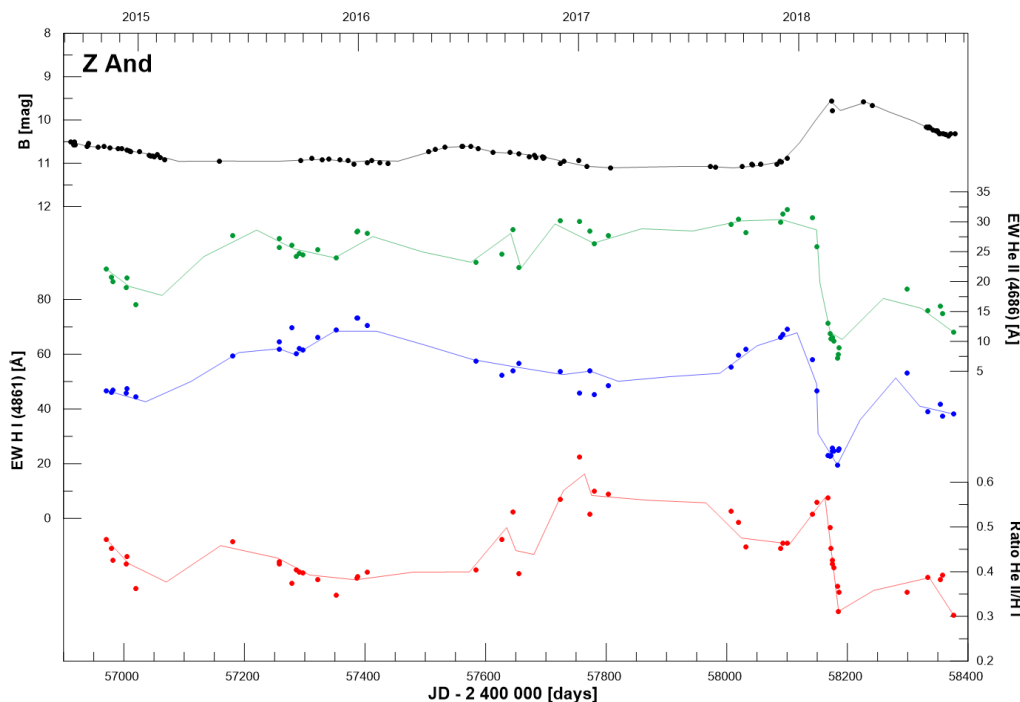


Figure 4: The EW ratio of the two strong emission lines He II and H β together with their EWs and AAVSO light curve in the B filter. The solid lines represent a spline fits to the data points.

The Raman-scattered O VI lines

The Raman-scattered O VI lines are broad emission features in optical spectra at 6825 and 7082 Å which are a product of Raman-scattering of the photons of the O VI resonance lines at 1032 and 1038 Å off the atoms of neutral hydrogen (Schmid, 1989). They occur almost exclusively in the spectra of symbiotic stars. During recent outburst of Z And, the Raman-scattered O VI line at 6825 Å disappeared due to cooling of the ionizing source (fig. 2 and 4). Similar vanishing was observed during the outburst of AG Dra in 2006, confirming a drop in the white dwarf's temperature (Leedjäv et al., 2016).

It is worth to note, that similar disappearance of the O VI lines was also observed during the recent *hot* outbursts of AG Dra and AG Peg (Skopal et al., 2017; Merc et al., 2019) when the temperature of the ionizing source in these symbiotic systems has risen. In these cases, vanishing of the O VI lines could be probably caused by an increase of mass-loss rate from the hot component which makes O VI zone optically thick (Skopal et al., 2017). It is possible that a similar effect also played a role in the recent outburst of Z And because the O VI lines were undetectable long after other highly ionized lines reappeared in the spectrum. On the other hand, according to the new ARAS observations, during the current post-outburst decline of the new symbiotic star HBHa 1704-05 (Munari et al., 2018), the Raman-scattered O VI lines have appeared, while the [Fe VII] lines were still very weak.

Conclusions

In the present paper, we investigated the latest outburst of symbiotic binary Z And. We analysed photometric and spectroscopic observations covering this brightening with focus on the evolution of the EWs of selected prominent emission lines and their profile changes. As we have shown, the recent outburst manifested the decrease of the emission line EWs and the steep decrease of the ionising source temperature. Similar behaviour of Z And was observed in the past, especially during the major outburst in 2006 which was accompanied by the ejection of bipolar jets, signatures of which were observed in the profile of hydrogen lines. Despite the significant similarity between the outbursts in 2006 and 2018, no jet components were observed in the spectra during the latter one. Nevertheless, it is worth observing this interesting symbiotic system further. Only long-term monitoring can help to uncover the physical mechanisms responsible for the unusually long active stage of Z And lasting now for almost two decades.

Moreover, the presented results showed also the importance of professional/amateur collaborations. ARAS Group is a perfect example that such collaboration can be very successful and can bring important results. Thanks to amateur photometric and spectroscopic data, we are now able to monitor the evolution of symbiotic systems on timescales which were not previously available.

Acknowledgement

We are grateful to all ARAS members that contributed their observations to this paper, particularly we acknowledge and thank Paolo Berardi, Joan Guarro Flo, Tim Lester, Jacques Montier and Peter Somogyi. We acknowledge with thanks the variable star observations from the AAVSO International Database contributed by observers worldwide and used in this research. This work was supported by the Slovak Research and Development Agency grant No. APVV-15-0458 as well as by the Estonian Ministry of Education and Research institutional research funding grant IUT 40-1.

References

- Bailer-Jones, C. A. L., Rybizki, J., Fouesneau, M., Mantelet, G., & Andrae, R., 2018, *AJ*, 156, 58, [2018AJ....156..58B](#)
- Brocksopp, C., Sokoloski, J. L., Kaiser, C., et al., 2004, *MNRAS*, 347, 430, [2004MNRAS.347..430B](#)
- Burmeister, M. & Leedj arv, L., 2007, *A&A*, 461, L5, [2007A&A...461L...5B](#)
- Formigini, L. & Leibowitz, E. M., 1994, *A&A*, 292, 534, [1994A&A...292..534F](#)
- Gaia Collaboration, Brown, A. G. A., Vallenari, A., et al., 2018, *A&A*, 616, A1, [2018A&A...616A...1G](#)
- Iijima, T., 1981, in *Photometric and Spectroscopic Binary Systems*, 517, [1981psbs.conf..517I](#)
- Kafka, S., 2018, *Observations from the AAVSO International Database*, <https://www.aavso.org>
- Leedj arv, L., 2004, *Baltic Astronomy*, 13, 109, [2004BaltA..13..109L](#)
- Leedj arv, L., G alis, R., Hric, L., Merc, J., & Burmeister, M., 2016, *MNRAS*, 456, 2558, [2016MNRAS.456.2558L](#)
- Merc, J., G alis, R., & Leedj arv, L., 2018, in *The Golden Age of Cataclysmic Variables and Related Objects IV, Proceedings of Science*, 315, 60, [2017gacv.workE..60M](#)
- Merc, J., G alis, R., Teysmier, F., 2019, *Contributions of the Astronomical Observatory Skalnat  Pleso*, submitted
- Mikolajewska, J. & Kenyon, S. J., 1996, *AJ*, 112, 1659, [1996AJ....112.1659M](#)
- Munari, U., Dallaporta, S., Valisa, P., et al., 2018, *The Astronomer's Telegram*, 11937, 1, [2018ATel11937....1M](#)
- Schmid, H. M., 1989, *A&A*, 211, L31, [1989A&A...211L..31S](#)
- Skopal, A., Vaňko, M., Pribulla, T., et al., 2002, *Contributions of the Astronomical Observatory Skalnat  Pleso*, 32, 62, [2002CoSka..32...62S](#)
- Skopal, A., Pribulla, T., Vaňko, M., et al., 2004, *Contributions of the Astronomical Observatory Skalnat  Pleso*, 34, 45, [2004CoSka..34...45S](#)
- Skopal, A. & Pribulla, T., 2006, *The Astronomer's Telegram*, 882, 1, [2006ATel.882....1S](#)
- Skopal, A., Vaňko, M., Pribulla, T., et al., 2007, *Astronomische Nachrichten*, 328, 909, [2007AN....328..909S](#)
- Skopal, A., 2008, *Journal of the American Association of Variable Star Observers*, 36, 9, [2008JAVSO..36....9S](#)
- Skopal, A., Pribulla, T., Budaj, J., et al., 2009, *ApJ*, 690, 1222, [2009ApJ...690.1222S](#)
- Skopal, A., Shugarov, S., Vaňko, M., et al., 2012, *Astronomische Nachrichten*, 333, 242, [2012AN....333..242S](#)
- Skopal, A., Shugarov, S. Y., Seker as, M., et al., 2017, *A&A*, 604, A48, [2017A&A...604A..48S](#)
- Skopal, A., Tarasova, T. N., Wolf, M., Dubovsk y, P. A., & Kudzej, I., 2018, *ApJ*, 858, 120, [2018ApJ...858..120S](#)
- Sokoloski, J. L. & Bildsten, L., 1999, *ApJ*, 517, 919, [1999ApJ...517..919S](#)
- Sokoloski, J. L., Kenyon, S. J., Espey, B. R., et al., 2006, *ApJ*, 636, 1002, [2006ApJ...636.1002S](#)
- Tomov, N. A., Tomova, M. T., & Bisikalo, D. V., 2007, *MNRAS*, 376, L16, [2007MNRAS.376L..16T](#)

Improvement of Simplified Models of Variability of Stars: A review

IVAN L. ANDRONOV¹

(1) Department "Mathematics, Physics and Astronomy", Odessa National Maritime University, Mechnikova, 34, 65029 Odessa, Ukraine, tt_ari@ukr.net

Abstract: Astronomical data are typically irregular in time, e.g. the space (HIPPARCOS/TYCHO, KEPLER, GAIA, WISE etc.) and ground-based CCD (NSVS, ASAS, CRTS, SuperWASP etc.) and photographic (Harvard, Sonneberg, Odessa etc.) photometrical surveys. This leads to cancellation of the conditions, which lead to the orthogonality of the basic functions, and thus the simplified methods give biased parameters of the approximations. In the common methods, there is a "matrix-phobia", as it was later called by Prof. RNDr. Zdeněk Mikulášek, CSc. (MUNI).

We have elaborated a series of algorithms and programs for statistically correct analysis, and have applied them to 2000+ variable stars of different types. The data were obtained from an international collaboration in a frame of the "Inter-Longitude Astronomy" (ILA) campaign. Some highlights of our studies are presented, with an extended list of our original publications.

The main improvements were done: 1) for the periodogram analysis - the parameters are determined from a complete set of equations containing the (algebraic polynomial) trend superimposed on the (multi-) harmonic wave, so no "detrending", no "prewhitening" are used; 2) for the approximations - we use additional (multi-) harmonic waves, and also "special shapes" (patterns) for parts of the light curve, which correspond to relatively fast changes (minima of the eclipsing binaries, minima and maxima for the pulsating variables); 3) "auto correlation analysis" (ACF) - taking into account the bias due to a trend removal (previously - only a subtraction of the sample mean was taken into account); ACF for the irregularly spaced data; 4) for the signals with bad coherence, the "scalegram" analysis is proposed, which allows to estimate a characteristic cycle length and the amplitude, as well as to provide a realistic approximation; 5) the extension of the Morlet-type wavelet for more periodic signals and 6) "running" (parabola, sine) approximations for aperiodic and "nearly periodic" variations, respectively.

Introduction

Time series analysis (recently more often called the "Data analysis") is applied not only in astronomy, but also in geoscience, economics and other sciences. Among the best textbooks are the ones by Anderson (Anderson, 1971). The complexity of time series may vary from object to object and especially from one type of variable stars to another.

The majority of the methods of the time series had been elaborated for some standard cases of temporal behaviour. For real cases of multi component variability, some authors apply simplified (or even "oversimplified") methods, neglecting apparent correlations between different components of variability. This leads to shifts of values of the model parameters, and, consequently, may lead to wrong physical conclusions. This is generally true, even for linear model, with a summation of different contributions of variability, due too the orthogonality of the basic functions. In this case, the matrix of normal equations becomes non-diagonal, and the estimated values of the parameters depend on the number of coefficients. Obviously, this challenges their physical meaning.

We show some examples of wrong values of the coefficients and thus a mathematical model leading to wrong physical conclusions.

The basic equations started from Carl Gauss two centuries ago, and are published many textbooks and monographs (e.g. Anderson, Terebizh) and reviews (Andronov, 1994, 2003, Andronov & Marsakova, 2006, Mikulášek, 2007, 2015, Mikulášek et al., 2006, 2015). There may be some improvements, which are discussed below.

Least Squares

Let the approximation $x_C(t; C_\alpha)$ be the function with the corresponding parameters $C_\alpha, \alpha = 1..m$ are, which are to be determined.

In the vector notation, the test function is

$$\Phi(C_\alpha; \vec{t}; \vec{x}) = (\vec{x} - \vec{x}_C) \cdot (\vec{x} - \vec{x}_C), \quad (1)$$

where $\vec{x} = (x_k, k = 1..n)$ is the vector of observations obtained at times \vec{t} , and $\vec{x}_C = (x_{Ck}) = (x_C(t_k))$ is the vector of calculated values at times t_k . The best “quality of the approximation” corresponds to the minimal value of Φ . Assuming n – dimensional distribution of the error of observations, this corresponds to a maximum likelihood. As the data are fixed, the test function $\Phi(C_\alpha; \vec{t}; \vec{x})$ is to be minimized in respect to the parameters C_α only. The generalized scalar product may be written as

$$(\vec{a} \cdot \vec{b}) = \sum_{k,j=1}^n g(t_j, t_k, f; T_0) h_{jk} a_j b_k, \quad (2)$$

where h_{jk} is an analog of the metric tensor, and g is the function to make an approximations both local and dependent on the time scale and position of the central point (like in the wavelet and “running” approximations (Andronov, 1997, 1998).

Mikulášek et al. (2003) proposed an additional weight function dependent on $|x_k - x_{Ck}|$, the aim of which is dump the outliers. In this case, the iteration is “robust” and should converge after several iterations.

Assuming that the errors of the measurements have a covariation matrix μ_{jk} , it is usually recommended to use $h_{jk} = \sigma_0^2 \mu_{jk}^{-1}$, where σ_0^2 is any positive constant, which is called “the unit weight variance”. The inverse relation is $\mu_{jk} = \sigma_0^2 h_{jk}^{-1}$.

The simplest case of variability is the “linear model”

$$x_C(t; C_\alpha) = \sum_{\alpha=1}^m C_\alpha f_\alpha(t), \quad (3)$$

where $f_\alpha(t)$ are basic functions, and the coefficients C_α are generally dependent on f and T_0 , if the additional weight function g is not constant with time.

Practically, such complicated expressions are not used for the periodogram analysis. The matrix is usually oversimplified to $h_{jk} = \delta_{jk}$ (e.g. in the approximations in the electronic tables), or to $h_{jk} = w_k \delta_{jk}$, if assuming that $w_k = \sigma_0^2 / \sigma_k^2$, $\mu_{jk} = \sigma_k^2 \delta_{jk}$. Such approximations are used typically for “global” approximations, when all the data are used.

The cases of overlapping “running” approximations (improving the “running mean” = “moving average”) are discussed below.

Periodogram analysis

“Point – Point” Methods

The structural scheme of the methods of the periodogram analysis was presented by Andronov (1996). The main division is into the groups "point-point" (non-parametric) and "point-curve" (parametric). The first group has started from Lafler and Kinman (1965) and was modified by other authors. All these methods are based on minimizing weighted mean distance (or its square) between the points with times $t_k, k = 1..n$, values of the signal x_k , which are sorted according to phases ϕ_k computed for a given trial period P (or frequency $f = 1/P$). The test function may be generally expressed as a function of trial frequency and fixed (for a given sample) data:

$$\Theta(f; t_k; x_k) = A \sum_{k=1}^n \rho(|x_k - x_{k-1}|; |\phi_k - \phi_{k-1}|), \quad (4)$$

where the initial data $(x_k, \phi_k, k = 1..n)$ are extended by $x_0 = x_n, \phi_0 = \phi_n - 1$. The scaling coefficient $A > 0$. The summand $\rho(\delta_x; \delta_\phi)$ may be equal e.g. to $|\delta_x|^\gamma$ with a power index $\gamma = 1$ (appendix by T.J.Deeming to Bopp et al., 1970), $\gamma = 2$ (initial proposal by Lafler and Kinman, 1965), or any other positive value. Few variations of functions with a real dependence of ρ on δ_ϕ were proposed e.g. by Renson (1978) and Dworetsky (1983).

Detailed review and comparison of these methods was presented by Andronov and Chinarova (1997).

More general expression was presented in Eq. (3) by Pelt (1975) and may be reasonably rewritten using the “structure function”.

$$\Theta(f; t_k; x_k) = \frac{\sum_{j=1}^{n-1} \sum_{k=j+1}^n g(f; |t_k - t_j|) \rho(|x_k - x_j|)}{\sum_{j=1}^{n-1} \sum_{k=j+1}^n g(f; |t_k - t_j|)}, \quad (5)$$

where $\rho(\delta_x)$ is the “distance” between the points (e.g. again $|\delta_x|^\gamma$), and the structure function may be split into two parts:

$$g(f; |t_k - t_j|) = W(f; |t_k - t_j|) G(|\phi_k - \phi_j|), \quad (6)$$

where, in the simplest case, function $W(f; \delta_t) = 1$, if $|\delta_t| \leq \delta_{t,\text{lim}}$ (else $W(f; \delta_t) = 0$), and, similarly, $G(\delta_\phi) = 1$, if $|\delta_\phi| \leq \delta_{\phi,\text{lim}}$ or $1 - |\delta_\phi| \leq \delta_{\phi,\text{lim}}$ ($G(\delta_\phi) = 0$). In other words, the structure function is a sum of $\rho(|x_k - x_j|)$ only for the data points close either in phase, or in time. Another improvement may be of a “wavelet – style”, if $W(f; \delta_t) = 1$, if $|f \delta_t| \leq \delta_{E,\text{lim}}$. One may propose smooth functions, e.g. a Gaussian $W(f; \delta_t) = \exp(-c((f \delta_t)^2)$ or a limited-width function proposed by Andronov (1997). For the second function, Pelt (1975) suggested a cosine-type shape $G(\delta_\phi) = (1 + \cos(2\pi\delta_\phi))/2$, which is a good choice for nearly sinusoidal oscillations, but is much worse for periodic variables with more complicated curves (e.g. eclipsing binaries). Because of long computational time needed, these methods are not widely used, except the initial method of Lafler and Kinman (1965). It was realized in many programs (e.g. Breus, 2003, 2007; Vanmunster, 2018).

“Point – Curve” Methods

The "point-curve" methods are typically based on the least squares method by comparing the data with the approximation (“computed curve”) $x_c(t; C_\alpha)$, which is dependent on the frequency $f = \frac{1}{P}$, where P is a trial period, and (generally) on the initial epoch T_0 . Obviously, the test function $\Phi(C_\alpha; \vec{t}; \vec{x})$ depends on these two parameters as well. The simplest type of variability is a cosine wave. For it, the optimal mathematical model is:

$$x_c(t; C_\alpha) = C_1 + C_2 \cos \omega t + C_3 \sin \omega t = C_1 - R \cos(\omega(t - T_0)), \quad (7)$$

where $\omega = 2\pi f = 2\pi/P$, and T_0 is the “initial epoch” corresponding to a *minimum* signal value (which, if being a magnitude (in astronomy), as a *maximum* of brightness). The relations between the coefficients are well known: $C_2 = -R \cos(\omega T_0)$, $C_3 = -R \sin(\omega T_0)$, $R^2 = C_2^2 + C_3^2$, $T_0 = \arctan2(-C_3, -C_2) + P \cdot K$, where K is any integer number. The function $\arctan2(y,x)$ calculates $\arctan(y/x)$, and returns an angle in the correct quadrant (is present in Python, Delphi and other computer languages). For further period corrections, Andronov (1994) recommended to use such a value of K , which makes T_0 as closest as possible to a (weighted) sample mean of times of observations.

For mono-periodic multi-harmonic signals (e.g. “regular” pulsating variables and eclipsing binaries), this may be easily expanded to trigonometric polynomials (abbreviated Fourier series) of order s :

$$x_c(t; C_\alpha) = C_1 + \sum_{j=1}^s (C_{2j} \cos j\omega t + C_{2j+1} \sin j\omega t) = C_1 - \sum_{j=1}^s R_j \cos(j\omega(t - T_{0j})) \quad (8)$$

with similar relations: $C_{2j} = -R_j \cos(j\omega T_{0j})$, $C_{2j+1} = -R_j \sin(j\omega T_{0j})$, $R_j^2 = C_{2j}^2 + C_{2j+1}^2$, $T_{0j} = \arctan2(-C_{2j+1}, -C_{2j}) + \frac{P.K.}{j}$.

The test function is recommended to be computed at a grid of test frequencies $f_i = f_0 + i \cdot \Delta f$, where $\Delta f = \Delta\phi/(t_n - t_1)$, and the phase shift is recommended to be $0 < \Delta\phi \leq 0.1$ (cf. Andronov, 1994b). After determination of the largest peak at the periodogram, the period may be corrected by differential corrections. The realizations of the method were made initially in the Fortran programming language, but then implemented in the MCV (“Multi-Column Viewer”) by Andronov and Baklanov (2004).

Examples of periodograms for different degrees s and discussion on the statistically optimal degree of the trigonometrical polynomial are presented by Andronov et al. (2016).

Based on the statistically optimal fits of a group of Mira-type stars, Kudashkina and Andronov (2017) compiled an atlas of behavior of the light curves at the $(x_c; dx_c/d\phi)$ phase diagrams.

Multi-Periodic Multi-Harmonic Oscillations with Trend: Detrending / Prewhitening vs Complete Models

Similarly to multi-harmonic approximations, the fit may be expanded to few (L) independent periods $P_l, l = 1..L$, with corresponding degrees of the trigonometrical polynomial s_l , and the possible trend may be represented by an algebraical polynomial of degree s_0 :

$$x_c(t; C_\alpha) = \sum_{j=1}^{s_0+1} C_j \cdot (t - T_{mean})^{j-1} - \sum_{l=1}^L \sum_{j=1}^{s_l} R_{jl} \cos(j\omega_l \cdot (t - T_{0jl})) \quad (9)$$

In the software MCV (Andronov and Baklanov, 2004), the maximal number of independent periods is $L = 3$.

For the periodogram analysis, $L = 1$, but one may use a trend and a multi-harmonic approximation. The test function is

$$S = 1 - \Phi_{s_0+1+2s_1} / \Phi_{s_0+1}, \quad (10)$$

where Φ_m is the test function for the approximation with m parameters. For simpler approximations (e.g. in the electronic tables etc.), the value of S is expressed as r^2 . This value shows the ratio of the variance of the “signal” to the “signal+noise”, where the “signal” is in deviation of the “trend+periodic wave” approximation from the “pure trend”.

Detrending is a special type of prewhitening, when the characteristic time scale is much longer than the observations, so an algebraic polynomial is used instead of multi-harmonic approximation.

It is very important to note, that, due to the non-orthogonality of the basic functions, the coefficients C_j of the “trend” are *generally different* from that of the “trend+periodic wave”. In the simplified methods, the “detrending” is applied, and then the periodogram analysis is applied as for the signal without any trend. This biases the periodogram and may produce peaks at false periods (frequencies), what produces *fake results*. Similarly, “prewhitening” is a subtraction of a periodic wave, and further application of the periodogram analysis. For a “good” distribution of times of the signal (approximately filling a complete phase curve), this may not be very significant. But for real observations of superhumps or pulsations of the δ Sct-type stars, the periods of which are comparable with the duration of the observations, the errors may reach dozens of per cent.

In the light curves of the intermediate polars, there are two periodic components (orbital and spin, e.g. Patterson, 1994), thus it is effective to apply (e.g. Andronov and Breus, 2013). Andronov et al. (2008a) used trigonometrical polynomials to study night-to-night variations of the asynchronous polar BY Cam.

The total number of parameters should not exceed a default value of $m = 21$. Of course, all the parameters are computed with corresponding error estimates, as defined in the LSQ approximation.

Special Shapes for the Narrow Features of the Signal

Polynomial Splines

Trigonometrical polynomial fits are excellent approximating functions in a case of smooth curves. However, in a case of abrupt variations (eg. narrow eclipses in binary stars, or relatively short ascending branches of RR Lyr - type stars or HADS (high amplitude δ Scuti stars)), the number of the parameters becomes very large, causing apparent waves at the light curve (the Gibbs phenomenon). In this case, it is recommended to use a smaller number of basic functions.

In the case of one hump phase curves of pulsating variables, we have applied a two-interval model consisting of a parabola at the longer part and a cubic function in the smaller interval typically corresponding to a rapidly ascending branch. The function itself, and its derivative are continuous everywhere, including the borders between the intervals. There are 3 parameters obtained using linear LSQ, and 2 nonlinear parameters, including two positions of borders.

These cyclic spline approximations of variable order 2 and 3 were used for a period search and parameter determination of the pulsating variables from the HIPPARCOS-TYCHO photometrical survey (Andronov, Cuypers & Piquard, 2000).

Another approximation, based on splines of different order, is a "constant+parabola" one. There are also 3+2 parameters. Such an approximation is an effective one not only for the EA-type stars, but also for EB and EW. The position of the minimum and the eclipse width are the free parameters (Andronov, Cuypers & Piquard, 2000). This approximation has much better quality than e.g. the approximation in 4 overlapping intervals, proposed by Papageorgiou et al. (2014), which is good for the maxima (out-of-eclipse) phases, but has systematic underestimate of the eclipse depth.

Cubic splines with periodic bound conditions were used by Andronov (1987) for the periodogram analysis and studies of the period variations without using the (O-C) diagrams for the times of extrema, using a trial "time correction" to compute phases taking into account not only the initial epoch and period, but a term proportional to the period derivative. As the splines are dependent not only on the number of basic points, but also on the shift, there were two versions – the "shift-averaged" spline and the "shift-optimized" spline.

Local Special Shapes (Patterns)

Further improvements are due to using other functions rather than algebraic or trigonometric polynomials. Andronov (2010) proposed to use a combination of the trigonometrical polynomial of only second order with "eclipse parts" with a local "special shape" $H(z) = (1 - |z|^\alpha)_+^{1.5}$, where the index "+" denotes that negative values of the function are set to zero. The function may be scaled and shifted to fit the minimum, and the parameter α describes the shape at the center. The minimal (physically reliable) value $\alpha = 1$ corresponds to a total eclipse of stars with equal radii, and $\alpha \rightarrow \infty$ corresponds to an extremely "flat" minimum. The fixed power index 1.5 corresponds to asymptotic behavior of the light curve close to the phases of the outer contacts at the eclipse (Andronov and Tkachenko, 2013).

This approximation was referred as to the NAV ("New Algol Variable") one, and was initially applied to four newly discovered variable stars by Kim et al. (2010) and then to other "newbees". Andronov (2012a) argued that this local approximation seems the best among others with the same number of parameters because, with the same quality of the fit, it allows to determine, in an addition to other parameters, an important characteristic for the "General Catalog of Variable Stars" (Samus' et al., 2017) – the eclipse full half-width. Unfortunately, this important parameter (making a relation between the summary dimensionless size of the components and the inclination) is recently typically ignored, as the popular programs do not determine it.

This parameter is, in principle, may not be determined using functions with formally infinite width, e.g. a Gaussian or its "hyperbolic cosine" improvement by Brat et al. (2012), implemented as a standard on-line tool at the B.R.N.O. (O-C gate) web page. For further details, see Mikulášek (2015) and Mikulášek et al. (2015),

Andronov (2012b) compared the "NAV" function to others, including the function $H_2(z) = (1 - z^2)_+^\beta$, which has a classical parabolic shape at the center $|z| \ll 1$: $H_2(z) \approx (1 - \beta z^2)$, contrary to the "NAV" shape with another $H(z) \approx (1 - 1.5 \cdot |z|^\alpha)$. At the eclipse borders, $|z| \approx 1$, $H(z) \approx \alpha^{1.5}(1 - |z|)^{1.5}$, and $H_2(z) \approx 2^\beta(1 - |z|)^\beta$ – both functions have power shape, but different. The function $H_2(z)$ was applied to 26121 LMC and 6138 SMC eclipsing binaries from the OGLE III LMC database (Graczyk et al., 2011) photometric survey by Juryšek et al. (2018).

The “New Algol Variable” (NAV) algorithm may be effectively applied not only to Algol-type stars, as was initially suggested, but also to β Lyr and even W UMa stars. The curves for the prototype stars of these subclasses are presented by Tkachenko et al. (2016).

Contrary to the approximations of complete light curves, the phenomenological modeling of the partial light curves covering only the vicinities of extrema (to determine only the ToM=Time of Minimum/Maximum) is a more frequent task. The previous review on the statistically optimal determination of the characteristics of extrema (not only ToM, but the approximating function as well) was presented by Andronov (2005).

The polynomial of a statistically optimal order was used for compiling the catalogue of the characteristic of individual extrema of 173 semi-regular variables by Chinarova and Andronov (2000). This method was later implemented by Breus (2003).

For the intervals, completely covering the eclipses, Andronov et al. (2017) proposed few improvements of the methods proposed by Andronov (2012a) and Mikulášek (2015). For the intervals, covering the symmetric eclipses, or maxima of the pulsating variables, Andrych et al. (2015, 2017) proposed a series of which split the interval into two or three parts. These more recent methods were implemented in the software MAVKA, and are presented in the same volume by Andrych and Andronov (2018). The first version (Andronov et al., 2015) implemented the approximations using (general and symmetric polynomials as well as the asymptotic parabola (Marsakova and Andronov, 1996).

Andrych et al. (2017) introduced the “wall-supported” functions which are more effective for total eclipses and transits. Finally, the 3-interval parabolic spline was implemented.

The program MAVKA allows to apply up to 20 functions for a given interval and may automatically choose the best approximation, which corresponds to the best accuracy of the ToM.

Previous versions of the program were applied to observations of some eclipsing binary stars (Savastru et al, 2017; Tvardovskyi et al., 2017, 2018) and symbiotic variables (Marsakova et al., 2015).

An alternate approach is to determine moments of crossing of the approximation and some constant level (cf. Andronov et al., 2008b, Andronov and Andrych, 2014).

“Running” Approximations

Thus the one may use T_0 as an argument of the “super-function”, which is constructed from the middle points of the original functions computed by taking into account the Eq. (6):

$$\tilde{x}_c(T_0) = \sum_{\alpha=1}^m C_\alpha(f; T_0) f_\alpha(T_0). \quad (11)$$

A complete theory of the statistical properties of such functions and their derivatives was presented by Andronov (1997) with an application to “running parabola” (RP) with an additional weight function

$$g(t_j, t_k, f; T_0) = (1 - ((t_j - T_0)f)^2)_+ \cdot \delta_{jk}. \quad (12)$$

Here the bottom index “+” denotes that the value is computed in this way, only if the result is positive (else $g = 0$). The statistically optimal value of $f = 1/\Delta t$ (in the original paper) may be determined using the scalegram analysis

The application to the sine functions leads to two branches: the running sines and the wavelet analysis.

Running Sines (RS)

For the “Running Sines” (RS), the function is defined by Eq. (1), and is an effective tool for (nearly) periodic functions with a (relatively slow) trend, e.g. semi-regular variables, intermediate polars. The review on the “stress test” of the method for the signals with variable periods was presented by Andronov and Chinarova (2013).

Running sines are an intermediate between the wavelet and a running parabola, discussed below. Contrary to the wavelet, the period is fixed, as well as as the filter half width. The weight functions is constant inside the interval of smoothing, i.e. the filter (weight) function is rectangular.

The recommended filter half-width is $\Delta t = P/2$, but the pulsational periods of many Mira-type stars are close to a year, thus seasonal gaps in the observations cause large errors if the smoothing function, thus, for these signals, the recommendation is $\Delta t = P$. Generally, it is as a free parameter. Larger values of Δt may be recommended for

relatively stable light curves, in which the shape of the light curve changes at a time scale exceeding Δt , so will hide possible real variations of the characteristics of the light curve.

Theoretically, for pure multiharmonic signal and an interval, uniformly filled with observations, the smoothing function is a purely sinusoidal function. For the data with gaps, the shape becomes a-sinusoidal.

Wavelet Analysis

Wavelet analysis is a popular tool for analysing nearly periodic data with time scale of variability of characteristics of the individual cycles, which exceeds the period by a factor of a few times. The over-simplified method is based on a simple replacement of the integrals from minus to plus infinity by discrete sums over the moments of observations, similarly to the method of Deeming (1975). Foster (1995) proposed the WWZ ("weighted wavelet Z – transform"), which is based on a determination of the parameters of the fit using the least squares method with weights. Andronov (1998) proposed improvements of the method, introducing the wavelet periodogram, and using for the period determination the test function $S(f)$ similar in sense to that one, which was introduced by Andronov (1994a).

Depending on the time distribution of the observations, the improvement of the "signal-to-noise" ratio may reach "gain" from dozens of per cent to dozens of times (for a very disjointed distribution in time).

The recommendation for the wavelet analysis (based on the improved Morlet-type wavelet) is to use the logarithmically constant scale step for the trial periods, contrary to usually used periods. Also as an analog of the Nyquist interval between the data, for the Morlet type wavelet, the optimal time step for smoothing is $P/3$.

Detailed reviews were presented by Andronov (1998, 1999).

Running Parabolae

This method was elaborated by Andronov (1997) for irregular signal and the signals of low coherence, e.g. quasi-periodic oscillations (QPO) or regular outbursts with variable occurrence rate. The free parameter to be determined for the statistically optimal smoothing is the filter half-width Δt . Similarly to the periodogram analysis, the scalegram analysis is used. The corresponding test functions may be different. Among them - the unbiased estimate of r.m.s. deviation of the observations from the fit; the r.m.s. accuracy of the approximation at the arguments of the signal; the "signal-to-noise" ratio. The weight function (in the notation of the Eq. (12)) is:

$$g(t_j, t_k, f; T_0) = (1 - ((t_j - T_0)/\Delta t)^2)_+ \cdot \delta_{jk} \quad (13)$$

Andronov (2003) introduced an additional test function (Δt), which may be interpreted as a "scalegram periodogram". It may be used for determination of "period" (cycle length) of quasi-periodic signals (QPO) and effective amplitude. Obviously, for pure sinusoidal signals with "good" (dense, uniform) distribution of the times of observations, all these methods (global fit, running sines, wavelet analysis and the scalegram analysis) should result in the same (within accuracy estimates) parameters. However, for real data, the results may be significantly different. Also, the scalegram analysis an effective tool for the flickering (red noise, fractal) variability, e.g. in cataclysmic and symbiotic variables.

Autocorrelation Functions (ACF) of Detrended Signals

Autocorrelation analysis is widely used for the analysis of regularly spaced time series i.e. when the times of the observations are related as $t_k - t_j = (k - j) \cdot \delta$ (e.g. Anderson, 1971).

This classical relation may be improved for the ACF analysis of the residuals of the observations from the smoothing function, what is an often case e.g. for cataclysmic variables with orbital variability and quasi-periodic oscillations (QPO) and/or flickering, as well as for binary systems with pulsations of one of the components

The removal of the mean was studied by Sutherland et al. (1978), whereas the complete theory of statistical properties of the ACF was presented by Andronov (1994a). This may help to prevent false interpretation of flickering as the quasi-periodic oscillations.

Acknowledgement

We thank Lewis M. Cook and Prof. RNDr. Zdeněk Mikulášek for discussions. This work is related to the international projects "Inter-Longitude Astronomy" (ILA, Andronov et al., 2003, 2014, 2017) and "Ukrainian Virtual Observatory", "Astroinformatics" (Vavilova et al., 2017).

References

- Anderson T.W., 1971. The Statistical Analysis of Time Series, Wiley, NY - 704p.
- Andronov I. L., Publ. Astron. Inst. Czechoslovak Acad. Sci., 1987, 70, 161, [1987PAICz..70..161A](#)
- Andronov I. L., 1994a, Astronomische Nachrichten, 315, 353, [1994AN....315..353A](#)
- Andronov I.L., 1994b, Odessa Astronomical Publications, 7, 49, [1994OAP....7...49A](#)
- Andronov I.L., 1996, The Proceedings of the 27th Conference on Variable Star Research. November 10-12,1995. Brno, Czech Republic. editor M. Zejda. ISBN 80-85882-05-1, 6, [1996vsr.conf...6A 1994](#)
- Andronov I.L., 1997, A&AS, 125, 207, [1997A&AS..125..207A](#)
- Andronov I.L., 1998, Kinematika Fiz. Nebesn. Tel, 14, No. 6, 490, [1998KFNT...14..490A](#)
- Andronov I.L., 1999, Self-Similar Systems, Dubna, Russia, 29 July – 3 August 1998, eds. V.B.Priezzhev and V.P.Spiridonov, Joint Inst. Nucl. Res., 1999, p. 57-70, [1999sss.conf...57A](#)
- Andronov I.L., 2003, ASPC, 292, 391, [2003ASPC..292..391A](#)
- Andronov I.L., 2005, ASPC, 335, 37, [2005ASPC..335...37A](#)
- Andronov I.L., 2010, Int. Conf. KOLOS-2010 Abstr. Booklet, Snina, Slovakia, 1, <http://www.astrokarpaty.net/kolos2010abstractbook.pdf>
- Andronov I.L., 2012a, Astrophysics, 55, 536, [2012Ap.....55..536A](#)
- Andronov I.L., 2012b, arXiv preprint arXiv:1212.6707; Częstochowski Kalendarz Astronomiczny 2013, ed. Bogdan Wszolek, Vol.VIII, p. 133-138, [2012CKA.....8..133A](#)
- Andronov I.L., et al., 2003, Astron.Astroph.Trans., 22, 793, [2003A&AT...22..793A](#)
- Andronov I.L., et al., 2008a, Central European Journal of Physics, 6, 385, [2008CEJPh...6..385A](#)
- Andronov I.L., et al., 2008b, Astronomy and Astrophysics, 486, 855, [2008A&A...486..855A](#)
- Andronov I.L., et al., 2017, ASPC, 511, 43, [2017ASPC..511...43A](#)
- Andronov I.L., Andrych K.D., 2014, Odessa Astronomical Publications, 27, 38A, [2014OAP....27...38A](#)
- Andronov I.L., Baklanov A.V., 2004, Astronomical School's Report, 5, 264, [2004AstSR...5..264A](#)
- Andronov I.L., Breus V.V., 2013, Astrophysics, 56, 518, [2013Ap.....56..518A](#)
- Andronov I.L., Chinarova L.L., 1997, Kinematika Fiz. Nebesn. Tel, 13, No. 6, 67, [1997KFNT...13f..67A](#)
- Andronov I.L., Chinarova L.L., 2013, arXiv e-print (arXiv:1308.1129); Częstochowski Kalendarz Astronomiczny 2014, ed. Bogdan Wszolek, Vol. X, p. 171-188, <http://adsabs.harvard.edu/abs/2013CKA....10..171A>
- Andronov I.L., Cuypers J., Piquard S., 2000, 2000ASPC..203...64A, [2000ASPC..203...64A](#)
- Andronov I.L., Marsakova V.I., Kudashkina L.S., Chinarova L.L., 2014, AASP, 4, 3, [2014AASP....4...3A](#)
- Andronov I.L., Marsakova V.I., 2006, Astrophysics, 49, 370, [2006Ap.....49..370A](#)
- Andronov I.L., Tkachenko M.G., 2013, Odessa Astronomical Publications, 26, 204, [2013OAP....26..204A](#)
- Andronov I.L., Tkachenko M.G., Chinarova L.L., 2017, Astrophysics, 60, 57, [2017Ap.....60...57A](#)
- Andronov I.L., Shakhovskoj N.M., Kolesnikov S.V., 2003, NATO Science Series II – Mathematics, Physics and Chemistry, 105, 325, [2003whdw.conf..325A](#)
- Andrych K.D., Andronov I.L., 2018, eprint arXiv:1812.06949, [2018arXiv181206949A](#); OEJV, this volume
- Andrych K.D., Andronov I.L., Chinarova L.L., Marsakova V.I., 2015, OAP, 28, 158, [2015OAP....28..158A](#)
- Andrych K.D., Andronov I.L., Chinarova L.L., 2017, OAP, 30, 57, [2017OAP....30...57A](#)
- Brát L., Mikulášek Z., Pejcha O., 2012, http://var2.astro.cz/library/1350745528_ebfit.pdf
- Bopp B.W., Evans D.S., Laing J.D., Deeming, T. J., 1970, MNRAS, 147, 355, [1970MNRAS.147..355B](#)
- Breus V.V., 2003, Odessa Astronomical Publications, 16, 24, [2003OAP....16...24B](#)

- Breus V.V., 2007, Odessa Astronomical Publications, 20, 24, [2003OAP....20...32B](#)
- Chinarova L.L., Andronov I.L., 2000, Odessa Astronomical Publications, 13, 116, [2000OAP....13..116C](#)
- Deeming T. J., 1975, Ap&SS, 36, 137, [1975Ap&SS..36..137D](#)
- Dworetsky M.M. 1983, MNRAS, 203, 917, [1983MNRAS.203..917D](#)
- Foster. G., 1996, Astronomical Journal, 112, 1709, [1996AJ....112.1709F](#)
- Graczyk D., Soszynski I., Poleski R., et al., 2011, Acta Astron., 61, 103, [2011AcA....61..103G](#)
- Juryšek J., Zasche P., Wolf M., Vraštil J., Vokrouhlický D., Skarka M., Liška J., Janík J., Zejda M., Kurfürst P., Pauanzen E., 2018, Astron. & Astrophys., 609, A46, 30 pp., [2018A&A...609A..46J](#)
- Kim Chun-Hwey, Lee Jae Woo, Duck Hyun Kim, Andronov Ivan L. Odessa Astronomical Publications, 2010, 23, 62, [2010OAP....23...62K](#)
- Kudashkina L.S., Andronov I.L., 2017, Odessa Astronomical Publications, 30, 93, [2017OAP....30...93K](#)
- Lafler J., Kinman T.D., 1965, ApJ Suppl., 11, 216, [1965ApJS...11..216L](#)
- Marsakova V.I., Andronov I.L., 1996, OAP, 9, 127, [1996OAP.....9..127M](#)
- Marsakova V.I., Andronov I.L., Chinarova L.L., Chyzyk M.S., Andrych K.D., 2015, Częstochowski Kalendarz Astronomiczny 2016, 269, <http://adsabs.harvard.edu/abs/2015CKA....12..269M>
- Mikulášek Z. 2007, Odessa Astronomical Publications, 20, 138, [2007OAP....20..138M](#)
- Mikulášek Z. 2015, A&A, 584A, 8, [2015A&A...584A...8M](#)
- Mikulášek Z., Žižňovský J., Zverko J., Polosukhina, N.S. 2003, Contributions of the Astronomical Observatory Skalnaté Pleso, 33, 29, [2003CoSka..33..29M](#)
- Mikulášek Z., Wolf M., Zejda M., Pecharová P., 2006, ApSS, 304, 363, [2006Ap&SS.304..363M](#)
- Mikulášek Z., Zejda M., Pribulla T., Vaňko M., Qian S.-B., Zhu L.-Y., 2015, ASPC, 496, 176, [2015ASPC..496..176M](#)
- Papageorgiou A., Kleftogiannis G., Christopoulou P.-E., 2014, Contrib. Astron. Obs. Skalnaté Pleso, 43, 470, [2014CAOSP..43..470P](#)
- Pelt J. Methods for search of variable star periods, 1975, Tartu Astrofüüs. Obs. Teated, Nr. 52, 24 p., [1975TarOT..52....1P](#)
- Renson P., 1978, A&A, 63, 125, [1978A&A....63..125R](#)
- Samus' N.N., Kazarovets E.V., Durlevich O.V., Kireeva N.N., Pastukhova E.N., 2017, ARep, 61, 80, [ARep, 61, 80](#)
- Sutherland P. G., Weisskopf M. C., Kahn S. M. 1978, ApJ, 219, 1029, [1978ApJ...219.1029S](#)
- Savastru S.V., Marsakova V.I., Andrych K.D., Dubovsky P., 2017, OAP, 30, 126, [2017OAP....30..126S](#)
- Tkachenko M.G., Andronov I.L., Chinarova L.L., 2016, JPhSt, 20, 4902, [JPhSt, 20, 4902.](#)
- Tvardovskiy D.E., Marsakova V.I., Andronov I.L., 2017, OAP, 30, 135, [2017OAP....30..135T](#)
- Tvardovskiy D.E., Marsakova V.I., Andronov I.L., Shakun L.S., OAP, 2018, 31, 103, [2018OAP....31..103T](#)
- Vanmunster T., 2018, Peranso software, <http://www.cbabelgium.com/peranso/>
- Vavilova I.B., Yatskiv Ya.S., Pakuliak L.K., Andronov I.L., Andruk V.M., Protsyuk Yu.I., Savanevych V.E., Savchenko D.O., Savchenko V.S., 2017, IAU Symposium, 325, 361, [2017IAUS..325..361V](#)
- Wehlau W., Leung Kam-Ching, 1964, ApJ, 139, 843, [1964ApJ...139..843W](#)

The Informatics in the Doppler Tomography Modeling of the Envelopes of the Close Binaries Systems

V. BAHYL¹, M.GAJTANSKA², P. HANISKO¹, PHAM VAN TINH³

(1) Júlia observatory, Zvolenská Slatina, Slovak Republic, basoft@zv.psg.sk

(2) KFEAM, DF TU vo Zvolene, Masarykova 24, 960 53 Zvolen, Slovak Republic

(3) Fac. of Inform. Technol., Nong Lam Univ. Thu Duc District, Ho Chi Minh City, Vietnam

Abstract: We present our software which is able to realize the Doppler tomography models of the close binaries surroundings. We prove the correctness of our software and we suggest the possibilities and access for the tomographic modeling of the binaries with eccentric orbits and with rather high motion of the line of apsids.

Introduction

The effort to model the components of the close binaries is very old. The same is true for modeling the surroundings of these stars no matter if they are detached, semi-contact or contact. The list of authors which scientifically treated the problems of the dynamics and structures of the close binaries is very long so we allow us to select to mention the works of Z.Kopal (1959), T.B.Horak (1974) and/or J.Hekela (1972). Of course since them a lot of time has passed and new scientists obtained new results, mainly T.M. Richards. We are allowed to build on this work in private our results. Before time we have realized the software which allowed us to study the internal structures of matter by the computer tomography methods.

Very shortly, there is not important if the object under the computer tomography is not in move and the radiation source and detectors are going round the object as there is in the medical computer tomography or if the object is rotating and the detectors are stable. The software access is the same. And the binary system is the case in which the object is rotating and the detectors are nom mowing. In the computer tomography terminology the so called “projection” is the same. This is why there were no problems to transfer our software from technics to the Doppler tomography of the close binaries surroundings at all.

We would like shortly remark that according to our opinion the mathematical principles of the computer tomography or the mathematical principles of the Doppler tomography are widely known and described so we will not waste time and space to describe them. We present only the Figure 1 where there is the computer tomography picture of the circular and rectangular structures. And on the tomograms the circle is a circle and the square is a square.



Figure 1: The sample and its tomographic image.

First attempts

Of course we have not started these days the applications of the computer tomography methods in the astronomy. Already in the year 2004 (In the frame of the A Star Puzzle conference.) we have applied the computer tomography

reconstruction method on the changes of the primary minima of the β Lyrae system. Our results are here on the Figure 2. Left there are the changes in the primary minima structures and right there is the corresponding picture. Of course there is no miracle there but our result is well accepted proof that the application of the computer tomography methods is applicable in the study of the light curves changes and it is able to give us new results or it is able to give us new views on these systems too.

Doppler tomography

We have checked our software on the data of two selected binary systems. There are TT Lincis and U Sagittae systems. The corresponding data we have obtained from Dr. Jan Budaj from the Astronomical Institute of the SAV Skalnaté Pleso. These "line profiles we have inserted as the input data into our software and we have realized the back projections computations. Our results we have compared with the relevant results from the paper Richards et al (2014). The comparative images are given on the Figure 3 for the TT Hydrae system and on the Figure 4 for the U Sagittae system.

From these results we allow us to conclude that our Doppler tomography software is correct and the back projections obtained with this software represents the true distribution of the velocity vectors (fields) in the surrounding of the studied close binaries.

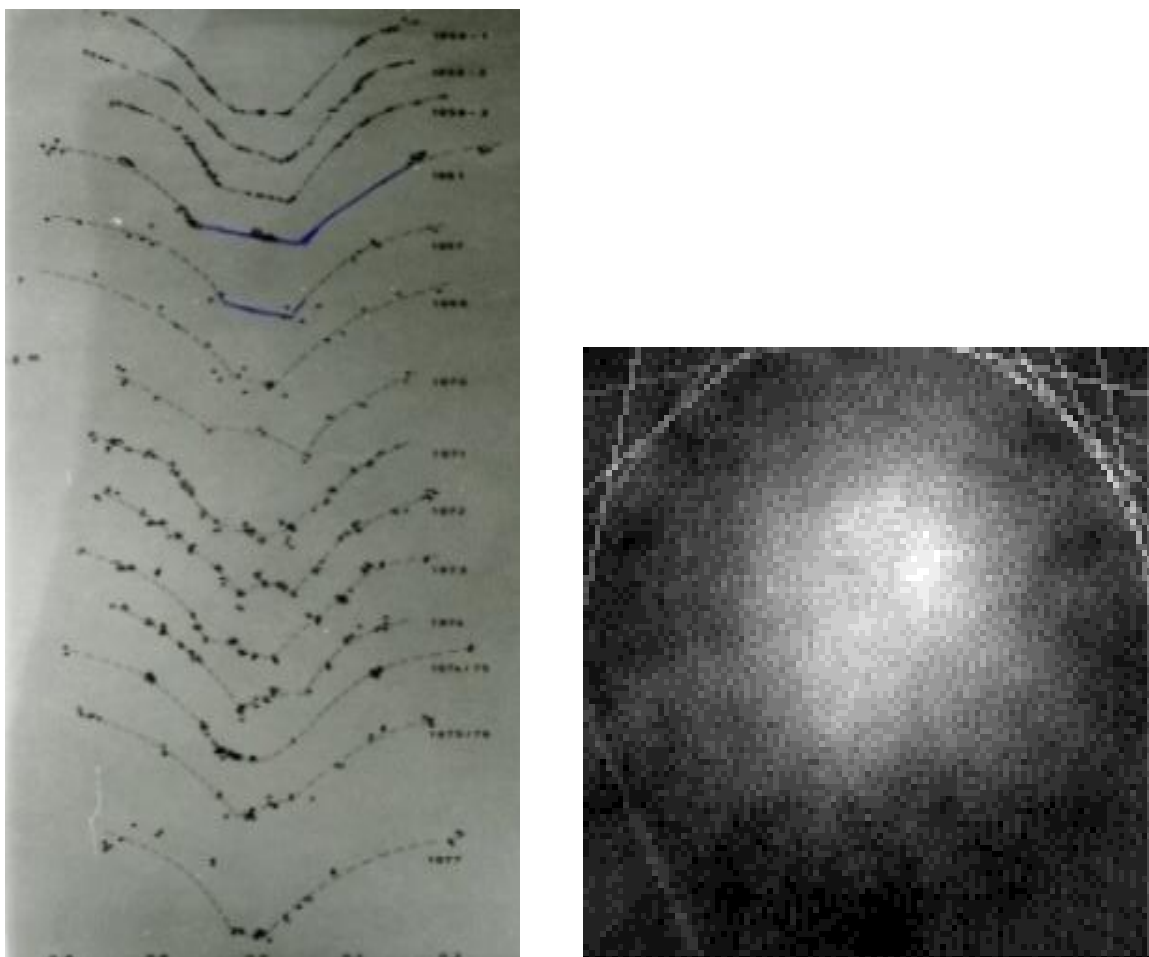


Figure 2: Our Computer tomography attempts with the sets of the β Lyrae minima photometric structures.

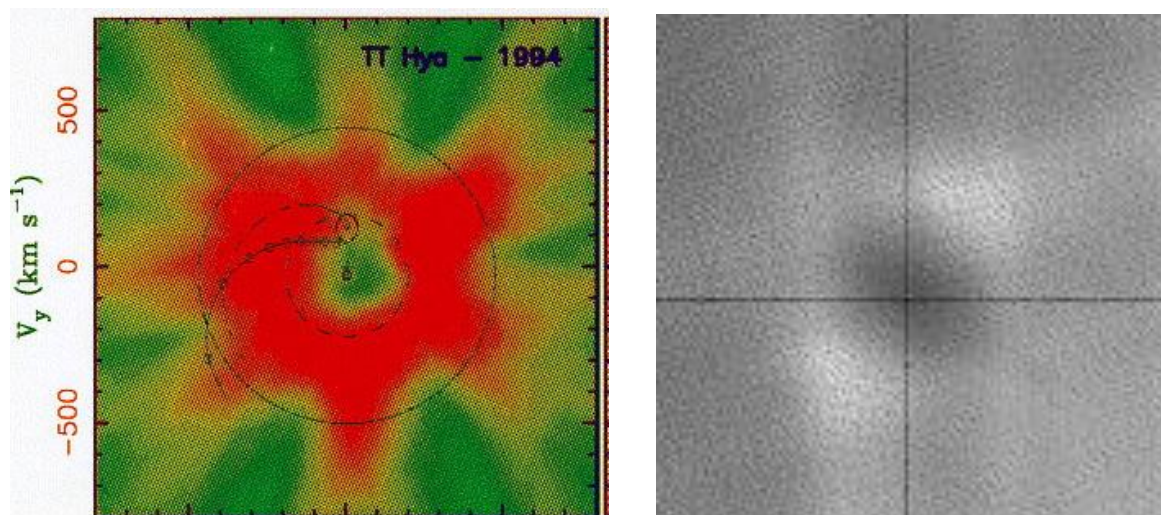


Figure 3: The velocity vectors distribution for the TT Hydrae system. Richards at al (2014) – left; our results – right.

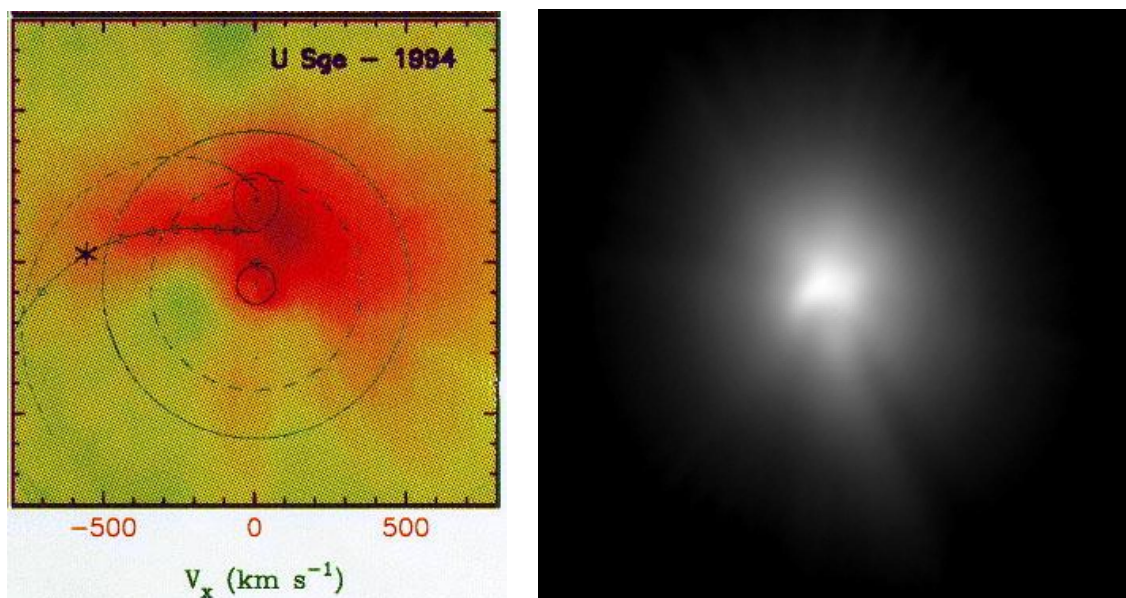


Figure 4: The velocity vectors distribution for the U Sagittae system. Richards at al (2014) – left; our results – right.

The old Latin proverb tells us „Sic duum faecit idem, non est idem“. Of course our pictures are little different from those of Richard et al (2014) but not in the subject. The left and right pictures are different in details only according to our opinion. The differences (on the pictures) go out from the fact that the input data have not been the same (numerically) even if the algorithms are the same. This is, of course, natural.

BM3 models

We have realized the BM3 models of the both systems as we have at our disposal the photometric data for the both systems. The results are very interesting according to our opinion and to some extent they may be the suggestion of the way of research for the future in this branch of science. Our results are given on the next figures. The Figure 5 represents the model of the TT Hydrae system and the Figure 6 represents the model of the U Sagittae system.

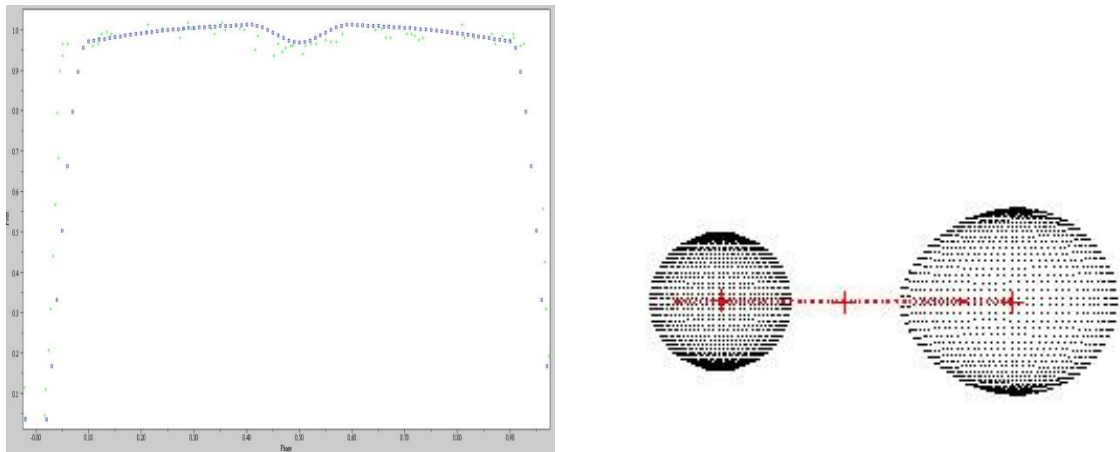


Figure 5: The BM3 model for the photometric data of the TT Hydare system.

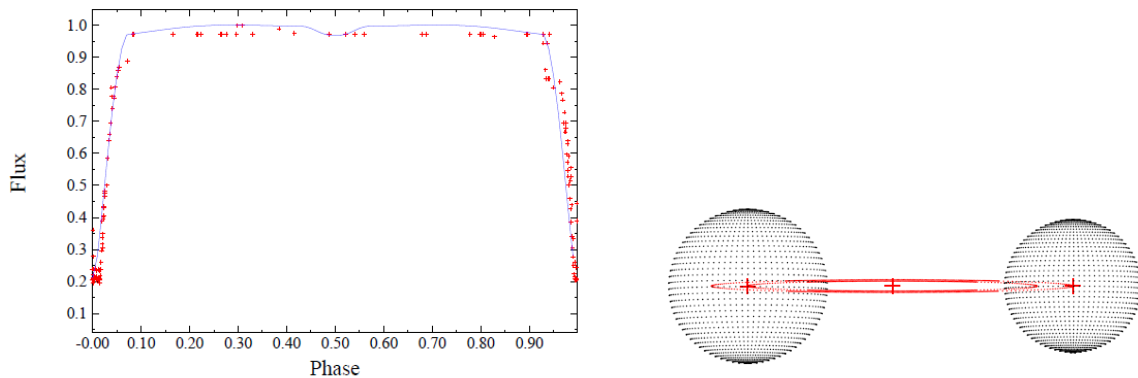


Figure 6: The BM3 model for the photometric data of the U Sagittae system.

We guess that TT Hydrae and U Sagittae are both semi-detached systems according to the data given in the CALEB (Catalog and Atlas of Eclipsing Binaries) which is the integral part of the BM3 system.

Even if the Doppler tomography of the close binaries surrounding and the BM3 modeling of the close binaries are quite different branches of science we allow us to express our opinion that they should be complementary and their results are to be added. And this there is easy to seen from the given above.

Future ideas

Let us have the binary system with the elliptical orbit. See e.g. the Figure 7 where there is binary system with the elliptical orbit. Of course the period is many years and such a systems are not suite to be studied with us in this moment. But there are many systems with the elliptical orbits in which the rotation of the apsidal line is expressed in the years. Such a system is e.g. SMC-ECL-1634 (Kyeongsoo Hong et al. 2016).

These systems is according to our opinion worth to study with the methods of the computer tomography.

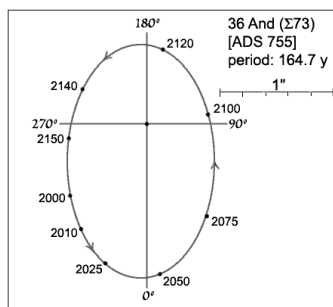


Figure 7: The binaries (Not close of course) with an elliptical orbit.

Having this idea we realized the model of such a system and we have found that the secondary minimum should move itself on the light curve in agreement with the position of the line of apsids. So having the light curves which well cover the half the period of the apsid line we can quietly realize the computer tomography model of such kind a close binary system. Our preliminary and theoretical results are given on the final Figure 8.

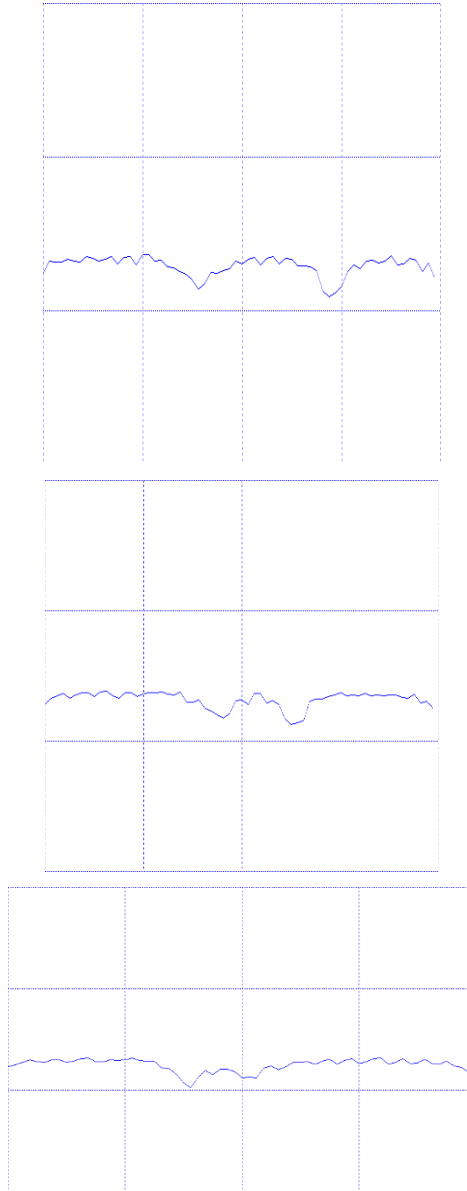


Figure 8: The theoretical light curve models for the close binaries with eccentric orbit.

And back projecting of these theoretical light curves there is possible to obtain e.g. model given on the Figure 9.

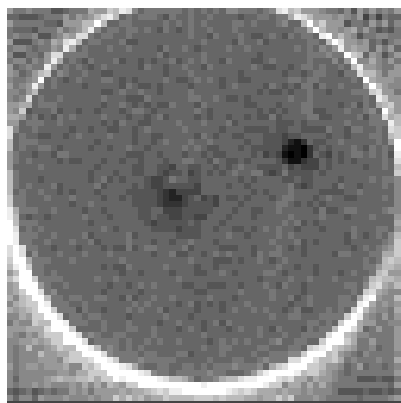


Figure 9: The theoretical model for the eclipsing binaries with high eccentricity and with high movement of the apsid line.

Conclusion

We have succeeded in our work that we have fully working software for the Doppler tomography and that there is possible to model the close binaries components by the method of the computer tomography under special conditions, specifically if the eccentricity of the orbit is high and the apsid line rotates quickly.

In future we would like to obtain the relevant and real astronomical data and to apply our software to them.

Acknowledgement

We would like to express our thanks to the Slovak Union of Astronomers for the obtained support. And we express our thanks also to prof. Ilian K. Iliev Rozhen National Observatory for kindly giving the spectral data of the U Sagittae system at the disposal to us.

References

- Budaj, Ján; Richards, Mercedes T.; Miller, Brendan, A Study of Synthetic and Observed H α Spectra of TT Hydrae, 2005, [ApJ...623..411B](#).
- Brandstreet, D. H., 2017, **BM3**, Eastern University, PA, www.euastronomy.com
- Grygar, J., Horák, T. B., 1974, BV Observations of W UMa Type Binaries CK Boo, BI CVn and AH Vir, BACSI **25**, 275.
- Hekela, J., 1972, Spatial Spectroscopic Diagnostic of Planetary Nebulae. I. Formation of Synthetic Problem for Optically Thin Lines. BACSI, **23**, 197., [1972BAICz..23..197H](#)
- Kopal, Z., 1969, Dynamics of Close Binary Systems, Springer Verlag.
- Kyeongsoo Hong et al., 2016, Apsidal motion of 90 eccentric binary systems in the Small Magellanic Cloud., Mon. Not. R. Astron. Soc., [2016MNRAS.460..650H](#)
- Miller, Brendan; Budaj, Ján; Richards, Mercedes; Koubský, Pavel; Peters, Geraldine J., Revealing the Nature of Algol Disks through Optical and UV Spectroscopy, Synthetic Spectra, and Tomography of TT Hydrae., [2007ApJ...656.1075M](#).
- Motl, D., 2010, MuniWin V2.0.10, <http://c-munipack.sourceforge.net>
- Plavec M., 1966, Period Changes of Eclipsing Binaries I. Astron. Soc. Of the Pacific, Leaflet No. 440, 321p., [1966ASPL....9..321P](#)
- Richards, T. M. et al. 2014, Images of Gravitational and Magnetic Phenomena Derived from Two-dimensional Back-projection Doppler Tomography of Interacting Binary Stars. ApJ, 795, 160 (18pp), [2014ApJ...795..160R](#)
- Scientific Image Processing System (SIPS), 2016, Moravské Přístroje a.s. V3.3 32 bit (x86)
- StatSoft, Inc, 2011, STATISTICA (data analysis software system), V10, www.statsoft.com
- Známé zákrytové dvojhvězdy, 2018, ČAS, http://var2.astro.cz/brno/eclipsing_binaries.php

Modeling variability of Be stars

P. KURFÜRST^{1,2} & J. KRČIČKA¹

- (1) Department of Theoretical Physics and Astrophysics, Masaryk University, Kotlářská 2, 611 37 Brno, Czech Republic, petrk@physics.muni.cz
 (2) Institute of Theoretical Physics, Charles University, V Holešovičkách 2, 180 00 Praha 8, Czech Republic,
 (4) petr.kurfurst@utf.mff.cuni.cz

Abstract: Be stars are rapidly rotating non-supergiant B-type stars surrounded by equatorial Keplerian disks. The characteristic property of all Be stars is their multiperiodic variability driven for example by pulsations in isolated Be stars or by the effects of binarity. We assume in our models the equatorial decretion disk that stems from the angular momentum loss needed to keep the central object at or below the critical rotation. Using our hydrodynamic code, we calculate the 2D profile of Be stars' disk structure under various physical and geometrical configurations of the star-disk system as well as various profiles of the circumstellar medium. The tidal interactions in binary systems facilitate the matter ejection from the equatorial region of the star, and there is also evidence of warping of the disk in binaries. The important subclass is the Be/X-ray binaries, consisting of a Be star and mostly a neutron star (NS), which belong to the brightest objects in the X-ray sky. Intensive matter accretion from the optical donor companion onto the compact object in a relatively close binary system produces transient phases of the high energy X-ray emission which dramatically vary in brightness and whose timescales may range from milliseconds to years. We calculate the effects of X-ray irradiation on the temperature structure of the Be stars' disk. Using the Bondi-Hoyle-Littleton approximation, we estimate the NS accretion rate and the excess of X-ray luminosity during various phases of NS-disk interaction.

Introduction

Be stars are “non-supergiant B-type (late O - early A) stars with Balmer spectral lines in emission.” The typical representatives are γ Cas, α Eri (Achernar), β Cmi, X Oph, ζ Tau, 28 Cma, etc. Be stars are the fastest rotators among all other (nondegenerate) types of stars on average, their equatorial rotation rate is closest to its critical limit (e.g., Rivinius et al. 2013). The mechanism that brings these stars so close to the critical rotation rate is uncertain. It is believed that the evolution of stellar angular momentum distribution results from the effects of convective motion, meridional circulation, etc. (Maeder & Meynet 2000).

We identify two-component circumstellar envelopes of Be stars: fast polar wind + equatorial (nearly) Keplerian disk. Although the exact mechanism of disk creation is still unknown (probably non-radial pulsations, Rivinius et al. 2013), the viscosity is then responsible for the further outward transportation of the angular momentum and thus for the disk building and broadening (Lee et al. 1991). We regard the viscous decretion disks (VDD) as the typical examples of the equatorial stellar decretion disks with the Keplerian rotation velocity.

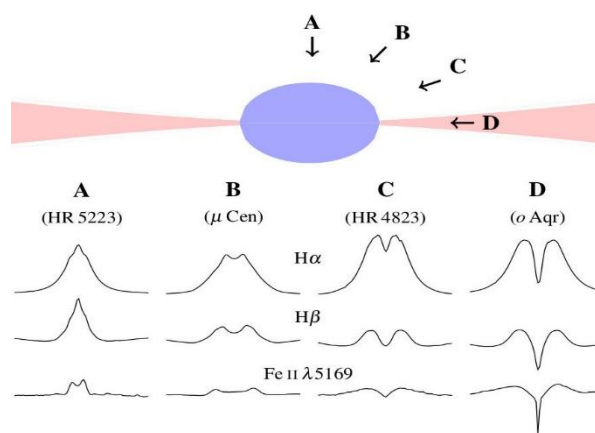


Figure 1: Schematic spectra of various Be stars according to the line-of-sight orientation ordered from pole-on to the equator-on line-of-sight directions (A - D). The Be star o Aqr is a shell star (Hanuschik 1996). The upper part shows the equator-on scheme of critically rotating Be star with a flared disk. Adapted from Rivinius et al. (2013).

These are stellar pulsations that likely drive the multiperiodic variability of Be stars, besides other variabilities on basically all timescales. Only the variability of the early spectral subtypes is large enough to be observed from the ground, the late types pulsate as well but with smaller amplitudes (e.g., Saio et al. 2007). We divide the Be stars variability into numerous classes, according to different mechanisms that excite the pulsation modes.

The binarity strongly affects the physics of Be stars' disks. One estimates the fraction of Be stars binary (or multiple) systems to be 30 - 35% (Porter & Rivinius 2003). In "closer" systems (with the orbital period a year or less) the tidal interactions help to eject the matter from the equatorial region of Be star and feed the disk. The spin-up of Be stars can also be strongly affected by binary interactions (Harmanec et al. 2002). The binarity causes the disk truncation at the radius where the tidal torque balances the viscous torque (Okazaki et al. 2002). The accretion of the disk material onto the compact companion (mostly a neutron star (NS)) in the Be/X-ray binaries produces the intense X-ray emission (Reig 2011).

Dynamics of Be disks around single Be stars

The viscosity is the fundamental factor in building the disk since it causes the mass and angular momentum outward transport throughout the Keplerian disk. However, the decretion disks are never steady; the positive viscous torque causes the growth of the disk while the negative or no torque causes the disk decay.

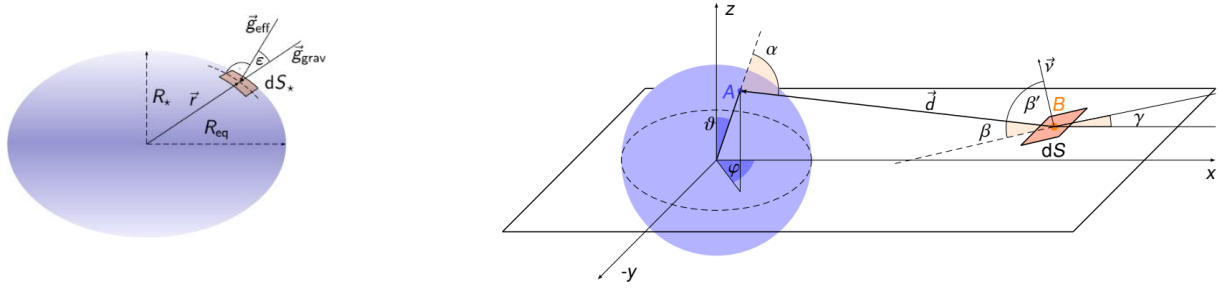


Figure 2: *Left panel* - Schema of the rotationally oblate star with polar radius R_* , equatorial radius R_{eq} , and stellar surface element dS_* whose position vector is \vec{r} . Vector \vec{g}_{eff} of the effective gravity (see Eq. 2) is normal to the stellar surface element dS_* . *Right panel* - Geometry of the irradiation of the disk by the central star. The disk "surface" element dS (with the central point B) is impinged by the stellar irradiation along the line-of-sight vector \vec{d} from the stellar surface element dS_* (with the central point A). The angle α denotes the deviation between vectors \vec{r} and \vec{d} , the angle β is the deviation of the inclination of the surface element dS and the vector \vec{d} (the angle β is defined as the complementary angle to the deviation angle β' of the the line-of-sight vector \vec{d} and the normal vector \vec{v} of the surface element dS). The angle γ denotes the inclination of the surface element dS from the xy plane (Kurfürst et al. 2018, the idea is adapted from Smak (1989)).

The Be decretion disks are in an approximate thermal balance with irradiation from a central star. We can represent the irradiative flux that impinges the disk "surface" by the following relations: regarding the rotationally oblate star (see left panel of Fig. 2), we write the von Zeipel theorem that describes the latitudinally dependent stellar radiation \vec{F}_* that emerges from each point on the star's surface (von Zeipel 1924) as

$$\vec{F}_*(\Omega, \vartheta) = -\frac{L_*}{4\pi GM_* \left(1 - \frac{\Omega^2}{2\pi G \langle \rho \rangle}\right)} \vec{g}_{eff}(\Omega, \vartheta), \quad (1)$$

where Ω is the angular velocity of the stellar rotation, ϑ is the colatitude of the surface point, L_* is the stellar luminosity, M_* is the total mass of the star, G is gravitational constant, $\langle \rho \rangle$ is the mean stellar density. Assuming most of the mass of the star is concentrated to its center (Roche model), the effective gravity

$$\vec{g}_{eff} = \left(-\frac{GM_*}{r^2} + \Omega^2 r \sin^2 \vartheta, \Omega^2 r \sin \vartheta \cos \vartheta, 0\right), \quad (2)$$

in the spherical coordinate directions r, ϑ, ϕ . The right panel of Fig. 2 illustrates the geometry of the disk irradiation by the central star. The irradiative flux that impinges each point B in the disk (Smak 1989) is

$$F_{irr} = \frac{F_*}{\pi} \iint_{\vartheta, \phi} R_*^2 \sin \vartheta \frac{[1-u(1-\mu)]\mu \sin \beta}{(1-u/3)d^2} d\vartheta d\phi, \quad (3)$$

where $\mu = \cos \alpha$, d is the magnitude of the vector \vec{d} , and u is the coefficient of the limb darkening. The "linear limb darkening law" then takes the form $I = I_0(1 - u + u\mu)$, where I is the specific intensity of radiation and $I_0 = F_*/\pi$ (e.g., Heyrovský 2007).

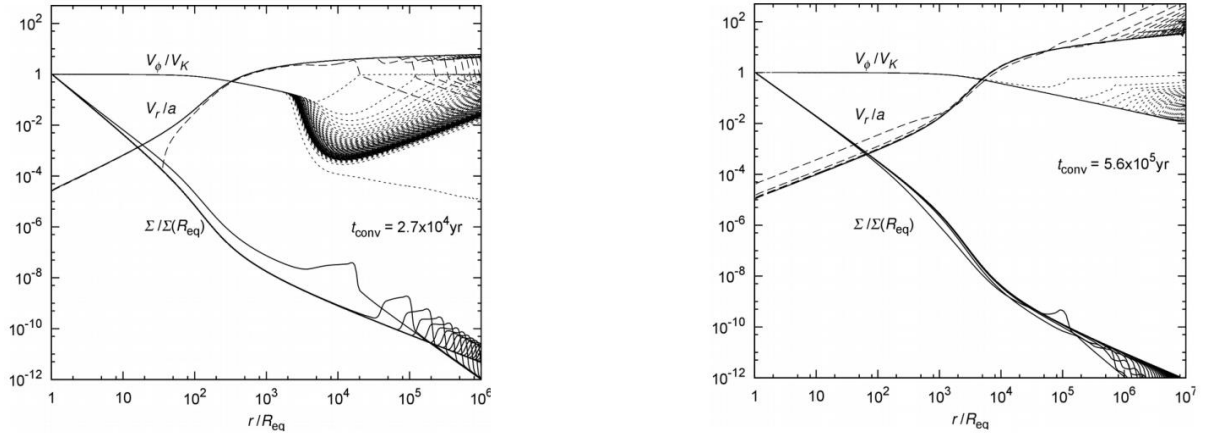


Figure 3: *Left panel* - The composite graph of time snapshots of surface density, radial, and azimuthal velocity demonstrates the propagation of the transforming wave in the dynamical timescale t_{dyn} and the final converged profiles of the surface (column) density Σ , radial velocity V_r (scaled to the speed of sound a), and azimuthal velocity V_ϕ (scaled to the Keplerian velocity V_K), of the isothermal model of B0-type (with parameters described in the text) star's disk with constant viscosity parameter α . The first wave at the distance (roughly) $10^4 r/R_{\text{eq}}$ represents $t_{\text{dyn}} \approx 65$ yrs. The time t_{conv} denoted in the graph, is the minimum time needed for the model to converge into the final stationary state. *Right panel* - Similar model with radially decreasing viscosity ($\alpha \sim r^{-0.2}$) and decreasing temperature ($T \sim r^{-0.4}$). The first wave at the distance $10^5 r/R_{\text{eq}}$ represents $t_{\text{dyn}} \approx 3800$ yrs. Adapted from Kurfürst (2015).

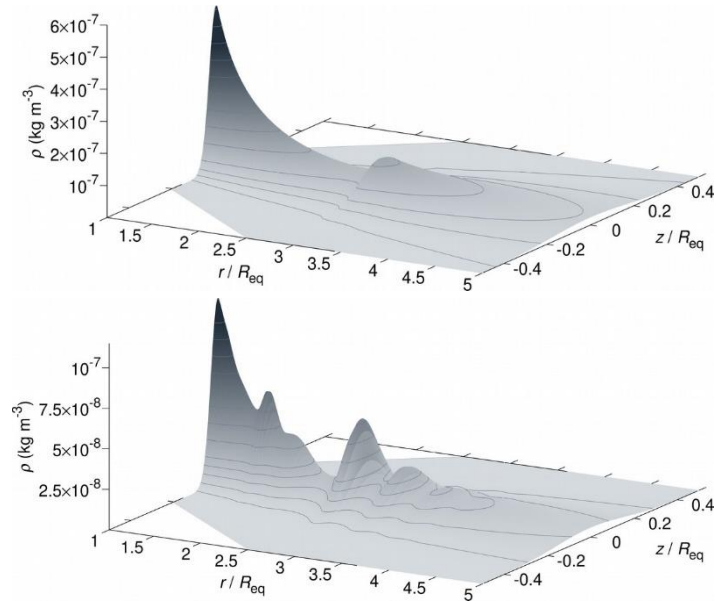


Figure 4: *Upper panel* - 2D density graph of a self-consistently calculated circumstellar disk of a critically rotating B0-type star with the same parameters as for the 1D model. The disk mass-loss rate $\dot{M} = 10^{-8} M_\odot \text{yr}^{-1}$, the viscosity parameter $\alpha = 0.1$ is constant. The sonic point radius $r_s \approx 2.5 \times 10^4 R_{\text{eq}}$. Contours mark the densities $2.5 \times 10^{-8}, 5 \times 10^{-8}, 10^{-7}, 1.5 \times 10^{-7}, 2 \times 10^{-7}$ (in SI units), etc. *Lower panel* - Corresponding graph with the constant viscosity coefficient $\alpha = 1$. The density profile in the $\alpha \gtrsim 0.5$ models roughly periodically oscillates. The contours mark the densities $2.5 \times 10^{-8}, 5 \times 10^{-8}, 7.5 \times 10^{-8}, 10^{-7}$, etc. Adapted from Kurfürst et al. (2018).

We show the particular results of our time-dependent 1D calculations (see Fig. 3) of the fundamental quantities Σ (density), V_r (radial velocity), and V_ϕ (azimuthal velocity) that determine the decretion disk hydrodynamic behaviour (Kurfürst et al. 2014) at least to the sonic point distance where V_r equals the speed of sound a . We calculate the models either for isothermal disks with constant viscosity parameter α (Shakura & Sunyaev 1973) or for the cases where one or both of these parameters vary with the distance. We also recognize in the models the

wave that converges the initial state to the final stationary state. Figure 3 represents two 1D models of a classical Be star's disk, $M_{\star} = 14.5M_{\odot}$, $R_{\star} = 5.8R_{\odot}$, $T_{\text{eff}} = 25000\text{K}$ (Harmanec 1988), with the two different modes of initial temperature and viscosity profiles.

We also performed the self-consistent (density+velocity vs. temperature) time-dependent 2D calculations of a disk structure up to 100 stellar radii in the R - z plane of a unique cylindrical - conical computational grid (see Fig. 4). We assumed the vertical hydrostatic and radiative equilibrium and calculated the irradiative flux taking into account the limb darkening as well as the stellar equatorial darkening that results from its rotational oblateness (Kurfürst et al. 2018). We calculate the thermal disk structure using the flux diffusion approximation (see, e.g., Mihalas 1978) and taking into account the radiative loss of energy in the optically thin approximation (e.g., Rosner et al. 1978). Figure 4 shows two 2D models of the density structure up to $5R_{\text{eq}}$ for two different parameters of an initial state.

The 1D dynamic simulations (e.g., Haubois et al. 2013) of the disk growth and dissipation confirm the approximate validity of the analytical formula (cf. Pringle 1981)

$$\frac{\partial \Sigma}{\partial t} = \frac{1}{r} \frac{\partial}{\partial r} \left[\frac{\partial}{\partial r} (r^2 \alpha a^2 \Sigma) \right]. \quad (4)$$

They show the time-evolution of the surface density of a newly formed disk with a constant rate of mass supply for more than 50 years. The steady-state solution $\Sigma \sim r^{-2}$ (Okazaki 2001) is shown as the temporally asymptotic limit; this implies that the disks are never steady except at the time $t \rightarrow \infty$. Moreover, the disk surface density grows with time but with entirely different rates according to the distance from the star. In the simplified model when a disk is supplied with the material at a constant rate, the viscosity parameter α scales the disk growth and dissipation time up and down. According to Eq. (4), changes of the α parameter lead to different scaling of the time at least in case of the constant ratio between the azimuthal speed and the sound speed. Therefore, the higher the α , the faster the growth of the disk. For instance, a disk with $\alpha = 1$ will evolve ten-times faster than a disk with $\alpha = 0.1$ (Haubois et al. 2013).

These theoretical predictions are supported for example by the retroactive compilation of V-band photometric observations of ω (28) Cma, by Ghoreyshi et al. (2018). Older data were of poor quality, the study thus involves the measurements only since the year 1982. Since that time, ω Cma exhibited four quasi-regular cycles with lengths varying between 7.0 to 10.5 years. Each cycle includes two main sub-epoches: an outburst phase characterized by a brightening of 0.3 mag to 0.5 mag during about 2.5 - 4.0 years (corresponding to the disk growth phase) and a quiescence phase that lasts about 4.5 - 6.5 years (corresponding to the disk partial dissipation). Comparing the observational features to a theoretical model, the authors conclude that the VDD model is fully capable of reproducing the variability of the disk. Different values of α (typically higher) are required during the disk growth phase than during the dissipation ($\alpha = 1$ vs. $\alpha = 0.1$). A similar trend was also found for a sample of Be stars in the Small Magellanic Cloud by Rímulo et al. (2018).

Dynamics of Be disks around binary Be stars

We mainly focus to Be/X-ray binaries which are the largest sub-class of high mass X-ray binaries (more than 2/3 of the identified systems). A Be/X-ray binary system usually consists of a Be star + NS while the X-ray emission comes from accretion onto NS (Reig 2011). The orbits are usually eccentric ($e \leq 0.9$) with periods $12\text{d} < P_{\text{orb}} < 300\text{d}$. Most Be/X-ray binary systems show only a transient activity. We identify the following schematic types of X-ray activity (Negueruela 1998):

- 1) low-luminosity with persistent X-ray emission where the X-ray luminosity $L_X \leq 10^{27}\text{W}$,
- 2) periodical (type I) outbursts with $L_X \approx 10^{28}\text{-}10^{30}\text{W}$, and
- 3) giant (type II) outbursts with $L_X \geq 10^{30}\text{W}$.

For example, the observations of X-ray source 2S 1417-62 (Bildsten et al. 1997) show the type II outburst where the X-ray flux increases 10-times during 20 days and then decreases during about 90 days back to the original value. This is succeeded by the sequence of quasi-periodic type I outbursts with average periods of about 50 days. The maxima of the type I outbursts are approximately 3-times lower than that of the type II outburst. It is believed that type I outbursts occur during the periastron passage of the NS.

The binarity also causes a truncation of the disk. In systems with low eccentricity is expected the disk truncation at 3:1 resonance radius (Okazaki & Negueruela 2001), that is, $r_{\text{trunc}}/r_{\text{orb}} \approx 0.48$, where r_{trunc} is the disk truncation radius and r_{orb} is the radius of the NS orbit. The truncation radius decreases with increasing eccentricity; the

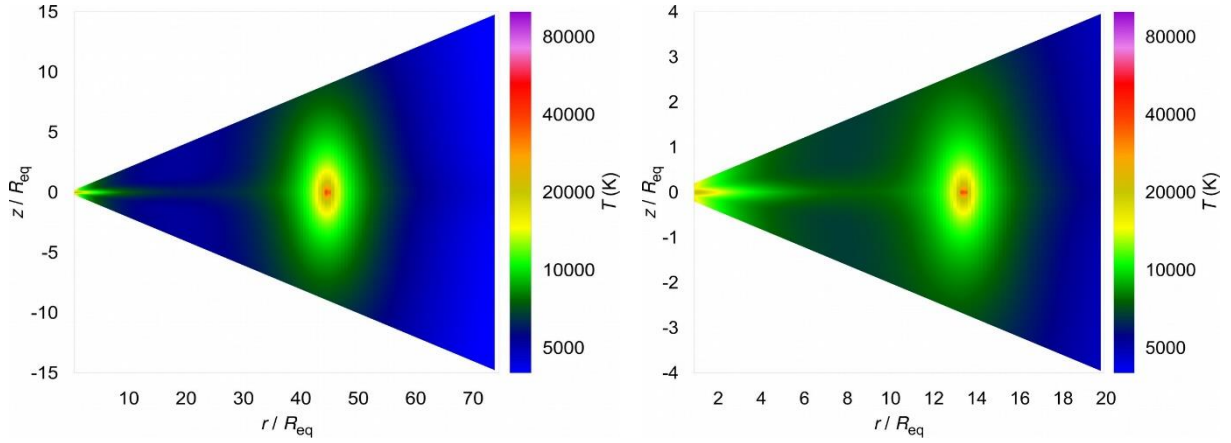


Figure 5: *Left panel* - 2D temperature structure of Be/X-ray binary GRO J1008-57. The main sequence star is of spectral type B0eV with $T_{\text{eff}} \approx 32\,000$ K. The other parameters are: $L_X \approx 3 \times 10^{30}$ W, $\dot{M} = 2.85 \times 10^{-9} M_{\odot} \text{yr}^{-1}$, $D \approx 390 R_{\odot} \approx 45 R_{\text{eq}}$, $r_{\text{acc}}/H \sim 10^4$, $T_X \geq 51\,000$ K. *Right panel* - 2D temperature structure of Be/X-ray binary HD215770. The main sequence star is of spectral type O9.7IIIe with $T_{\text{eff}} \approx 22\,500$ K. The other parameters are: $L_X \approx 6.5 \times 10^{29}$ W, $\dot{M} = 6 \times 10^{-10} M_{\odot} \text{yr}^{-1}$, $D \approx 260 R_{\odot} \approx 13.5 R_{\text{eq}}$, $r_{\text{acc}}/H \sim 10^4$, $T_X \geq 60\,000$ K.

reason is that the disk radius has to be smaller than the periastron distance. Resonant truncation works for Be disks in misaligned systems (in the systems where the orbital plane is inclined from the disk plane) as well.

We model the hydrodynamic situation of co-rotating aligned Be/X-ray binary systems with low eccentricity. The binary separation D thus constraints the outer disk radius as the disk truncation radius r_{trunc} . We use the Bondi-Hoyle-Littleton (BHL) approximation where NS accretes within the range of accretion radius (cf. Krtička et al. 2015)

$$r_{\text{acc}} = \frac{2GM_X}{V_{\text{rel}}^2},$$

where M_X is the mass of NS and $V_{\text{rel}}^2 = V_r^2 + V_{\phi}^2$. If the accretion radius $r_{\text{acc}} > H$ (where the disk vertical scale-height $H = a/\Omega$, that is, the ratio of the sound speed and the local disk angular velocity), NS accretes all the disk material within r_{acc} . The X-ray luminosity in this case is

$$L_X = \frac{GM_X \dot{M}}{R_X},$$

where \dot{M} is the accretion rate and R_X is the NS radius.

Using the above principles, we calculated the density and temperature structure of the sample of Be/X-ray binaries with $r_{\text{acc}} > H$ and $\dot{M} \sim 10^{-9} - 10^{-13} M_{\odot} \text{yr}^{-1}$, listed in the following Table (see Krtička et al. 2015):

Binary	Spectral Type	$T_{\text{eff}} [10^3 \text{K}]$	$R_{\star} [R_{\odot}]$	$D [R_{\odot}]$	$L_X [\text{W}]$
V831 Cas	B1V	24	4.5	480	2×10^{28}
IGR J16393-4643	BV	24	4.5	18.8	4×10^{28}
V615 Cas	B0Ve	26	4.9	43	5×10^{28}
HD 259440	B0Vpe	30	5.8	510	1.2×10^{26}
HD 215770	O9.7IIIe	28	12.8	260	6.5×10^{29}
CPD-632495	B2Ve	34	7.0	177	3.5×10^{27}
GRO J1008-57	B0eV	30	5.8	390	3×10^{30}

We show two examples of our models in Fig. 5 that illustrates the 2D temperature profile of the disk in radial-vertical plane, in the direction of aligned co-rotating NS. For the self-consistent density vs. temperature calculation, we took into account the NS gravity and X-ray heating of the ambient disk gas. We denote T_X the maximum disk gas temperature in the proximity of NS.

Conclusions

Be disks around single stars exhibit a long term photometric variability due to the disk growth and decay whose amplitude may reach up to 1 magnitude. The presence of a companion adds interesting complexities on the dynamics of Be decretion disks and their host systems. In the binary systems with low eccentricity the disk truncation begins approximately at 3:1 resonance radius while in more eccentric systems the truncation radius even decreases (Okazaki & Negueruela 2001). In Be/X-ray binaries also the accretion rate increases with eccentricity. Highly eccentric coplanar systems are believed to be the producers of Type I X-ray outbursts that occur during the periastron passage of the compact companion. The Mechanism(s) for Type II outbursts are uncertain; they are still one of the unresolved mysteries of Be stars study (Okazaki et al. 2013).

Acknowledgement

The access to computing facilities owned by 225 the National Grid Infrastructure MetaCentrum, provided under "Projects of Large Infrastructure for Research, Development, and Innovations" (LM2010005) is appreciated. This work was supported by grant GAČR 18-05665S and by the grant Primus/SCI/17.

References

- Bildsten L., Chakrabarty D., Chiu J., Finger M. H., Koh D. T., Nelson R. W., Prince T. A., Rubin B. C., Scott D. M.; Stollberg M., and 3 coauthors, 1997, *ApJS*, 113, 367, [1997ApJS..113..367B](#)
- Ghoreyshi M. R., Carciofi A. C., Rímulo L. R., Vieira R. G., Faes D. M., Baade D., Bjorkman J. E., Otero S., & Rivinius Th., 2018, *MNRAS*, 479, 2214, [2018MNRAS.479.2214G](#)
- Hanuschik R. W., 1996, *A&A*, 308, 170, [1996A&A...308..170H](#)
- Harmanec P., 1988, *BAICz*, 39, 329, [1988BAICz..39..329H](#)
- Harmanec P., Bisikalo D. V., Boyarchuk A. A., et al., 2002, *A&A*, 396, 937, [2002A&A...396..937H](#)
- Haubois X., Carciofi A. C., Rivinius Th., Okazaki A. T., & Bjorkman J. E., 2012, *ApJ*, 756, 156, [2012ApJ...756..156H](#)
- Heyrovský D., 2007, *ApJ*, 656, 483, [2007ApJ...656..483H](#)
- Krtička J., Kurfürst P., & Krtičková I., 2015, *A&A*, 573, 20, [2015A&A...573A..20K](#)
- Kurfürst P., Feldmeier A., Krtička J., 2014, *A&A*, 569, 23, [2014A&A...569A..23K](#)
- Kurfürst P., 2015, PhD thesis, Masaryk University, Brno, Czech Republic
- Kurfürst P., Feldmeier A., Krtička J., 2018, *A&A*, 613, 75, [2018A&A...613A..75K](#)
- Lee U., Saio H., & Osaki Y., 1991, *MNRAS*, 250, 432, [1991MNRAS.250..432L](#)
- Maeder A. & Meynet G., 2000, *ARA&A*, 38, 143, [2000ARA&A...38..143M](#)
- Mihalas D., 1978, *Stellar atmospheres /2nd edition/* (San Francisco: W. H. Freeman and Co., 1978), [1978stat.book.....M](#)
- Negueruela I., 1998, *A&A*, 338, 505, [1998A&A...338..505N](#)
- Okazaki A. T., 2001, *PASJ*, 53, 119, [2001PASJ...53..119O](#)
- Okazaki A. T. & Negueruela I., 2001, *A&A*, 377, 161, [2001A&A...377..161O](#)
- Okazaki A. T., Bate M. R., Ogilvie G. I., et al., 2002, *MNRAS*, 337, 967, [2002MNRAS.337..967O](#)
- Okazaki A. T., Hayasaki K., & Moritani Y., 2013, *PASJ*, 65, 41, [2013PASJ...65...41O](#)
- Porter J. M. & Rivinius T., 2003, *PASP*, 115, 1153, [2003PASP..115.1153P](#)
- Pringle J. E., 1981, *ARA&A*, 19, 137, [1981ARA&A..19..137P](#)

Reig P., 2011, Ap&SS, 332, 1, [2011Ap&SS.332....1R](#)

Rímulo L. R., Carciofi A. C., Vieira R. G., Rivinius Th., Faes D. M., Figueiredo A. L., Bjorkman J. E., Georgy C., Ghoreyshi M. R., & Soszyński I., 2018, MNRAS, 476, 3555, [2018MNRAS.476.3555R](#)

Rosner R., Tucker W. H., & Vaiana G. S., 1978, ApJ, 220, 643, [1978ApJ...220..643R](#)

Rivinius T., Carciofi A. C., & Martayan C., 2013, A&ARv, 21, 69, [2013A&ARv..21...69R](#)

Saio H., Cameron C., Kuschnig R., et al., 2007, ApJ, 654, 544, [2007ApJ...654..544S](#)

Shakura N. I., & Sunyaev R. A. 1973, A&A, 24, 337, [1973A&A....24..337S](#)

Smak J., 1989, Acta Astronomica, 39, 201, [1989AcA....39..201S](#)

von Zeipel H., 1924, MNRAS, 84, 665, [1924MNRAS..84..665V](#)

Using neural networks in searching for variable stars

P. CAGAŠ^{1,2}

- (1) BSObservatory, Modrá 587, 760 01 Zlín, Czech Republic, pc@bsobservatory.org
- (2) Variable Star and Exoplanet Section of the Czech Astronomical Society, Vsetínská 941/78, CZ-757 01 Valašské Meziříčí, Czech Republic

Abstract: Neural networks recently prove to be a very powerful tool in the field of machine learning and artificial intelligence. Neural networks operation principle is non-algorithmic and thus can be used for some tasks better suited for a human's mind rather than traditional computer algorithms. One such task is a recognition of stars within astronomical images. However, an algorithmic recognition already reached a very good quality and requires significantly less computational resources and, therefore, the motivation to replace algorithms with neural networks is low in this case. Possibly more interesting application is a recognition of variable stars in a set of time-based light curves of all stars within a field of view, for which neural networks provide better results compared to algorithm-based methods. At the same time, computational time of the neural network detection is comparable to the algorithm-based ones.

Introduction

Neural networks now often surpass humans in tasks which were traditionally considered to be solvable only by human intellect (e.g., the board game “Go”). Even though the first experiments with artificial neurons and neural networks closely followed the invention of practically usable computers, enormous demand for computational resources and a necessity to “manually” configure network parameters by human programmers prohibited the usage of neural networks in real applications.

The first step to the current boom of neural networks was the introduction of the backpropagation algorithm for automatic learning (determining of network parameters) from learning data set (Werbos 1975).

Still, achieving convincing results demanded a development of computational devices capable of handling a very large amount of calculations performed during neural network learning and inferring. Such devices proved to be graphical cards (GPU – Graphics Processing Unit), which evolved from simple rasterization accelerators to generally programmable vector processors, equipped with hundreds or even thousands floating point calculation units (Krizhevsky et al., 2012). With a rapid increase of neural network-based applications, more specialized hardware is introduced into commonly used computers – CPUs (Central Processing Units) are enhanced with wider vector instructions and new neural network optimized data types, GPUs are equipped with tensor processors and even specialized neural network handling co-processors are introduced.

Principles of neural networks are described in many widely available publications (e.g., Nielsen 2015) and their description is beyond the scope of this article.

Recognizing stars in astronomical images

Finding stars in astronomical images seems easy for humans and virtually everybody is capable to mark stars even without any previous experience or special training. With some experience, humans can recognize stars with very high fidelity and distinguish them from non-star objects, for instance, background galaxies or various artifacts (traces of particles passing through the silicone detector, etc.). This makes the star recognition a good candidate for a neural network application.

Experimental neural network for star recognition is implemented as a part of the Astrometry tool of the SIPS (Scientific Image Processing System) software package (Cagaš 2017).

Simple 3-layer neural network is organized as follows:

- First (input) layer of 961 neurons represents a matrix of 31×31 pixels.
- Second layer consists of 240 neurons.
- Third (output) layer contains only one output neuron. Its value in the range 0.0 to 1.0 represents the probability a star is contained within the input subframe.

Input neurons are fed with pixels of the particular image sub-frame. While image pixels are typically in the integer range 0 to 65535 (astronomical cameras often provide images with 16-bit dynamic range), all input pixels are

scaled to span range from -1.0 to 1.0 (the used neural network handles all calculation in single-precision floating point numbers).

The number of neurons in the middle layer is chosen according to neural network response. The ability to recognize stars decreases with lowering the number of neurons in the middle layer (networks with 40 and 100 neurons in the middle layer were tested). On the other hand, increasing of the number of the middle layer neurons does not bring any measurable increase in the network reliability. All neurons in the network use sigmoid activation function (Nielsen 2015).

The crucial point in any neural network application is the ability to gather good learning set. Luckily, current algorithmic methods are reliable enough to provide thousands or tens thousands of stars within single image, depending on image resolution and position of the field of view on the sky. Training of the neural network needs both positive samples (this is a star) and negative samples (there is no star in this area). Algorithmically found star positions are, therefore, complemented with the same number of random patches within the image, in which no star is detected.

Neural network is trained on real astronomical images, containing ~50000 detected stars. Including the same number of empty patches, representing non-star areas, the learning set contained ~100000 samples. Learning is performed using stochastic gradient descent (Nielsen 2015) with each mini-batch containing 10 samples. 50 iterations are performed to achieve 98.5% reliability in recognition stars from the learning data set.

The trained neural network is surprisingly efficient in recognition of stars. Still, using of neural network for this task did not prove to be a better way compared to algorithms from the following reasons:

- Neural network can find more stars compared to algorithm. The reason is mainly the normalization of the network input bitmap – this efficiently equalizes weak and bright stars. However, the algorithm can be also modified to find weaker stars simply by lowering the threshold, expressed in terms of the standard deviation of the examined aperture. Still, finding more (weaker) stars is not desirable, because their S/N ratio is too low for extracting any valuable information. Their inclusion in the set, therefore, only increases the computational cost of the image processing.
- Neural network cannot properly distinguish very close stars, because the network response to weak stars close to bright ones is low. However, it is worth noting that the same problem affects the algorithms also, because the bright stars within tested aperture strongly increases the aperture standard deviation and pixels belonging to nearby weak star do not pass the threshold. Therefore, algorithmic search uses two apertures in dense fields. The first pass is using a small aperture to find weak stars and the subsequent pass with greater aperture detects bright stars omitted during the first pass. Training two neural networks, one with smaller input bitmap and another one with greater bitmap would probably result in the same reliability in finding close stars. This approach was not tested because of the reasons mentioned below.
- The main problem of the neural network used to find stars is a speed. Neural network results are not expressed, for example, as coordinates of the found star centroid. Instead, the network provides probability of star detection over every pixel in the image, i.e., a star probability map. Then, it is again necessary to algorithmically pass through the probability map to find points of the greatest probability, calculate centroids, and create data structures describing stars found on the image. So, inherent computational complexity of the neural network, combined with the overhead necessary to create data structures usable by other algorithms, results into very low efficiency of neural network in this task.

Let us note that the neural network used in this example is implemented using CPU only with no GPU accelerated calculations. However, the code detects the level of the vector instructions supported by the used CPU and utilizes SSE3, AVX, or AVX2 instruction set to speed up calculations. If the CPU does not support at last SSE3 instruction set, the code falls back to using scalar instructions. All tests mentioned in this article use the AMD Ryzen 7 1700X CPU supporting the AVX2 instruction set.

There certainly is a room for improvement of neural network execution speed, probably more than by an order of magnitude. Unfortunately, the algorithmic method is many orders of magnitude faster, depending on the particular image, so a neural network probably cannot match the speed of algorithm. There is no need to improve and speed up the processing based on neural networks.

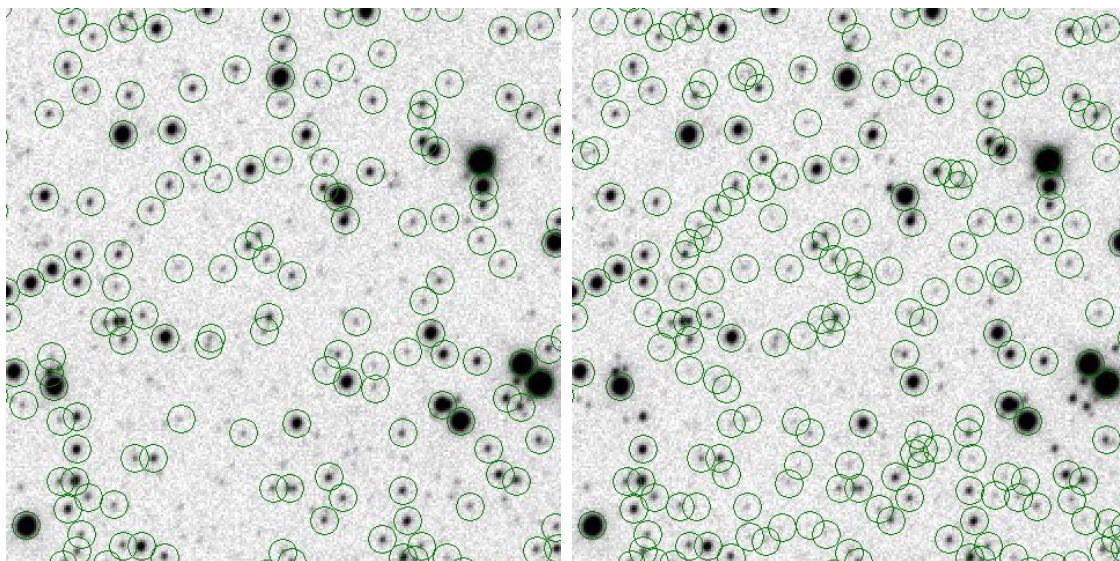


Figure 1: Comparison of a portion of the field of view with stars found by SIPS algorithmic method (left) with the same field with stars found using a neural network. Notice that the neural network finds more stars within the field of view while misses some weak stars close to bright ones. Possible modifications of algorithm to find more stars or neural network to find weak stars close to bright ones are discussed above.

Using neural networks to recognize variable stars

Recognizing typical shapes of light curves of variable stars is another task, in which a human brain excels, even though some level of previous experience and knowledge is needed. If an image of a certain field contains tens or possibly hundreds of thousands of stars, software can generate the same number of light curves. Manually inspecting tens of thousands of light curves to check whether some light curve could indicate new variable star is time consuming, exhausting, and not much reliable, as the human's ability to keep focus and concentrate on every single light curve is limited.

Certain statistical methods were developed to distinguish brightness changes of variable stars from other steady stars within the field of view. Unfortunately, statistical methods struggle in wide and dense fields with a lot of stars, many of which are angularly close and mutually contaminate photometry apertures. Also, matching individual stars on such series can fail for weak stars, which are not reliably detected in all images of the series (as observing conditions change, weak star may not surpass detection threshold on some images, etc.). What is more, number of various artifacts, exhibiting very high statistical deviations compared to regular steady stars and thus very high "variability indexes", typically exceeds number of real variable stars by an order of magnitude in such wide, dense fields.

Neural network results are compared with two such methods in this article.

- The "RMS method" calculates standard deviation of the time series for every star. For steady stars, the standard deviation increases with magnitude. Variable stars (and unfortunately also artifacts) show standard deviation above the average of steady stars of certain magnitude. Higher than average RMS of time series indicates possible variability.
- The "VDI method" (Variability Detection Index – name chosen in SIPS to denote this method) is based on a method originally proposed to detect the Blazhko effect of RR Lyrae variable stars (Jaimes 2013). In SIPS, the VDI method is slightly modified to better indicate fast physical variable stars, which light curve crosses the mean brightness many times during a single observation.

Simple neural networks have fixed structure. The neural network designed here for the detection of a star variability has three layers. All neurons use the sigmoid activation function.

- First (input) layer of 512 neurons represents isochronous brightness points of the light curve.
- Second layer consists of 256 neurons.
- Third (output) layer contains only one output neuron. Its value in the range 0.0 to 1.0 represents the probability the input light curve belongs to variable star.

The 512-neuron input layer is chosen as this number exceeds typical number of brightness points recorded over a course of an observation night. Because the neural network requires exactly 512 input points and these points must be isochronous, the input light curve must be pre-processed (interpolated). Also, possible gaps in the input light curve (interruptions in observation, caused, e.g., by clouds, GEM pier swap, etc.) must be interpolated with equidistant brightness points. The brightness points are also scaled to fit range from -1.0 to 1.0 for each input light curve.

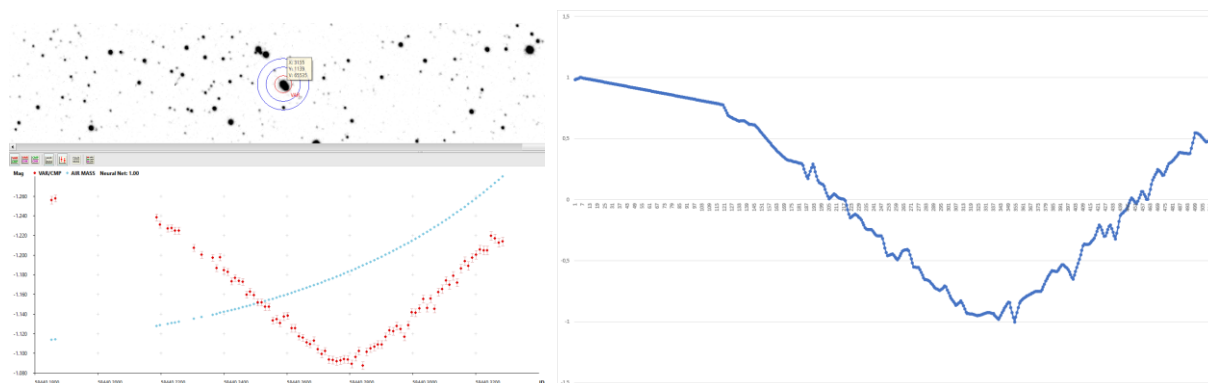


Figure 2: Example of real light curve of randomly chosen star (left panel). Certain portion of the light curve is missing, because the star saturated the detector and photometry software removed these brightness measurements as unreliable. The same light curve interpolated to 512 equidistant brightness points and scaled to fit the range from -1.0 to 1.0 (right panel).

Let us note that the interpolation of gaps may lead to false positives in some special cases. If both the last point just before the gap and the first point after the gap are below the average, interpolation fills the gap with points below the mean value and thus creates a false minimum, which can result in high output the neural network.

Training of neural network to recognize variable stars

As it is mentioned above, obtaining good training set is crucial for every neural network application. The empirical rule states that the learning set should contain at least thousands of individual samples.

SIPS Photometry tool is extended to allow creation of a variable star detection learning set. The learning set is a simple text file, with each line containing desired output (1 for variable star, 0 for non-variable star) followed by 512 equidistant brightness points, scaled to range from -1.0 to 1.0.

After each observing night is processed with SIPS Photometry, the tool allows to add any chosen light curve to learning set as variable or non-variable. The current learning set presented here contains 2165 variable star samples and 2079 non-variable star samples from approx. 10 fields monitored at BSObservatory.⁴

It is worth mentioning that the learning set is created iteratively. Neural network is trained on a smaller set, then the learning set is extended especially with non-variable stars (typically artifacts), to which the network assigned high variability index. This allows to subsequently train the network to limit recognition of particular artifacts as variable stars and to improve reliability. Still, such simple network cannot completely avoid false detection.

The network was trained using the stochastic gradient descent with mini-batch size of 10 samples for 50 iterations. The achieved reliability of proper recognizing of 4000+ light curves, contained in the learning set, as variable or non-variable was 98.8%.

Comparison of statistical and neural network methods of variable star detection

The first example shows response from all three compared methods to newly found variable star UCAC4 554-108577 ($\alpha = 20^{\text{h}} 19^{\text{m}} 45.27^{\text{s}}$, $\delta = +20^{\circ} 40' 20.2''$) in a field in Sagitta. The star exhibits V-shaped minima only ~ 60 mmag deep, which makes its detection by statistical methods particularly difficult.

⁴ <http://www.bsobservatory.org/>

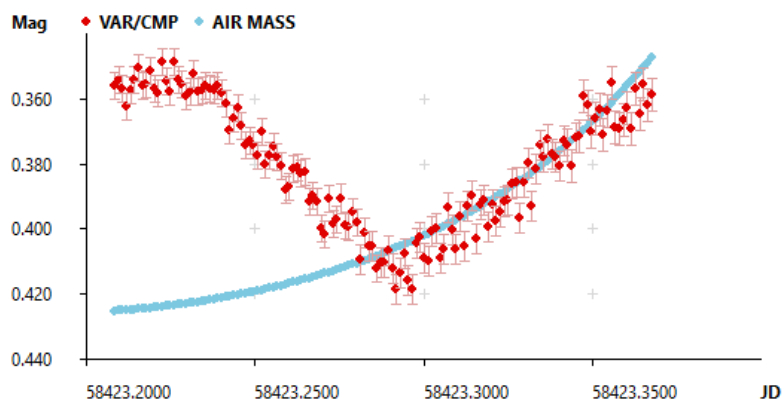


Figure 3: Light curve of the newly found Algol-type variable star UCAC4 554-108577, captured on October 31st, 2018.

The position of the above-mentioned star is highlighted by a red circle in the following charts. Please note that the SIPS Photometry tool displays already known variable stars with red dots, comparison stars with green dots and all other stars with gray dots.

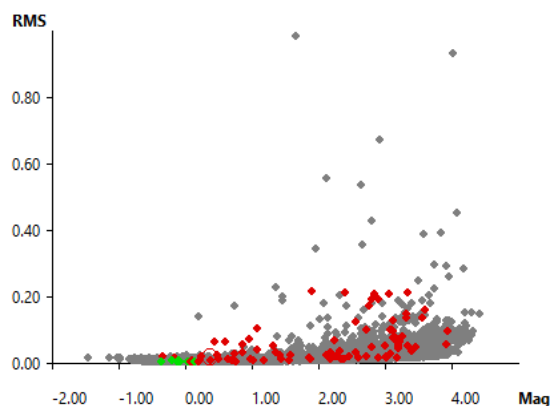


Figure 4: Response of the “RMS” method to star on Figure 3. The red circle very close to zero value shows the very low response, not allowing to recognize this star as variable. Also note the high number of gray dots at the upper-right portion of chart – all these dots are artifacts with very high RMS index response. Already known variable stars are marked with red dots.

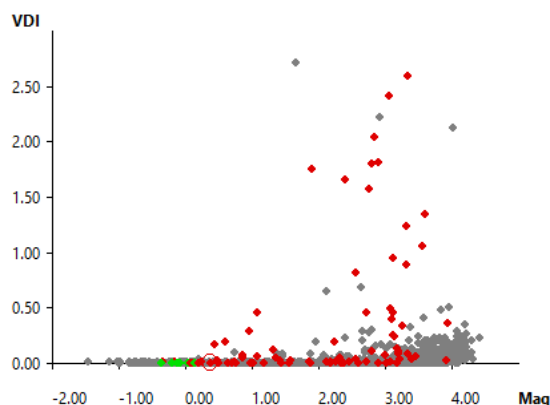


Figure 5: Response of the “VDI” method to star on Figure 3. Despite the VDI shows much better results compared to RMS method (fewer artifacts and more actual variable stars have high response), the particular star response is still very close to zero, so it would probably remain undetected.

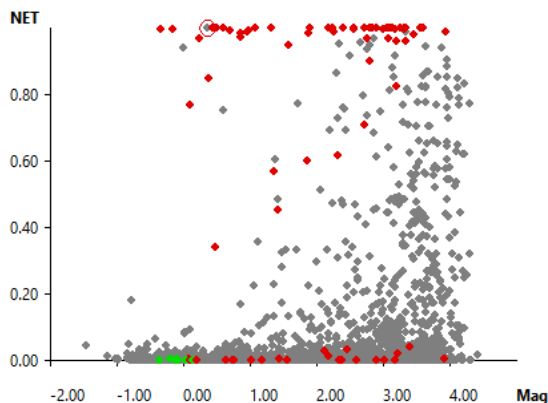


Figure 6: Neural network response to star on Figure 3 is 1.00 and clearly indicates this is a new variable star.

The second example shows response of compared methods to a very shallow (only ~20 mmag) minimum of the star UCAC4 552-114582 ($\alpha = 20^{\text{h}} 17^{\text{m}} 57.49^{\text{s}}$, $\delta = +20^{\circ} 20' 50.7''$) in the field in Sagitta, mimicking possible exoplanet transit (further observations proved this is only a secondary minimum of Algol-type variable star).

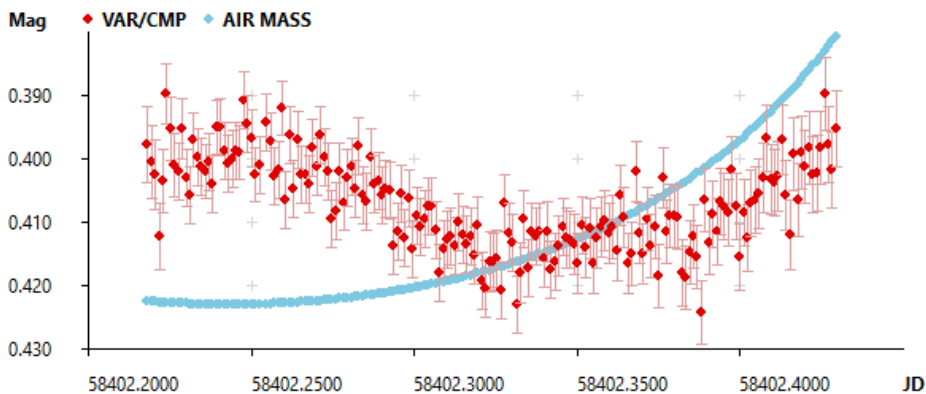


Figure 7: Light curve of the secondary minimum of a newly found Algol-type variable star UCAC4 552-114582, captured on October 10th, 2018.

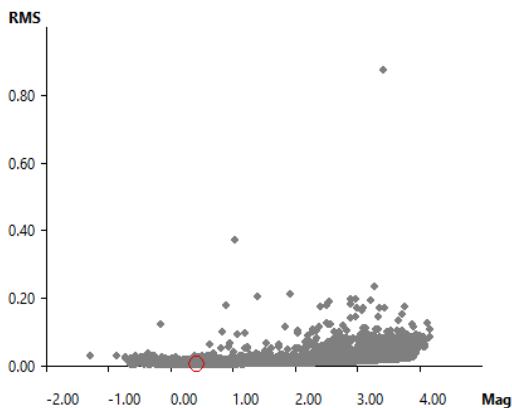


Figure 8: “RMS” method response to star on Figure 7 is among the lowest possible in this set.

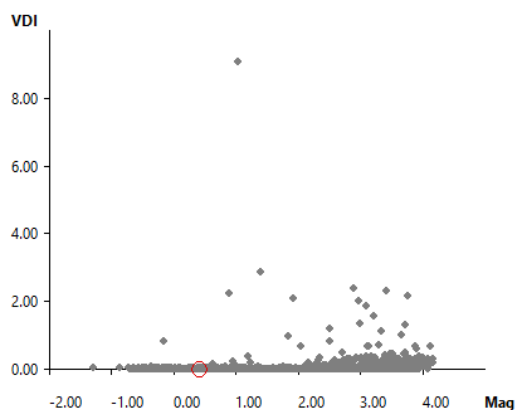


Figure 9: “VDI” method response to star on Figure 7 is also virtually zero.

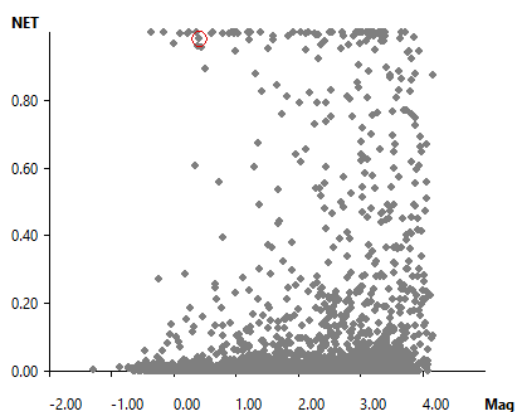


Figure 10: Neural network response to star on Figure 7 is 0.98, which allowed detection of this star as variable.

Conclusion

Neural network proves to be highly effective mean of detecting of new variable stars. Despite the neural network generate false positives, its reliability is much higher compared to statistical methods.

References

- Nielsen, M., Neural Networks and Deep Learning, Determination Press, 2015
- Werbos, P., Beyond Regression: New Tools for Prediction and Analysis in the Behavioral Sciences, Harvard University, 1975
- Krizhevsky, A., Sutskever, I., Hinton, G., Imagenet classification with deep convolutional neural networks, Advances in neural information processing systems, 2012
- Cagaš, P., Proceedings of the 48th Conference on Variable Stars Research, Open European Journal on Variable stars, vol. 180
- Jaimes, R. F. et al, Variable stars in the globular cluster NGC 7492, A&A, 2013, [2013A&A...556A..20F](#)

Modeling the effects of interaction between supernova ejecta and dense circumstellar material

P. KURFÜRST^{1,2}, J. KRTIČKA¹ & M. ZEJDA¹

(1) Department of Theoretical Physics and Astrophysics, Masaryk University, Kotlářská 2, 611 37 Brno, Czech Republic, petrk@physics.muni.cz

(2) Institute of Theoretical Physics, Charles University, V Holešovičkách 2, 180 00 Praha 8, Czech Republic, petr.kurfurst@utf.mff.cuni.cz

Abstract: Progenitors of core-collapse supernovae (SN) lose a significant fraction of their mass before explosion via stellar winds, circumstellar disks, or bipolar lobes. The kinetic energy of the SN ejecta may be partially converted into radiation, giving rise to luminous transients comparable to the luminosities of the actual SN. We study the hydrodynamics of collisions between expanding SN ejecta and circumstellar medium (CSM). We calculate the rate of deceleration as well as the behavior of density, pressure, expansion velocity and temperature structure in the interaction zone with various geometrical configurations and initial density structures of CSM. The theoretical conclusions of our models will help to improve the determination of SN progenitors properties and CSM density distribution.

Introduction

Explosions of supernovae (SN) are the well-observable and one of the most brilliant events within the whole universe. They also serve as the prominent source of data for studying the enormous range of physics. We investigate the interaction of the SN with the surrounding circumstellar matter (CSM) which may provide the fundamental information about the progenitor type and its pre-explosion mass loss. Although most of the type II SN progenitors are red supergiants (RSG) stars (Smartt 2009, Pejcha & Prieto 2015), there were also detected a few hydrogen-rich massive blue supergiant (BSG) progenitors of type II SNe (Vanbeveren et al. 2013). In this point, many studies found the interaction of SN with CSM may significantly boost the observed luminosity, and so the super-luminous SNe are believed to explode inside a dense (mostly anisotropic) circumstellar matter (e.g., Smith 2017). After the SN shock reaches the progenitor surface, it continues to propagate through CSM. If the CSM is optically thick, the radiation is absorbed, and the energy accumulates in the region of the shock (Svirski et al. 2012). After the CSM becomes optically thin, this energy releases as an overluminous shock breakout (comparing to SN without CSM), which is represented by the characteristic slowly increasing light curve (e.g., Chevalier & Irwin 2011).

Expansion of SN envelope

We perform the models of the interaction of expanding SN envelope with CSM including the dense equatorial disk. We use our 2D hydrodynamic code (Kurfürst et al. 2018) for the calculation. We assume the stellar parameters corresponding to a typical RSG star: $M_{\star} = 15M_{\odot}$, $R_{\star} = 10^{12}\text{m}$, where the pre-explosion mass loss rate $\dot{M} = 10^{-6}M_{\odot}\text{yr}^{-1}$ (see the left panel of Fig. 1) or to a BSG star: $M_{\star} = 45M_{\odot}$, $R_{\star} = 80R_{\odot}$, where the pre-explosion mass loss rate $\dot{M} = 10^{-2}M_{\odot}\text{yr}^{-1}$ (the right panel of Fig. 1, with Figs. 2 and 3). In both the models the explosion energy $E = 10^{44}\text{J}$. We initiate the simulation as the “thermal bomb” within the radius $0.1R_{\star}$ inside of which we set the initial photon gas pressure as $p_{\text{ini}} = E/(3V)$, where V is the volume of the “bomb” region. We pre-calculate the initial stellar internal density and temperature profiles outside the “thermal bomb” region using the MESA models. The early phase of SN envelope expansion can be described in terms of a self-similar adiabatic process, using the equation of state of an isothermal ideal gas (Nadezhin 1985, Chevalier & Soker 1989).

We neglect in our models the effects of radiative cooling, magnetic fields, or the energy input from the compact remnant. The enormous SN energy strongly overlaps most of these effects, and so their influence on the dynamics of the problem is minimal (Truelove & McKee 1999), or are connected only with a specific situation or remnant type (like magnetars, see, e.g., Metzger et al. 2017).

Circumstellar medium

We consider a spherically symmetric CSM with an axisymmetric equatorial circumstellar disk. The initial density profile of a spherically symmetric CSM (which may be created by the stellar wind of the progenitor) is $\rho \propto r^{-2}$ while its initial base density ρ_0 (the density of CSM near the surface of the star) corresponds to stars' pre-explosion mass loss rate \dot{M} . Vertical density profile of the disk is Gaussian (e.g., Pringle 1981),

$$\rho_{\text{disk}}(r, z) = \rho_{\text{eq,disk}}(r) e^{-\frac{GM_{\star} z^2}{a^2 r^3}},$$

where $\rho_{\text{eq,disk}}$ is the disk midplane density that radially decreases as $\rho_{\text{eq,disk}}(r) \approx \rho_{0,\text{disk}}(R_{\star}/r)^{7/2}$ (e.g., Okazaki 2001), $a^2 \propto T_{\text{disk}} \propto p_{\text{disk}}/\rho_{\text{disk}}$ is the (squared) isothermal speed of sound, G is the gravitational constant, and z is the “vertical” distance from the disk midplane. The disk equatorial base density $\rho_{0,\text{disk}}$ roughly corresponds to the spherically symmetric CSM. We assume the constant disk temperature T_{disk} as corresponding to the stellar pre-explosion effective temperature that may be approximately 3500K for RSG and 25000K in case of BSG star.

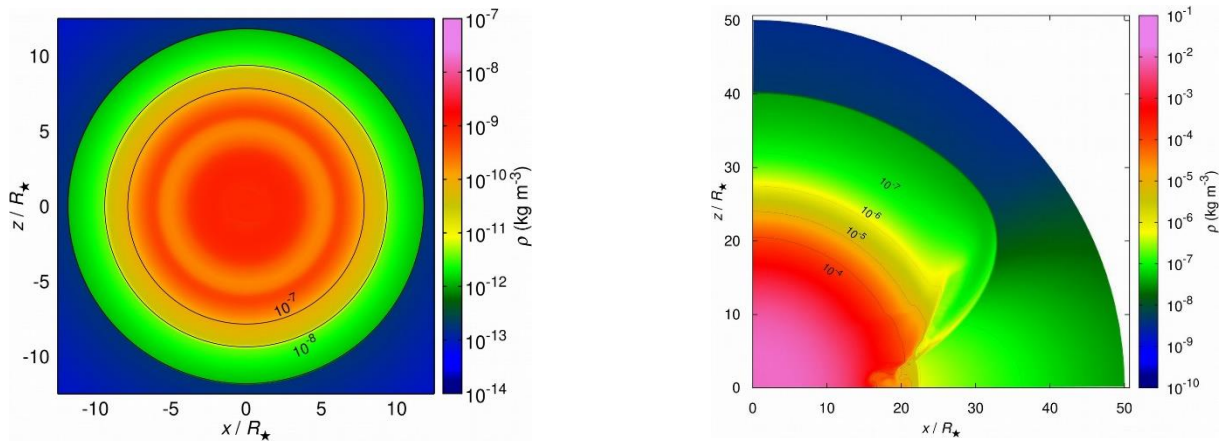


Figure 1: *Left panel* - 2D density structure of the interaction of SN (RSG progenitor) with perfectly spherically symmetric CSM at $t = 30$ d. We describe the stellar and CSM parameters in the text. *Right panel* - density structure of interaction of SN (BSG progenitor) with asymmetric CSM that includes the dense circumstellar disk, at the time $t = 125$ h. Contours mark the densities $\rho = 10^{-7}, 10^{-6}, 10^{-5},$ and 10^{-4}kgm^{-3} . Characteristic 1D sections of the model are in Figs. 5 and 6.

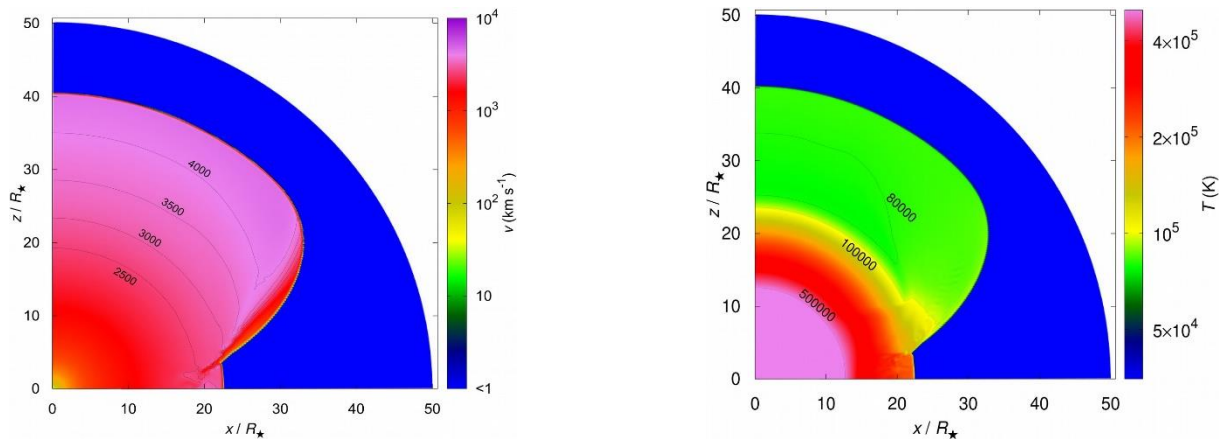


Figure 2: *Left panel* - 2D structure of expansion velocity of the model described in (right panel of) Fig. 1 at the same time. Contours mark the velocities 2500, 3000, 3500, and 4000 kms^{-1} . *Right panel* - 2D temperature structure of the model described in (right panel of) Fig. 1 at the same time. Contours mark the temperatures $8 \times 10^4, 10^5,$ and $5 \times 10^5 \text{K}$.

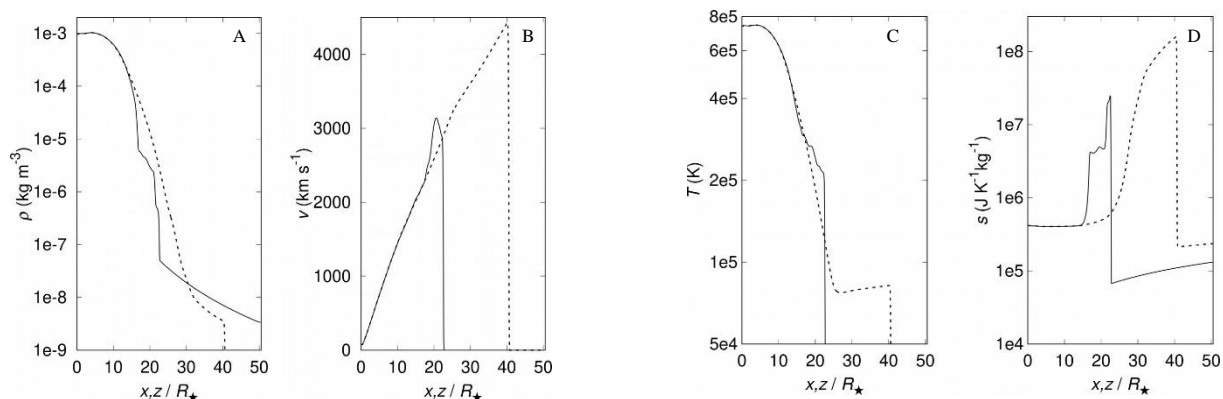


Figure 3: *Panel A* - 1D slices of the density in the equatorial (solid line, x -coordinate) and polar (dashed line, z -coordinate) direction of the model described in Figs. (right panel of) 1 and 2. *Panel B* - 1D slices of the velocity in the equatorial (solid line, x -coordinate) and polar (dashed line, z -coordinate) direction of the same model as in Panel A. *Panel C* – corresponding 1D slices of the temperature. *Panel D* – corresponding 1D slices of the specific entropy.

Numerical models

The left panel of Fig. 1 illustrates the 2D snapshot of the density profile (RSG progenitor) of the SN - CSM interaction for comparison. We show in the right panel of Fig. 1 the 2D snapshot of the density profile (BSG progenitor) of the SN - CSM interaction. We show in Fig. 2 the corresponding snapshots of the radial velocity and the temperature in the time $t \approx 180\text{h}$ since shock breakout (regarding the shock emergence from the surface of the progenitor star), up to the radius $50R_{\star}$. We performed the numerical calculations on the 2D grid with 2400 radial vs. 480 azimuthal grid cell intervals. We can distinguish the details of the selected quantities, especially the remarkable wings of over-dense and over-heated gas near the shear zone between the disk and the spherically symmetric CSM as well as the developing of Kelvin-Helmholtz and Rayleigh-Taylor instabilities. We also demonstrate the 1D equatorial and polar slices of the density and expansion velocity (panels A and B of Fig. 3) as well as the temperature and specific entropy (panels C and D of Fig. 3) that correspond to the instant time shown in Figs. 1 and 2. We quantify some of the particular values of the described quantities in the captions enclosed to the corresponding figures.

Summary and future work

The model demonstrates the aspherical expansion of the SN ejecta where the material preferably expands to the area outside the dense equatorial disk. In case of the disk initial base density values, such disk may effectively decelerate or even block the SN expansion with significant over-dense and over-heated regions near the SN-disk interaction zones. The density and temperature gradients also decrease with time, showing the steeper slopes for lower pre-explosion mass loss rates. The model also indicates the development of Kelvin-Helmholtz as well as Rayleigh-Taylor instabilities in the zone of shear between the disk and non-disk CSM where the flow of matter is re-directed to the regions of lower density, forming thus the over-dense gaseous wings along the disk - other CSM interaction zone.

We plan to calculate the SN light curves powered by the excess of the thermal energy caused by the effects of SN-CSM interaction as the following step. The comparison of the directionally split 2D light curve models with observations may significantly improve our understanding of the geometry and the details of the studied processes.

Acknowledgement

The access to computing facilities owned by 225 the National Grid Infrastructure MetaCentrum, provided under "Projects of Large Infrastructure for Research, Development, and Innovations" (LM2010005) is appreciated. This work was supported by grant GAČR 18-05665S and by the grant Primus/SCI/17.

References

- Chevalier R. A. & Soker N., 1989, ApJ, 341, 867, [1989ApJ...341..867C](#)
- Chevalier R. A. & Irwin C. M., 2011, ApJ, 729, L6, [2011ApJ...729L...6C](#)
- Kurfürst P., Feldmeier A., Krtićka J., 2018, A&A, 613, 75, [2018A&A...613A..75K](#)
- Metzger B. D., Berger E., Margalit B., 2017, ApJ, 841,14, [2017ApJ...841...14M](#)
- Nadezhin D. K., 1985, Ap&SS, 112, 225, [1985Ap&SS.112..225N](#)
- Okazaki A. T., 2001, PASJ, 53, 119, [2001PASJ...53..119O](#)
- Pejcha O. & Prieto J. L., 2015, ApJ, 806, 225, [2015ApJ...806..225P](#)
- Pringle J. E., 1981, ARA&A, 19, 137, [1981ARA&A..19..137P](#)
- Smartt S. J., 2009, ARA&A, 47, 63, [2009ARA&A..47...63S](#)
- Smith N., 2017, Interacting Supernovae: Types II_n and Ib_n, ed. A. W. Alsabti & P. Murdin, 403, [2017hsn..book..403S](#)
- Svirski G., Nakar E., & Sari R., 2012, ApJ, 759, 108, [2012ApJ...759..108S](#)
- Truelove J. K. & McKee C. F., 1999, ApJS, 120, 299, [1999ApJS..120..299T](#)
- Vanbeveren D., Mennekens N., Van Rensbergen W., & De Loore C., 2013, A&A, 552, 105, [2013A&A...552A.105V](#)

FLEXIBLE VARIABLE STAR EXTRACTOR: new software for detection of variable stars

V. BREUS¹

(1) Department "Mathematics, Physics and Astronomy", Odessa National Maritime University, Mechnikova, 34, 65029 Odessa, Ukraine, bvv_2004@ua.fm

Abstract: We developed software for detection of variable stars using CCD photometry. It works with "varfind data" that could be exported after processing CCD frames using C-Munipack. Our goals were maximum automation and support of large fields of view with thousands of stars. The program chooses the comparison stars automatically, processes all time series using multiple comparison stars to get final light curves. Different filtering algorithms are used to reduce the impact of outlying points, imaging artifacts and low quality CCD frames without careful manual time series reduction. We implemented various variable detection indices and plotting two-channel diagrams of selected pair of indices and mean brightness of the star to distinguish variables from constant stars for further manual check of outlying points as variable candidates.

Introduction

An indisputable advantage of the CCD photometry vs. earlier technologies is that CCD observations allow us to measure brightness of thousands stars from the same field of view simultaneously. We may learn from the experience, that there is at least one more known variable star within 10-20 arc minutes of any primary object of investigation and sometimes we may be lucky and discover an unknown one. Over the years of using CCD photometry different techniques for detect variable stars were developed. It has improved in recent years also due to intensified interest to discovery of extrasolar planets using transit photometry.

One of the simplest algorithms is based on the dependency of noise level to mean brightness of the star. According to the statistics, if all stars were constant, the dependence of standard deviation of brightness vs. mean brightness of an object would have a parabola-like shape. A variable star obviously should have larger standard deviation than a constant object of the same mean brightness. Particularly, this algorithm is implemented in the C-Munipack software package (Motl, 2011). It requires manual review of all suspected variable stars' light curves to approve or reject the candidate.

However, this solution is sensitive to outlying points and sometimes fails if the data is noisy due to various reasons. In this case at the dependence of standard deviation on the mean brightness we may see variable stars in a heap of points corresponding to constant stars, and many constant stars with lack of data or outlying points will be located above the curve like they are variables. One of the reasons of this software development was the necessity of the solution capable to analyze few experimental CCD series with more then 10000 stars in each field of view for the purpose of searching unknown short period variables.

This paper contains a brief description of Flexible Variable Star Extractor software (hereafter named FVSE) and methods used for detection of variable stars.

Algorithms

We used the basic idea of classical analysis of standard deviation on the mean brightness dependence. Usually this chart is based on the differential magnitudes and user can make a decision if a star is variable or not. This way we discovered eclipsing binary 2MASS J18024395 + 4003309 (Andronov & Breus & Zola, 2012, Andronov et al., 2015). However, using of the artificial comparison star instead of the control star makes possible to increase accuracy estimates by a factor of 1.3-2.1 times for clear and cloudy nights, respectively (Kim & Andronov, 2004). The algorithm of the „mean weighted“ comparison star for the photometry using CCD-cameras was described by Andronov & Baklanov (2004) and implemented in MCV. Obviously, using final magnitudes obtained by this method instead of differential ones for standard deviation calculation allows to decrease the noise and influence of the scatter of some particular comparison star on the data. It is computationally more expensive so it takes relatively more time to process the same data set, but it does not require modern PCs even for large number of stars and long time series.

During the process of developing it turned out that standard deviation does not distinguish variables significantly in case of big number of stars, so we decided to implement also other indices. Recently Sokolovsky et al. (2017) analyzed 18 statistical characteristics quantifying scatter and/or correlation between brightness measurements and

compared their performance in identifying variable objects using time series obtained with different class telescopes. We choose Median absolute deviation, chi-squared, Robust median statistic, Normalized excess variance and von Neumann ratio based on performance and least computational expenses.

Implementation

FVSE reads magnitudes and error estimates from the “varfind” data exported from C-Munipack. The weighted mean magnitude and standard variance are calculated for every star in the data set where weight of each observation is inversely proportional to the square of the individual observation error estimates.

The selection of comparison stars may be done manually or automatically. FVSE chooses the comparison stars using experimentally derived criteria, which could be adjusted at the settings tab. First the star should not be close to the frame border because these data usually has lower quality (default value: 50 pixels). The comparison star should be measured at least at 70% of CCD frames of the time series. Its standard variance must not exceed the value of the mean variance of all stars multiplied by the factor of 1.5. This allows us to select less noisy stars as the comparisons. The total number of selected comparison stars is limited (default: 1000). Since the stars are ordered from bright to faint in varfind data, this cuts the faintest objects that usually do not fit one of previously mentioned criteria. For some data sets it's necessary to limit the number of comparison stars to traditional 10-15.

Following the algorithm of the „mean weighted“ comparison star, weights of selected comparison stars are determined and the final magnitudes of all stars are calculated using the obtained artificial comparison star and the known magnitude of selected comparison star (entered by user). Since this moment, user could view light curves of any star and export it to the text file. Here the raw instrumental magnitudes is presented with red points, final light curve with green points (see Fig. 1).

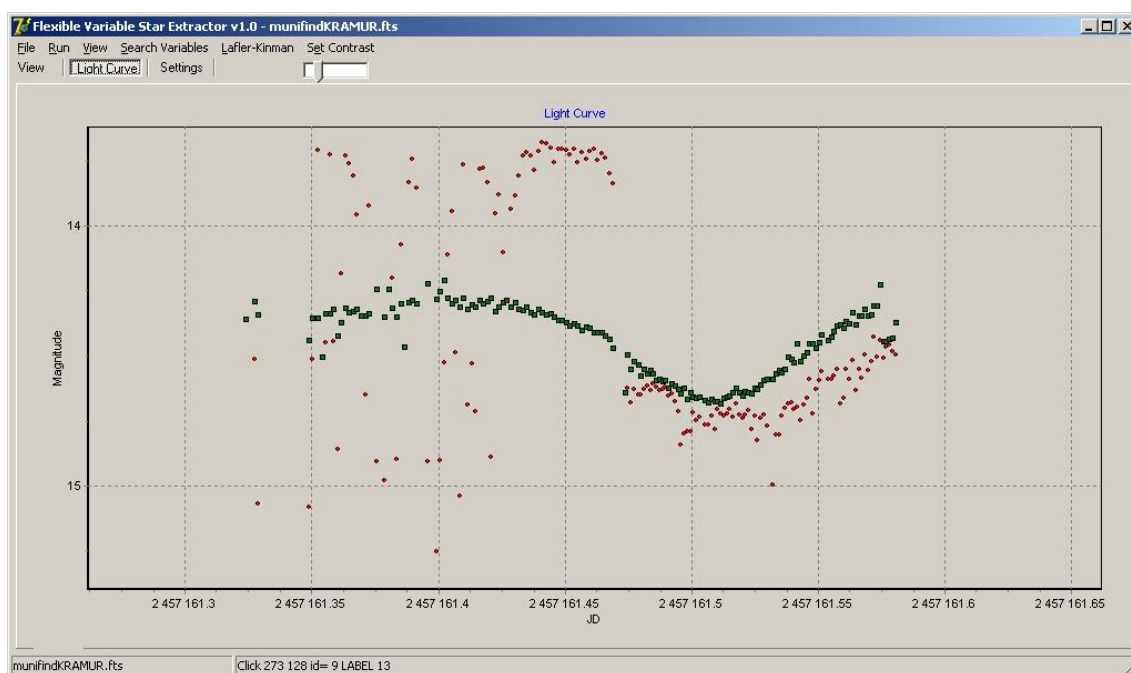


Figure 1: A sample light curve of the EW-type system V442 Cam during one night of observations (Breus et al., 2010). Large scatter at the beginning corresponds to the partially cloudy weather conditions that changed to clear sky later. The scatter of the final light curve (green) is also larger, but the influence of clouds is reduced using artificial comparison star method.

„Search Variables” menu item runs the calculation of variability detection indices used to distinguish variable stars from constant ones. We determine standard deviation σ , chi-squared χ^2 , Median absolute deviation, Robust median statistic, Normalized excess variance and von Neumann ratio. The chi-squared value is used in the form of square root and von Neumann ratio is calculated in inversed and simplified way. The detailed description of software and implementation of these algorithms was presented by Breus (2017).

User can plot any pair of standard deviation, mean brightness and these variability detection indices at the diagram. In any case, most of constant stars will form a group of points, and any outlying point may correspond to a variable star. The decision whether an object is a variable or not is left to the user who can view or save a light curve of any star in one click.

On this step it's necessary to mark the viewed star as variable or false alarm using context menu (see Fig. 2), this way it does not necessary to remember all objects in large field of view contrary to other solutions. At any step it is possible to remove some outlying points or even whole CCD frames from the data set and re-calculate the light curves and variability indices.

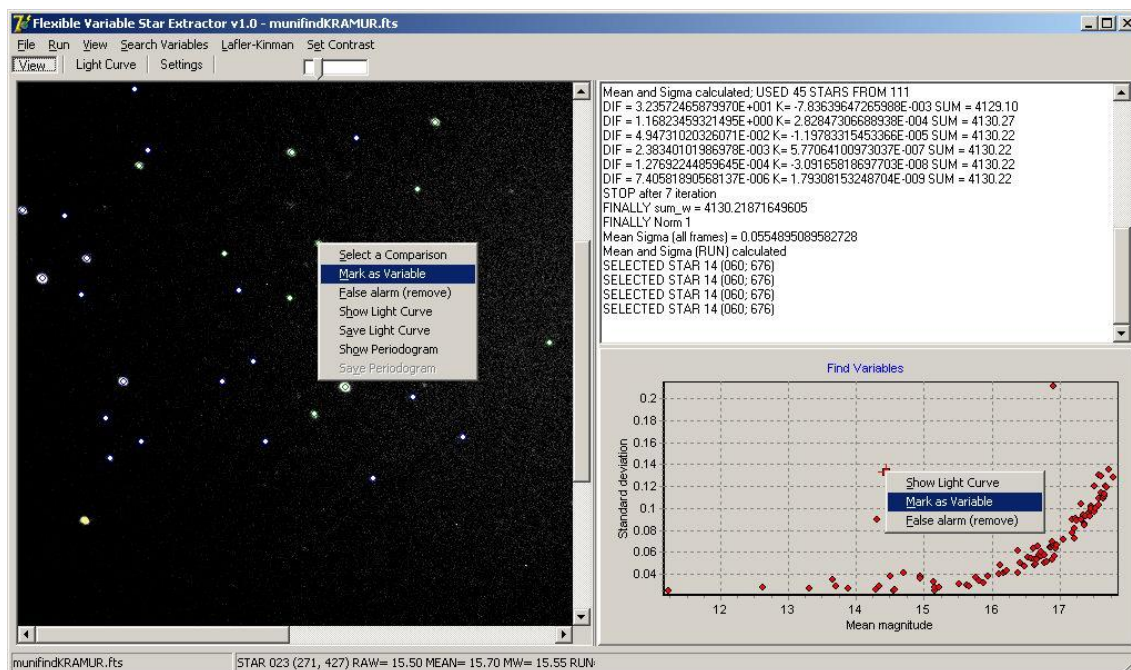
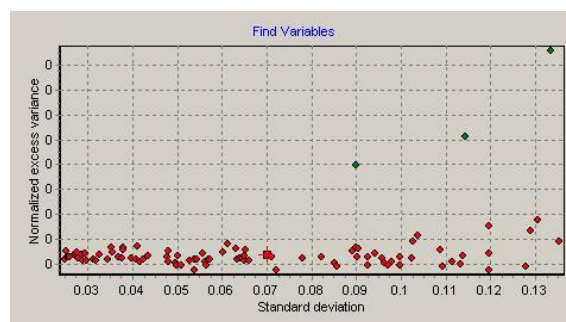
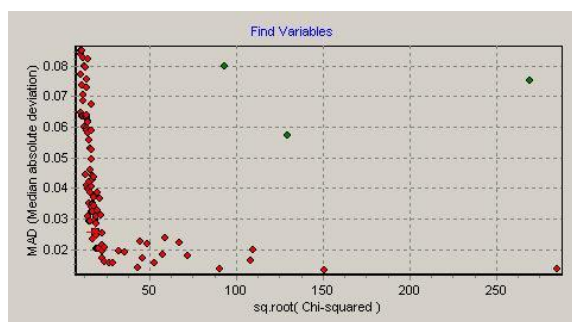


Figure 2: Graphical user interface of FVSE. Collage shows the context menu which may be called clicking on the star at the image or clicking the point at the diagram. It's possible to view the light curve of selected star, mark it as variable or false alarm.

It's possible to calculate periodograms of all stars in the data set. Originally there was an idea to use some parameters of the periodogram as one more variability detection index, but it has not yet been implemented. For this purpose, the Lafler – Kinman - Kholopov method was used (Lafler & Kinman, 1965, Andronov & Chinarova, 1997) and the implementation was borrowed from Variable Stars Calculator software (Breus, 2003, Breus, 2007).

Current version has hardcoded limits of the image size (5120x5120 pixels), 100000 points in the time series and 40000 stars in the field of view (may be changed upon request). This was done to increase performance in avoiding using dynamic arrays. These values are enough for most of the data and setting higher limits will raise RAM requirements.

FVSE is available as a freeware⁵.



⁵ <http://uavso.org.ua/varsearch/>

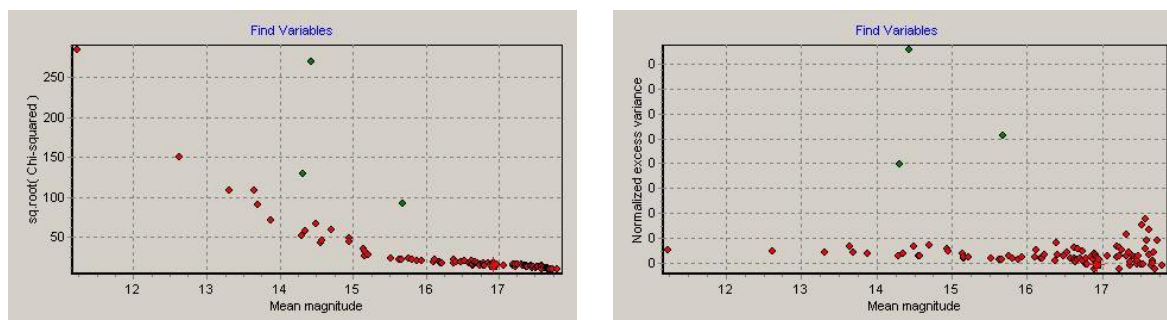


Figure 3: Samples of two-channel diagrams for the field of view of the intermediate polar MU Cam: dependence of MAD vs. chi-squared, NEV vs. standard deviation, chi-squared on the mean magnitude and NAV vs. mean magnitude. Green points correspond to MU Cam, V442 Cam and V440 Cam.

Results and Conclusion

We improved one of the most popular algorithms for variable stars detection in order to decrease the influence of noisy data and outlying points on the chart. “Flexible Variable Star Extractor” software was developed. It works with the data exported from C-Munipack, chooses the comparison stars automatically and processes all time series.

We implemented different variability detection indices. It turned out that some variability detection indices are effective to distinguish a star of particular variability type; other indices do not show significant difference for variable and constant stars, at the same time for another types of variability the situation is opposite. Innovative solution of viewing two-channel diagrams of any pair of parameters allows marking variable stars of all types by viewing 2 or 3 diagrams if the first one is not sufficient.

This style significantly improved the speed of semi-automatic search for variable stars in generic field of view of any size and time series of any duration.

Software was developed in the framework of the Ukrainian Virtual Observatory project (Vavilova et al., 2012). This program will be applied to the observations obtained within the “Inter-Longitude Astronomy” (Andronov et al., 2017) and “AstroInformatics” campaigns (Vavilova et al., 2017).

References

- Andronov I. L., Baklanov A. V., 2004, *Astron. School Rep.*, 5, 264, [2004AstSR...5..264A](#)
- Andronov I. L., Chinarova L. L., 1997, *KNFT*, 13, 67, [1997KFNT...13f..67A](#)
- Andronov I. L., Breus V. V., Zola, S., 2012, *OAP*, 25, 145, [2012OAP...25..150A](#)
- Andronov I.L. et al., 2015, *JASS*, 32, 127, [2015JASS...32..127A](#)
- Andronov I.L. et al., 2017, *ASPC*, 511, 43, [2017ASPC..511..43A](#)
- Breus V., 2003, *OAP*, 16, 24, [2003OAP...16...24B](#)
- Breus V., 2007, *OAP*, 20, 32, [2007OAP...20...32B](#)
- Breus V. V., Andronov I. L., Dubovsky P. A., Hegedus T., Kudzej I., Petrik K., 2010, *OAP*, 23, 19, [2010OAP...23...19B](#)
- Breus V., 2017, *AASP*, 7, 3, [2017AASP...7....3B](#)
- Kim Y., Andronov I. L., Jeon Y., 2004, *JASS*, 21, 191, [2004JASS...21..191K](#)
- Lafler J., Kinman T., 1965, *Ap.J.Suppl.*, 11, 216, [1965ApJS...11..216L](#)
- Motl D., 2011, C-Munipack project, <http://c-munipack.sourceforge.net/>
- Sokolovsky K. V., Gavras P., Karampelas A. et al., 2017, *MNRAS*, 464, 1, 274, [2017MNRAS.464..274S](#)
- Vavilova I.B., et al., 2012, *KPCB*, 28, 85, [2012KPCB...28...85V](#)
- Vavilova I.B., Yatskiv Ya.S., Pakuliak L.K., Andronov I.L., Andruk V.M., Protsyuk Yu.I., Savanevych V.E., Savchenko D. O., Savchenko V.S., 2017, *IAU Symposium*, 325, 361, [2017IAUS..325..361V](#)

MAVKA: Software for statistically optimal determination of extrema

KATERYNA D. ANDRYCH^{1,2}, IVAN L. ANDRONOV²

- (1) Department of Theoretical Physics and Astronomy, Odessa I.I. Mechnikov National University, 2 Dvoryanskaya St., Odessa 65026, Ukraine, katyaandrich@gmail.com
- (2) Department “Mathematics, Physics and Astronomy”, Odessa National Maritime University, Mechnikova, 34, 65029 Odessa, Ukraine, tt_ari@ukr.net

Abstract: We introduce the program MAVKA for determination of characteristics of extrema using observations in adjacent data intervals, with intended applications to variable stars, but it may be used for signals of arbitrary nature. We have used a dozen of basic functions, some of them use the interval near extremum without splitting the interval (algebraic polynomial in general form, "Symmetrical" algebraic polynomial using only even degrees of time (phase) deviation from the position of symmetry argument), others split the interval into 2 subintervals (a Taylor series of the “New Algol Variable”, “the function of Prof. Z. Mikulášek”), or even 3 parts (“Asymptotic Parabola”, “Wall-Supported Parabola”, “Wall-Supported Line”, “Wall-Supported Asymptotic Parabola”, “Parabolic Spline of defect 1”). The variety of methods allows to choose the “best” (statistically optimal) approximation for a given data sample. As the criterion, we use the accuracy of determination of the extremum. For all parameters, the statistical errors are determined. The methods are illustrated by applications to observations of pulsating and eclipsing variable stars, as well as to the exoplanet transits. They are used for the international campaigns “Inter-Longitude Astronomy”, “Virtual Observatory” and “AstroInformatics”. The program may be used for studies of individual objects, also using ground-based (NSVS, ASAS, WASP, CRTS et al.) and space (GAIA, KEPLER, HIPPARCOS/TYCHO, WISE et al.) surveys.

Introduction

Variable stars of different types are the most important sources of information about structure of stars and their evolution. Thus they are extensively observed in many countries.

For some types, like eclipsing or pulsating variables, there are many short time series of observations, which do not cover the whole photometrical period of the object. Typically this is due to a separation of the tasks to analyse precise multi-colour observations to determine parameters and get only one parameter from the incomplete light curve the “Time of Minimum/Maximum” (ToM) (cf. Tsevevich, 1970, 1971). The moments of extrema (also referred as “minima/maxima timings”) are used for the “O-C” studies of the period changes due to mass transfer and/or presence of a third/fourth body. The largest compilations were published as a paper monograph by Kreiner et al. (2001), whereas further catalogs are regularly improved and are accessible on-line. Among the most famous are the “O-C gate” (project BRNO, Czech Astronomical Society & Masaryk University) with an on-line possibility to determine the ToM (Brát et al., 2012), and the AAVSO (2018) database with recommended external software.

The popular methods of determination of ToM varied from “bisector” (Pogson’s) method using the light curve and its hand-written approximation to a polynomial (typically parabolic) approximation (e.g. Tsevevich 1970, 1971) or the method by Kwee and van der Woerden (1956). The software for determination of ToM using the polynomial fit, was presented e.g. by Breus (2006). The statistically optimal degree of the polynomial was used to compile a catalogue of characteristics of 173 semi-regular pulsating stars (Chinarova and Andronov, 2000). A review on long-period variables was presented by Andronov et al. (2014). The improvement of the “bisector” method (using only times of crossing of some constant value) was proposed by Andronov and Andrych (2014).

Newer methods of the ToM determination are based on the least squares, and were reviewed by Andronov (1994, 2005). For the complete light curves of intermediate polars, two-period (multi-)harmonic approximations were used (e.g. Andronov and Breus, 2013). For the complete light curves of the eclipsing binaries, Andronov (2010, 2012) proposed the “New Algol Variable” (NAV) algorithm, which is effective not only for Algols, but also for EB and EW-type systems (Tkachenko et al., 2016). Andronov et al. (2017) tested many functions to make a statistically optimal phenomenological approximation of the complete eclipse.

We focused on approximations for a common case, when time series are close to the extremum of brightness of the object. From such data needed to determine characteristics of extremum: moment, magnitude, width of flat part of eclipse (if there is transit) and corresponding accuracy estimates. Moreover, some types of functions are asymmetrical, what is generally the case for the pulsating variables, and may also be applied for eclipses of the binaries with the O’Connell effect.

For this task, the program MAVKA (“Multi-Analysis of Variables by Kateryna Andrych”) was elaborated initially in the Excel/VBA environment (Andrych et al., 2015) and then was rewritten in the Delphi 7 environment (Andrych et al., 2017) with adding these approximations to the Delphi version of the “Observation Obscurer” (OO) software, which was originally written in Free Pascal (Andronov, 2001). The software MAVKA allows to compute necessary parameters of the extrema using one out of nine realized methods.

In this paper, we discuss this program and algorithms, realised in it.

Methods of the analysis

Nine different methods were realized in program.

For all approximations linear parameters are determined by the method of least squares, and for non-linear - by the method of differential corrections.

- (1) Algebraic polynomial approximation of different degrees α . The program automatically chooses the most precise degree, which corresponds to the best accuracy of the moment of extremum.

$$x_c(u) = \sum C_\alpha \cdot f_\alpha(u), f_\alpha(u) = u^{\alpha-1}$$

- (2) "Symmetrical" algebraic polynomial approximation, which use only even degrees of deviation from point of symmetry.

$$x_c(u) = \sum C_\alpha \cdot f_\alpha(u), f_\alpha(u) = (u - u_0)^{2(\alpha-1)}$$

The next two methods are

- New Algol Variable, that was proposed by Andronov (2010, 2012):

$$x_c(u) = C_1 + C_2 \left(1 - \left(1 - \left(\frac{u - C_3}{C_4} \right) C_5 \right)^{1.5} \right)$$

- the function proposed by Mikulášek (2015), Mikulášek et al. (2015):

$$x_c(u) = C_1 + C_2 \left(1 - \left(1 - \exp \left(1 - \operatorname{ch} \left(\frac{u - C_3}{C_4} \right) \right) \right) C_5 \right)$$

In these forms, the functions are applied for approximation of the whole light curve. In the case, where the data are just close to the extremum, the matrix of normal equations becomes degenerate. The interval does not contain out-of-eclipse parts, and therefore we do not have enough data. Formally, the amplitude becomes infinite, and the error estimates are not available because of rounding errors.

To avoid degeneration of the matrix of the normal equation, the last two functions were expanded into the Taylor series, and the following approximations are used:

- (3) New Algol Variable (Andronov et al., 2017)

$$x_c(u) = C_1 + C_2 |z|^{C_6} + C_3 |z|^{2C_6}, \quad z = u - C_5$$

- (4) the function proposed by Prof. Z. Mikulášek (2015)

$$x_c(u) = C_1 + C_2 |z|^{C_6} + C_3 |z|^{C_6+2}, \quad z = u - C_5$$

These forms of functions realized in MAVKA.

In some cases, for example approximation of flat eclipses and exoplanet transitions, it is more precise to divide our data into three intervals, each of them is approximated by its own function. In this case, an additional parameter is the duration of the bottom part of the eclipse (total eclipse or a transit). This parameter is suggested to be listed in the “General Catalogue of Variable Stars” (GCVS, Samus’ et al., 2017).

The additional parameters (the borders between the three intervals) are determined by minimizing the test function (sum of the squares of the residuals of the data from the approximation) in respect to these parameters, and then corrected using differential equations. For the visualization, we have applied an own “gradient zebra” – type colour scheme (Andrych et al., 2017) instead of a classical “lines of constant level” (e.g. Tkachenko, 2016).

We have proposed some new methods for this case.

- (5) The Wall-Supported Parabola method (Andrych et al., 2017): part of data that is very close to extremum is approximated by parabola, but branches are approximated by a sum of a parabola and a contribution of another degree.

Let C_5 and C_6 be transition points from one function to another.

In the case of transition or eclipse for a small deviation of time from the point of the inner or outer contact, the flux increases/decreases proportionally to the difference $(C_5 - u)$ or $(u - C_6)$ in the non-integer power 1.5.

If $u < C_5$ then

$$x_c(u) = C_1 + C_2 \left(u - \frac{C_5 + C_6}{2} \right) + C_3(C_5 - u)^{1.5}$$

If $u > C_6$:

$$x_c(u) = C_1 + C_2 \left(u - \frac{C_5 + C_6}{2} \right) + C_3(u - C_6)^{1.5}$$

If $C_5 < u < C_6$:

$$x_c(u) = C_1 + C_2 \left(u - \frac{C_5 + C_6}{2} \right)$$

- (6) Wall-Supported Line (Andrych et al., 2017): it is nearly similar, but instead of the parabola, there is a constant line for the central interval. This method is useful for flat minima and it allows one to calculate the duration of the full eclipse or transition if the limb darkening effect can be neglected.

If $u < C_5$ then

$$x_c(u) = C_1 + C_2(C_5 - u)^{1.5} + C_3(C_5 - u)^{3.5}$$

If $u > C_6$:

$$x_c(u) = C_1 + C_2(u - C_6)^{1.5} + C_3(u - C_6)^{3.5}$$

If $C_5 < u < C_6$:

$$x_c(u) = C_1$$

- (7) Wall-Supported Asymptotic Parabola (this paper). The method improves the method of “Asymptotic parabola” (Marsakova and Andronov, 1996) by adding two parameters describing terms at the left and right interval, which correspond to ascending and descending branches. This method may be effective for approximation of the symmetric eclipses. For pulsating variables, it may be computed, but has no physical meaning.

If $u < C_5$ then

$$x_c(u) = C_1 + C_2(-D^2 - 2Dv) + C_3(C_5 - u)^{1.5}$$

If $u > C_6$:

$$x_c(u) = C_1 + C_2(-D^2 + 2Dv) + C_3(u - C_6)^{1.5}$$

If $C_5 < u < C_6$:

$$x_c(u) = C_1 + C_2v^2$$

where $D = \frac{C_6 - C_5}{2}$, $v = u - \frac{C_6 + C_5}{2}$.

- (8) Parabolic Spline (this paper). This approximation has more parameters than previous ones. Therefore, transition points from one function to another are C_6 and C_7 . The method improves the method of “Asymptotic parabola” (Marsakova and Andronov, 1996) by adding two parameters describing parabolic terms at the left and right interval. This method allows to extend the width of the interval (and so to increase the number of points) to get a same accuracy, as the “Asymptotic parabola”.

If $u < C_6$ then:

$$x_c(u) = C_1 + C_2u + C_3u^2 + C_4(C_6 - u)^2$$

If $u > C_7$:

$$x_c(u) = C_1 + C_2u + C_3u^2 + C_5(u - C_7)^2$$

If $C_6 < u < C_7$:

$$x_c(u) = C_1 + C_2u + C_3u^2$$

- (9) Asymptotic Parabola.

There are two lines “asymptotes”, which are connected with a parabola, so the function and it’s derivative are continuous. Previous experience had shown, that this is one of the best methods for asymmetrical maxima of generally pulsating variables. This method was originally proposed by Marsakova & Andronov (1996).

The transition points from one interval to another are C_4 and C_5 .

If $u < C_4$ or $u > C_5$ then:

$$x_c(u) = C_1 + C_2(2 \text{ abs}(v) - D)D + C_3v$$

If $C_4 < u < C_5$ then:

$$x_c(u) = C_1 + C_2v^2 + C_3v$$

where $D = \frac{C_5 - C_4}{2}$, $v = u - \frac{C_5 + C_4}{2}$.

MAVKA interface

The program was elaborated in the programming environment Delphi 7.

In MAVKA, the user can choose few methods and the algorithm automatically defines the method, which corresponds to the best accuracy of the moment of extremum (Fig. 1).

In an addition, the user can control results, because while the approximation may be mathematically accurate, formally the values of parameters may be out of physically realistic intervals (Fig. 2).

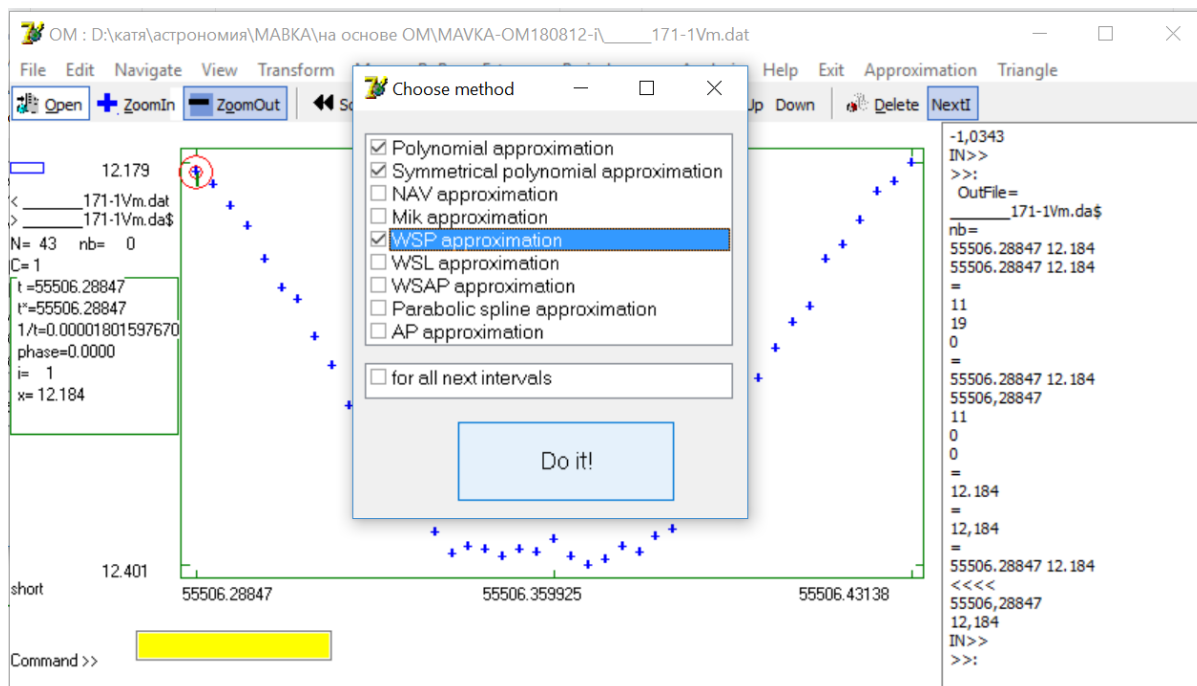


Figure 1: MAVKA submenu for choosing some approximation methods.

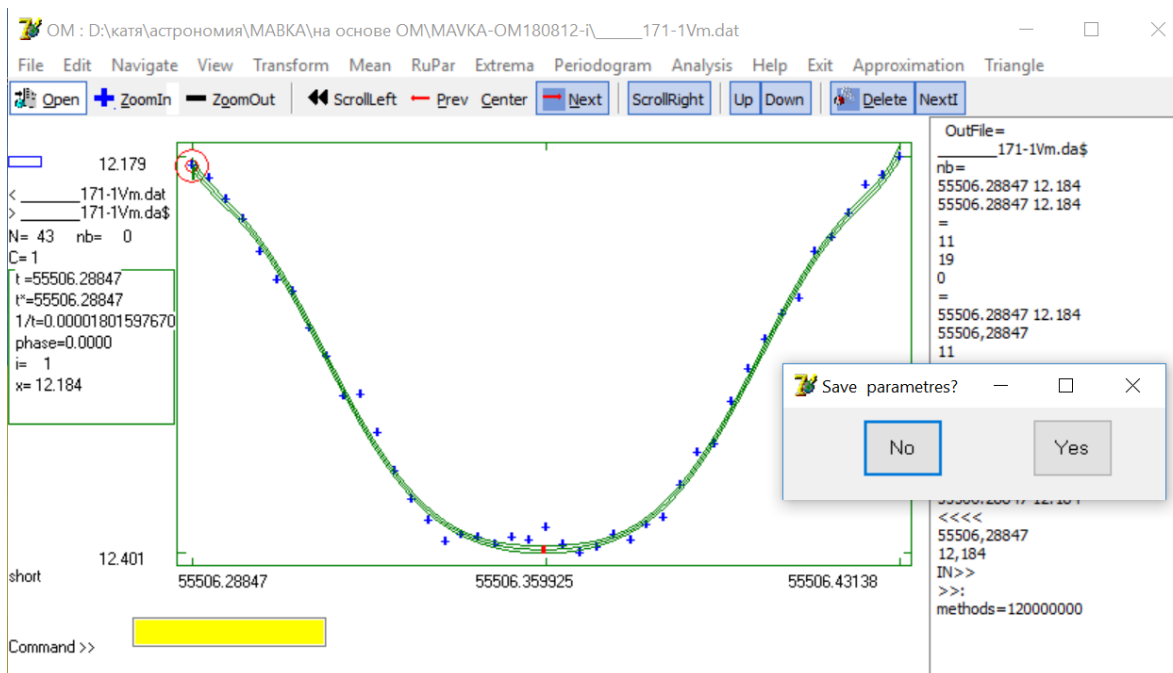


Figure 2: The possibility of visual control of approximation and results.

Application to Variable Stars of Different Types

Previous versions of the program, which was being improved for difficult cases of the distribution of the times (phases) of the observations in selected intervals near extrema, were applied to observations of some eclipsing binary stars (Savastru et al, 2017; Tvardovskyi et al., 2017, 2018) and symbiotic variables (Marsakova et al., 2015). This new version of the program is planned to be used for compilation of the characteristic of extrema of pulsating, eclipsing and interacting binary stars based on data from photometric surveys and own monitoring.

Discussion and Conclusion

We have introduced the program MAVKA. It allows the user to choose statistically optimal phenomenological approximation for a given data sample and determine characteristics of extrema with the best accuracy in case, when the data are just close to the extremum. This is the main mode of the observations by the “hunters” for the “extrema timings” = ”Times of Minima/Maxima” = ToMs”. Besides the ToM, the brightness at the extremum is determined, and (for the “3-interval” functions (5,6,7,9)) the duration of the full eclipse/transit. The error estimates for each parameter are determined.

The program allows one to determine the parameters either for the data at the screen, or by using a list of previously marked intervals – in this case, one may automatically determine the statistically optimal phenomenological approximations for all intervals and then check the quality of approximation by comparing with the data.

We have presented 9 different approximation functions, but we allow the determination of the statistically optimal degree of the polynomial or “symmetric polynomial”, so currently there are 20 functions to be used for the comparison.

The methods (1, 8, 9) may be recommended for approximation of generally asymmetric extrema, whereas the rest (2-7) are focused on the theoretically symmetric extrema.

Acknowledgement

We thank Doc. RNDr. Vladyslava I. Marsakova, Lewis M. Cook, Anton Paschke, Mgr. Kateřina Hoňková, Doc. RNDr. M. Zejda and Prof. RNDr. Zdeněk Mikulášek for discussions. This work is related to the international projects “Inter-Longitude Astronomy” (ILA, Andronov et al., 2003, 2017) and “Ukrainian Virtual Observatory”, “Astroinformatics” (Vavilova et al. 2017). The preprint was published in astro-ph [1812.06949](https://arxiv.org/abs/1812.06949).

References

- AAVSO, 2018, <https://sites.google.com/site/aavsoebsection/determining-time-of-minimum>
- Andronov I.L., 1994, OAP, 7, 49, [1994OAP.....7...49A](#)
- Andronov I.L., 2001, OAP, 14, 255, [2001OAP....14..255A](#)
- Andronov I.L., 2005, ASPC, 335, 37, [2005ASPC..335...37A](#)
- Andronov I.L., 2010, Int. Conf. KOLOS-2010 Abstr. Booklet, Snina, Slovakia, 1, <http://www.astrokarpaty.net/kolos2010abstractbook.pdf>
- Andronov I.L., 2012, Astrophysics, 55, 536, [2012Ap.....55..536A](#)
- Andronov I.L. et al., 2003, Astron.Astroph.Trans.,22, 793, [2003A%26AT...22..793A](#)
- Andronov I.L. et al., 2017, ASPC, 511, 43, [2017ASPC..511...43A](#)
- Andronov I.L., Breus V.V, 2013, Astrophysics, 56, 518, [2013Ap.....56..518A](#)
- Andronov I.L., Marsakova V.I., Kudashkina L.S., Chinarova L.L., 2014, AASP, 4, 3, [2014AASP....4....3A](#)
- Andronov I.L., Tkachenko M.G., Chinarova L.L. , 2017, Astrophysics, 60, 57, [2017Ap.....60...57A](#)
- Andronov I.L., Andrych K.D., 2014, OAP, 27, 38A, [2014OAP....27...38A](#)
- Andrych K.D., Andronov I.L., Chinarova L.L., Marsakova V.I., 2015, OAP, 28, 158, [2015OAP....28..158A](#)
- Andrych K.D., Andronov I.L., Chinarova L.L., 2017, OAP, 30, 57, [2017OAP....30...57A](#)
- Brát L., Mikulášek Z., Pejcha O., 2012, http://var2.astro.cz/library/1350745528_ebfit.pdf
- Breus V.V., 2007, OAP, 20, 32, [2007OAP....20...32B](#)
- Chinarova L.L., Andronov I.L., 2000, OAP, 13, 116, [2000OAP....13..116C](#)
- Kreiner J.M., Kim Chun-Hwey, Nha Il-Seong, 2001, “An Atlas of O-C Diagrams of Eclipsing Binary Stars”, Cracow, Poland: Wydawnictwo Naukowe Akademii Pedagogicznej, [2001aocd.book....K](#)
- Kwee K.K., van Woerden H., 1956, BAN, 12, 327, [1956BAN....12..327K](#)
- Marsakova V.I., Andronov I.L., 1996, OAP, 9, 127, [1996OAP.....9..127M](#)
- Marsakova V.I., Andronov I.L., Chinarova L.L., Chyzyk M.S., Andrych K.D., 2015, Częstochowski Kalendarz Astronomiczny 2016, 269, [2015CKA....12..269M](#)
- Mikulášek Z. 2015, A&A, 584A, 8, [2015A&A...584A...8M](#)
- Mikulášek Z., Zejda M., Pribulla T., Vaňko M., Qian S.-B., Zhu L.-Y., 2015, ASPC, 496, 176, [2015ASPC..496..176M](#)
- Samus' N.N., Kazarovets E.V., Durlevich O.V., Kireeva N.N., Pastukhova E.N., 2017, ARep, 61, 80, [ARep. 61, 80.](#)
- Savastru S.V., Marsakova V.I., Andrych K.D., Dubovsky P., 2017, OAP, 30, 126, [2017OAP....30..126S](#)
- Tkachenko M.G., 2016, AASP, 6, 73, [2016AASP....6...73T](#)
- Tkachenko M.G., Andronov I.L., Chinarova L.L., 2016, JPhSt, 20, 4902, [JPhSt. 20. 4902.](#)
- Tsevevich V.P., 1970, “Peremennye zvezdy i sposoby ikh issledovaniia.”, Moskva, Nauka, 240 p. [1970pzi.book....T](#)
- Tsevevich V.P., 1971, “Instationary stars and methods of their investigation. Eclipsing variables”, Moskva, Nauka, 352 p. [1971isme.conf....T](#)
- Tvardovskiy D.E., Marsakova V.I., Andronov I.L., 2017, OAP, 30, 135, [2017OAP....30..135T](#)
- Tvardovskiy D.E., Marsakova V.I., Andronov I.L., Shakun L.S., OAP, 2018, 31, 103, [2018OAP....31..103T](#)
- Vavilova I.B., Yatskiv Ya.S., Pakuliak L.K., Andronov I.L., Andruk V.M., Protsyuk Yu.I., Savanevych V.E., Savchenko D. O., Savchenko V.S., 2017, IAU Symposium, 325, 361, [2017IAUS..325..361V](#)

New tool with GUI for fitting O-C diagrams

P. GAJDOŠ & Š. PARIMUCHA

(1) Institute of Physics, Faculty of Science, Pavol Jozef Šafárik University, Košice, Slovakia,
pavol.gajdos@student.upjs.sk

Abstract: There are many different methods for fitting and analysing O-C diagrams. We present a new fitting tool for an analysis of O-C diagrams. Our package use Genetic Algorithms (GA) and Markov Chain Monte Carlo (MCMC) methods. Unlike many others fitting routines, our method does not need any initial values of fitted parameters. Fitting using presented software is quite simple thanks to a very intuitive graphic user interface. Currently, nine most common models of periodic O-C changes are included in this software.

1. Introduction

The precise timing of minima of eclipsing binaries (EBs) or extrema times of any other periodic events, which is a quite simple observational task and is also achievable with amateur's technique, could help us to discover interesting processes in the studied system. The most common phenomena are connected with a mass transfer between the components of EB, the presence of another body in the system, apsidal motion or angular momentum lost from the system.

Unfortunately, the exact physical model of many of these effects is complicated and strongly non-linear. Using classical fitting routines is problematic. The good initial values of parameters are needed by many of them. One can use the approximation of the model by Taylor or Fourier series but the physical properties of the model are loosening. In this paper, we present a new fitting tool for analysing the changes of times of minima of EBs or exoplanetary transits. We use Genetic Algorithms to remove the necessity of any input values of the model's parameters. Final values of them together with their statistically significant uncertainties are obtained using Markov chain Monte Carlo fitting. The combination of these two algorithms allows us to analyse the exact physical model of the observed variations.

2. Period changes models of eclipsing binaries and exoplanets

Minima times T_C of EBs or transits of extrasolar planets can be simply calculated by the linear ephemeris

$$T_C = T_0 + P \times E \quad (1)$$

which predicts minima times T_C of EB with orbital period P . Here E is an epoch of the observation and it counts how many eclipses elapsed since the zero epoch (i.e. from time T_0).

Minima times determined from observations for the same epoch (T_O) are in general different to times T_C . The behaviour of this difference (O-C), often shown in O-C diagrams, is caused by perturbation δT

$$T_O - T_C \equiv O - C = \delta T \quad (2)$$

This perturbation is generally a sum of different effects and it indicates period changes of the binary system. Formally, we can write

$$\delta T = (\Delta T_0 + \Delta P \times E) + Q \times E^2 + \delta T_i \quad (3)$$

where the part in bracket generates linear trend in (O-C)s and it is caused by wrong linear ephemeris (Equation 1), a quadratic term ($Q \times E^2$) describes changes due to mass transfer and δT_i means more complex periodic variations in (O-C)s (described in the next sections).

2.1 The light-time effect

The apparent changes of binary stars period caused by the distance variation of the system from the observer are often called the light-time effect (LiTE). The EB moves around the common barycentre of a wider triple system. It produces periodic variations in the observed minima times with respect to linear ephemeris of the EB with a period corresponding to the period of the third body. The secondary minima have identical behaviour in (O-C)s with primary ones.

Irwin (1952) determined analytical formula for O-C changes caused by LiTE, which can be written in the form

$$\delta T_{LiTE} = \frac{a_{12} \sin i_3}{c} \left[\frac{1-e_3^2}{1+e_3 \cos v_3} \sin(v_3 + \omega_3) + e_3 \sin \omega_3 \right] \quad (4)$$

where $a_{12} \sin i_3$ is the projected semi-major axis of the binary star around the barycentre of a triple system, i_3 is the inclination of the third body's orbit, e_3 is the eccentricity, v_3 is the true anomaly of the binary orbit around the system's barycentre and ω_3 is the longitude of pericenter. Two another orbital parameters, the period of the third body P_3 and the time of pericenter passage t_{03} are hidden in v_3 calculation, which have to be solved using Kepler equation. Equation 4 can be simply extended for another body(ies) in the system.

Because we are not able to find inclination of the orbit i_3 only from O-C analysis, we can determine only so-called mass function

$$f(M_3) \equiv \frac{(M_3 \sin i_3)^3}{M^2} = \frac{(a_{12} \sin i_3)^3}{P_3^2} \quad (5)$$

of the third body. Here, $M = M_1 + M_2 + M_3$ is a total mass of the system (M_i - masses of components).

Semi-amplitude of changes on O-C diagram generated by LiTE is given by equation:

$$K_3 = \frac{a_{12} \sin i_3 \sqrt{1-e_3^2 \cos \omega_3}}{c} \quad (6)$$

2.2 Agol's models

Agol et al. (2005) presented two models of O-C changes concerning on transits of exoplanets. O-C variations are caused by gravitational interaction with another body (planet) in the system. They assumed that the orbits of transiting exoplanet and the third body are coplanar with inclination $i = 90^\circ$.

The first one is the model of perturbations due to an interior planet on small orbit:

$$\delta T_{AgolIn} = -P \frac{\mu_3 r_3 \cos(v + \omega_3) \sqrt{1-e^2}}{2\pi a(1-e \sin \omega)} \quad (7)$$

where P is a period of transiting planet, a is its semi-major axis, e eccentricity of its orbit, v its true anomaly and ω its longitude of pericenter; r_3 is the radius of the orbit of the 3rd body, ω_3 its longitude of pericenter and $\mu_3 \equiv M_3/M$ ($M = \sum M_i$ is a mass of the whole system) is its reduced mass. Semi-amplitude of changes on O-C diagram generated by Agol's interior perturber is given by the equation:

$$K_3 = P \frac{\mu_3 r_3 \sqrt{1-e^2}}{2\pi a(1-e \sin \omega)} \quad (8)$$

For perturbations due to an exterior planet on a large eccentric orbit, Agol et al. (2005) determined the formula:

$$\delta T_{AgolEx} = \frac{\mu_3}{2\pi(1-\mu_3)} \frac{P^2}{P_3} (1-e_3^2)^{-3/2} (v_3 - l_3 + e_3 \sin v_3) \quad (9)$$

where P_3 is the period of the 3rd body, e_3 eccentricity of its orbit, v_3 its true anomaly and l_3 its mean anomaly. Other parameters are the same as for a case of interior perturber. Semi-amplitude of changes on O-C diagram generated by this model is given by the equation:

$$K_3 \approx \frac{\mu_3}{2\pi(1-\mu_3)} \frac{P^2}{P_3} (1-e_3^2)^{-3/2} 2 \left[\arctan \frac{e_3}{1+\sqrt{1-e_3^2}} + e_3 \right] \quad (10)$$

2.3 Apsidal motion

Apsidal motion is the precession of the orbit due to a gravitational quadruple moment induced by tidal distortion in a binary star. The secondary minima are in antiphase with primary ones in the O-C diagram. The pericenter position ω at epoch E is defined by the linear equation $\omega = \omega_0 + \dot{\omega} \times E$ where ω_0 is initial position of pericenter and $\dot{\omega}$ is angular velocity of line of the apsides.

Giménez & Bastero (1995) determined the formula for O-C changes in the form

$$\delta T_{APS} = \frac{P}{\pi} \sum_{n=1}^{\infty} (-\beta)^n \left(\frac{1}{n} + \sqrt{1-e^2} \right) \sin n v \quad (11)$$

where P is anomalistic period of EB (i.e. time between two primary or secondary eclipses), $v = \theta - \omega + \pi/2$ is true anomaly ($\theta = 0$ for primary minima and $\theta = \pi$ for secondary minima) and $\beta = e/(1 + \sqrt{1-e^2})$.

Semi-amplitude of changes on O-C diagram is

$$K_3 \approx \frac{Pe}{\pi}. \quad (12)$$

The sidereal period of EB is given by the equation

$$P_S = P \left(1 - \frac{\dot{\omega}}{2\pi}\right) \quad (13)$$

and the period of apsidal motion (and also period of the variation in O-C diagram) is

$$U = P_S \frac{2\pi}{\dot{\omega}} = P \left(\frac{2\pi}{\dot{\omega}} - 1\right). \quad (14)$$

3. Fitting methods

Many classical numerical methods based on the iterative minimization of the sum of squares (e.g. Levenberg-Marquardt algorithm or Simplex method) are used to obtain the optimal set of model's parameters. These algorithms can be simply implemented in many programming languages and data analysis packages and solution can be found relatively fast. However, the quality of the results (i.e. their convergence to the global optimum) is strongly dependent on an initial guess of fitted parameters which have to be close enough to the final one.

Here we introduce our approach to improve it. Our method does not require any starting values. It needs only searching interval where the values of parameters should be. The Genetic algorithms (GA) are used to obtain the first guess of parameters. They are improved by Markov Chain Monte Carlo (MCMC) fitting. MCMC is also used to calculating the realistic statistically significant estimation of uncertainties of the fitted parameters. These errors are underestimated in many cases if some classical fitting method, which calculates errors using the covariance matrix, is used.

3.1 Genetic Algorithms

Genetic Algorithms are commonly used for solving optimization problems which could not be solved using classical optimization methods (Weise, 2011). The basic scheme of GA is inspired by biologic evolution. The general principles of evolution could be summarized in several points:

1. There is a population of individuals.
2. There is a variability of properties of individuals.
3. Individuals with different properties have a different reproductive capacity.
4. Properties of descendant are correlated with properties of parents.

Similarly to biologic evolution, generating a new generation of individuals in GA include the impact of crossover and mutations which change individuals in the next generation. When fitting data using GA, individuals are made up of values of fitted parameters of the model. Crossover is realized by changing the values of some parameters between two individuals in parent generation. Mutations cause changing of the parameter by adding random value from a Gaussian distribution.

The main advantage of fitting data with GA is that start values of fitted parameters are unnecessary. We only need to know search limits for these parameters. In our case, we could set really wide limits which could be simply set from physics of the EBs or directly from O-C diagram. Fitting is not very computationally intensive and takes a relatively short time comparing to Monte Carlo method. On the other hand, GA fitting does not give any information about the errors of fitting parameters. This problem could be solved using MCMC fitting.

3.2 Monte Carlo method

Monte Carlo is one of the most used stochastic optimization methods (Brooks et al., 2011). The basic idea is to obtain states of the studied system which are from the required distribution, by generating random numbers from the uniform distribution. We use Metropolis algorithm which generates Markov chains. The MCMC method converges to the normal distribution of states. Uncertainties of all parameters can be easily estimated from this final distribution.

MCMC method gives us, unlike the GA, the estimation of errors of fitted parameters. However, MCMC fitting needs to know the initial values of parameters. For this reason, we have to use another fitting method before using MCMC itself. Fitting with MCMC is very computationally intensive and takes approx. five times longer than fitting with GA (with the same number of calculations of the model).

4. Package description

We developed a stand-alone package written in python for fitting O-C diagrams of EBs and exoplanets. Its name is OCFit. The package contents four main classes for fitting linear (FitLinear) and quadratic trends (FitQuad) and complex changes on O-C diagram (OCFit) and for loading the saving state of O-C analysis (OCFitLoad). There are also three auxiliary classes for working with GA and for analysis of GA and MCMC sampling.

The parameters of class OCFit could be saved to file using its function Save. After that, the state of class OCFit could be fully restored using function Load or using class OCFitLoad.

Our python package allows performing the complex study of O-C changes. Its detail description is above the scope of this paper. The manual for using our class in own python script could be found on our GitHub page⁶.

5. Graphic user interface

Our graphic user interface (GUI) can be used to basic control of class OCFit (see Sec. 4). Not all functions and control parameters are available here. However, the combination of this GUI with your own python script to work with OCFit class is still possible.

Design of GUI is quite simple (see Figure 1). It is created using standard python package Tkinter⁷. Many buttons are available only after successful executing previous necessary actions (e.g. showing the results is not available before fitting).

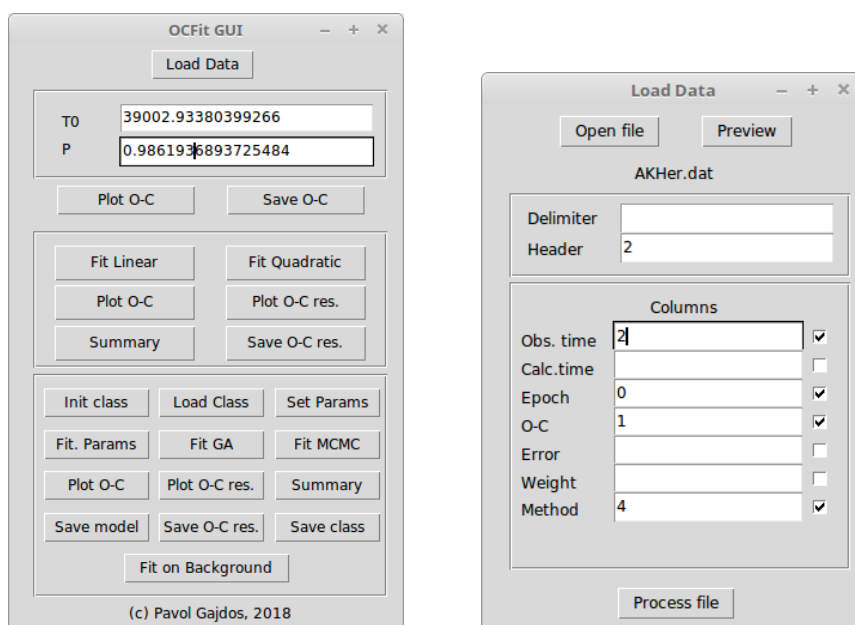


Figure 1: Main window of GUI (left). Window for loading data (right).

5.1 Loading data and linear ephemeris

Input O-C data can be loaded from any text file in which are data stored in columns. The columns could be separated by any character which is not used in data columns. Using header with an optional number of rows is also possible. Rows marked as python comments (i.e. started with "#") are skipped automatically.

The columns in input file could be:

- observed times of minima in Julian dates
- calculated times of minima in Julian dates
- epochs

⁶ <https://github.com/pavolgaj/OCFit>

⁷ <https://wiki.python.org/moin/TkInter>

- O-Cs in days
- errors of O-C in days
- weights
- used methods of O-C determination

Not all of them are necessary. The minimal required data are observed times of minima or calculated times with O-Cs. The setting of errors is also recommended. If the column with the used methods is presented, the error or weight of each individual method will be set in the next step. It is better to use errors of O-C measurements instead of their weights. Figure 1 shows the window for loading data. The parameters in this figure are set for loading data from a text file with O-C data from on-line database O-C gateway operated by the Czech Astronomical Society⁸ (Paschke & Brat, 2006).

The next step of the basic workflow is to enter the linear ephemeris of the studied system. The linear ephemeris should be very accurate. After that, the O-C diagram calculated from this ephemeris could be shown. If the linear ephemeris is not correct or also the quadratic trend is presented on the O-C diagram, it could be fitted separately before analysing more complicated changes. Now, the OCFit class could be initialized.

These steps could be skipped by loading already saved OCFit class from the file.

5.2 Parameters of model

Currently, there is nine model available for fitting. Adding other models is, of course, possible and it is planned. Available models are

- LiTE3 - LiTE caused by the 3rd body (see Sec. 2.1)
- LiTE34 - LiTE caused by the 3rd and 4th body (see Sec. 2.1)
- LiTE3Quad - combination of LiTE3 model and quadratic trend
- LiTE34Quad - combination of LiTE34 model and quadratic trend
- AgolInPlanet - model of inner perturber (see Sec. 2.2)
- AgolInPlanetLin - combination of AgolInPlanet model and linear trend
- AgolExPlanet - model of exterior perturber (see Sec. 2.2)
- AgolExPlanetLin - combination of AgolExPlanet model and linear trend
- Apsidal - model of apsidal motion (see Sec. 2.3)

It is necessary to set the values of all the fixed parameters of the model. If only the MCMC method (see Sec. 3.2) will be used, the values of fitted parameters are also required. The limits (minimum and maximum) and steps of all fitted parameters are needed in a case of using any of fitting method.

The limits of the parameters could be set extremely large in many cases (see Figure 2) and could be guessed from the O-C diagram. For example, eccentricity (e) and longitude of pericenter (w) could run in their whole possible range, i.e. e from 0 to 1 and w from 0 to 2π . The relative width of the interval of a period of the 3rd (or 4th) body could be about 40% and the same for its time of pericenter passage. The values of the projected semi-major axis of the binary star around the barycentre ($a_{\sin i}$) could go from very small values to values a few times larger than the real value. However, the interval for linear ephemeris should be as small as possible. In general, we recommend not to fit linear ephemeris together with more complicated models at all.

5.3 Fitting model

For the successful fitting of the model, setting good parameters of the fitting method is needed (see Figure 2). The parameters (together with their suggested values) of GA (see Sec. 3.1) are

- generation - the number of generations; 100 for testing and at least 1000 for final fitting
- size - size of one generation; 100 for testing and at least 1000 for final fitting

⁸ <http://var2.astro.cz/ocgate/>

The values of both parameters are the same in many cases. Generally, the extending the size of generation would produce a better solution than increasing the number of generation by the same value. The number of calculations of the model is *the number of generations* × *the size of one generation*.

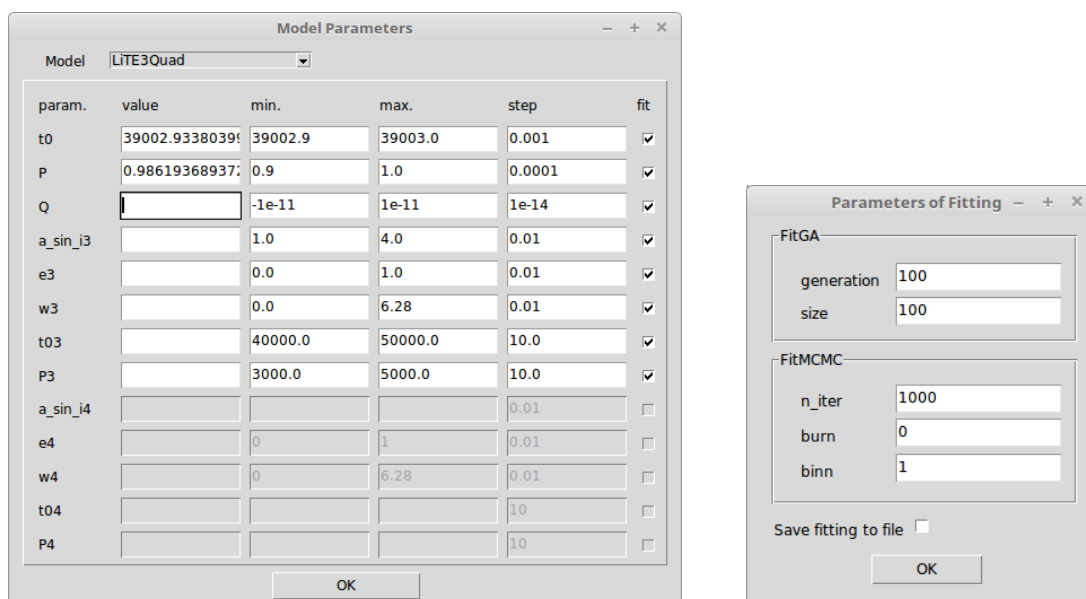


Figure 2: Windows for setting parameters of the model (*left*) and that of the fitting methods (*right*).

The setting of the good values of the MCMC method (Sec. 3.2) could be more complicated. They are

- `n_iter` - number of iterations; 1000 for testing and at least 10^6 for final fitting
- `burn` - number of the removed MC steps (before equilibrium); 0 for testing and at least 1000 for final fitting
- `bin` - size of one block for binning; 1 for testing and at least 10 for final fitting

In both fitting methods, it is necessary to set an appropriate number of iterations. This number is a compromise between computing time and the quality and accuracy of the results. The fitting routine (obtained sampling of the parameters) could be saved to file for later analysis. We use our own set of functions written in python for this purpose for GA sampling. Functions of python modules `pymc` (Patil et al., 2010) and `PyAstronomy` could be used to analyse MCMC sampling. These analyses are useful for evaluating the quality of the fitting.

The separate fitting using GA and MCMC is possible. We recommend using GA as a first fitting method. The first guess of values of parameters is obtained in this step. Their final values together with the estimation of their uncertainties are gotten using the MCMC method. It is possible to run fitting also on the background or to a generate fitting script which could be run later and/or on another computer (e.g. on computing server).

5.4 Working with results

We use python module `matplotlib` (Hunter, 2007) for displaying the final O-C diagram. The original O-C data together with model values could be displayed, e.g. O-C diagram of AD And in Figure 3. To check the quality of the fitting, the plot of residual O-Cs could be used.

All model's parameters are listed in a separated window (see Figure 3). The amplitude of (O-C)s (K) is also determined according to the used model (using the equations in Sec. 2). We also calculate the basic statistical indicators for evaluating the goodness of fit. They are the chi-squared error (χ^2), reduced chi-squared statistic (χ_r^2), Akaike information criterion (AIC), corrected Akaike information criterion (AICc) and Bayesian information criterion (BIC).

The model (O-C)s and residual (O-C)s could be saved to a text file. Eventually, the parameters of whole class `OCfit` could be saved to file and be used for later analysis. We strongly recommend to do it.

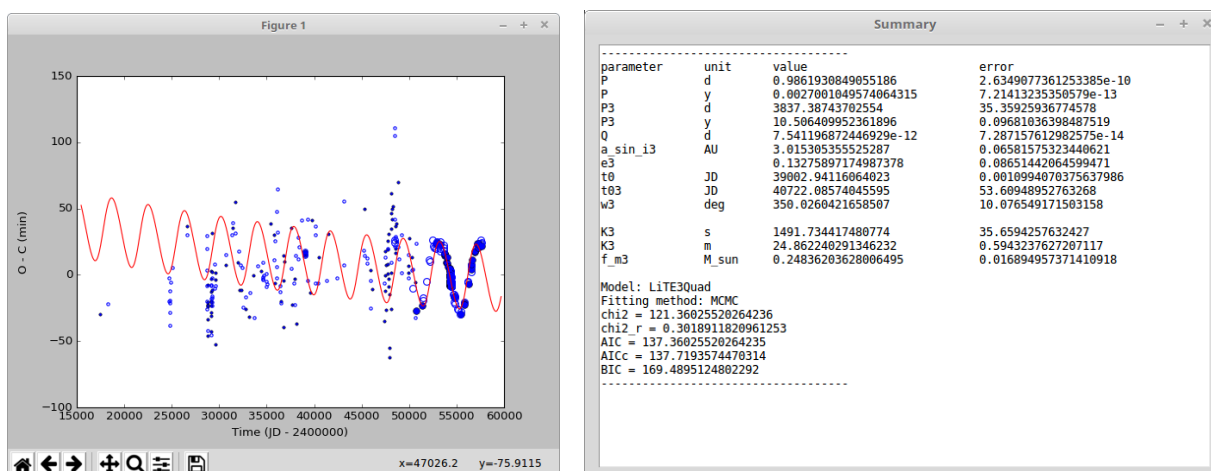


Figure 3: Graphic window with fitted O-C diagram of AD And (*left*) and window with summary of the model's parameters for the same O-C diagram (*right*).

6. Conclusion

The presented python package OCFit combines the advantages of GA and MCMC method to analyse O-C diagrams. The only disadvantage could be quite long computing time but this is not so big problem considering the current state of computer technology. We currently included nine models of O-C changes but it is possible to add other ones. We developed simple GUI to make work with our module easier. Both of them, python package and GUI, are available on our GitHub page⁹.

Our method gives very good results which are at least comparable with any other method. We already used it in two our papers (Gajdoš et al., 2017; Parimucha et al., 2018).

Acknowledgement

This paper has been supported by the grant of the Slovak Research and Development Agency with number APVV-15-0458. This article was created under project ITMS No.26220120029, based on the supporting operational Research and development program financed from the European Regional Development Fund. The research of P.G. was supported by internal grant VVGS-PF-2017-724 of the Faculty of Science, P. J. Šafárik University in Košice.

References

- Agol, E., Steffen, J., Sari, R., & Clarkson, W., 2005, MNRAS, 359, 567, [2005MNRAS.359..567A](#)
- Brooks, S., Gelman, A., Jones, G.L. & Meng, X., 2011. Handbook of Markov Chain Monte Carlo. Chapman & Hall/CRC, New York.
- Gajdoš P., Parimucha Š., Hambálek L., Vaňko M., 2017, MNRAS, 469, 2907, [2017MNRAS.469.2907G](#)
- Giménez, A., & Bastero, M., 1995, Ap&SS, 226, 99, [1995Ap&SS.226...99G](#)
- Hunter, J. D., 2007, Comput Sci Eng, 9, 90, [2007CSE.....9...90H](#)
- Irwin, J. B. 1952, ApJ, 116, 211, [1952ApJ...116..211I](#)
- Parimucha Š., Gajdoš P., Kudak V., Fedurco M., Vaňko M., 2018, RAA, 18, 47, [2018RAA...18...47P](#)
- Paschke, A., & Brat, L., 2006, OEJV, 23, 13, [2006OEJV...23...13P](#)
- Patil, A., Huard, D. & Fonnesbeck, C. J., 2010, J Stat Softw., 35, 1, [doi:10.18637/jss.v035.i04](https://doi.org/10.18637/jss.v035.i04)
- Weise, T., 2011. Global optimization algorithm - theory and application. 3rd ed. <http://www.it-weise.de/projects/bookNew.pdf>

⁹ <https://github.com/pavolgaj/OCFit>

Exoplanetary research in Czech Republic

M. SKARKA^{1,2,3}, P. KABÁTH², P. CAGAS^{3,4}

(1) Department of Theoretical Physics and Astrophysics, Masaryk University, Kotlářská 2, CZ-611 37 Brno, Czech Republic, maska@physics.muni.cz

(2) Astronomical Institute, Czech Academy of Sciences, Fričova 298, CZ-251 65 Ondřejov, Czech Republic

(3) Variable Star and Exoplanet Section of the Czech Astronomical Society, Vsetnska 941/78, CZ-757 01 Valasske Mezirc, Czech Republic

(4) BSObservatory, Modrá 587, CZ-760 01 Zlín, Czech Republic

Abstract: The investigation of extrasolar planets in Czech Republic is relatively new field. Recently, in times of many new exoplanetary discoveries, it is a very actual and prestigious topic. We focus on a brief summary of the research of exoplanets in Czech Republic, possible involvement of Czech observers in the exoplanetary research, and first results of observations with the Ondřejov Echelle Spectrograph regarding exoplanets.

Introduction

The motivation for studying exoplanets is closely tight with the basic natural questions about human origin and about the place of mankind in the Universe. However, there are, of course also questions related to the pure science such as: Is our Solar system unique? How many exoplanets are there? How do they look like? How do the planetary systems form and evolve? Investigation of exoplanets has a huge demands on the instrumentation and pushes the development of new instruments and analytical methods forward.

At the end of November 2018, we know almost 4000 exoplanets and about 3000 exoplanetary candidates (see e.g. <https://exoplanets.nasa.gov>). The diversity of the observed planets and planetary systems is stunning – we know planets of the size of Jupiter that orbit its host star with period of less than day (e.g. WASP-19b, Hebb et al. 2010), we know planets smaller than the Earth (e.g. Vanderburg et al. 2015), we can directly see alien planetary systems (e.g. Marois et al. 2008) and study the chemical composition of the planets themselves, as well as of their atmospheres (e.g. Zeng, Sasselov & Jacobsen 2016, Wytttenbach et al. 2015, Sedaghati et al. 2017).

The size of the needed telescope, the stability and capability of the instrument are defined by the purpose of observations and the desired accuracy. Study of Earth-sized planets and their characterization needs large telescopes and state-of-the-art instruments. However, Jupiter-size planets around bright low-mass main-sequence stars can be investigated with instruments and telescopes that are accessible to Czech observers. This is the topic that will be discussed in this proceedings.

Transit detection and observations.

Since the CCD cameras have become sensitive and cheap enough, the observations of exoplanetary transits is naturally the easiest way how to get involved in the exoplanetary research using small telescopes. Because the drop in brightness during the transit is defined as

$$\Delta F = \left(\frac{R_{\text{Planet}}}{R_{\text{star}}} \right)^2, \quad (1)$$

even amateur observers can easily detect and monitor exoplanetary systems with large planets compared to their host stars. Even a telescope with a few centimeters in diameter is sufficient for detection of an exoplanetary transit. This was well demonstrated during the summer school organized by the Czech Variable Star and Exoplanet Section of the Czech Astronomical Society (VSES CAS) in 2008 when the joint observation of HD 189733 took place (see Fig. 1). Transit observation is the most widespread activity of amateur observers regarding the exoplanetary research in the Czech Republic.

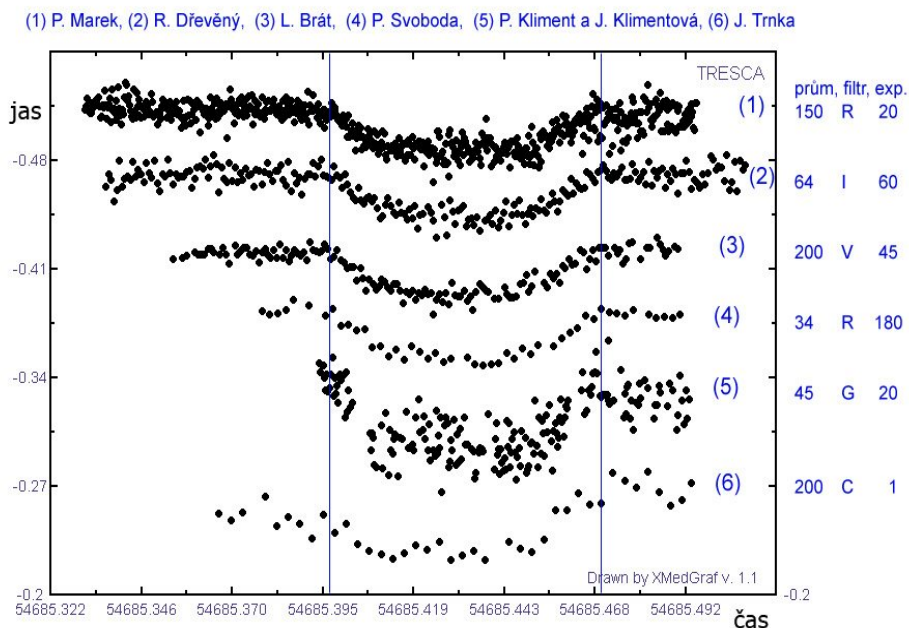


Figure 1: Joint observations of the transit of HD 189733. Figure taken from Sobotka (2008).

In 2008, the ETD and TRESKA databases maintained by VSES were launched (Poddaný, Brát & Pejcha 2010). In January 2019, ETD contains more than 8500 transit observations (336 exoplanets) similar to the one shown in Fig. 2. Most of the observations are produced by amateur observers not only from the Czech Republic but from all over the world.

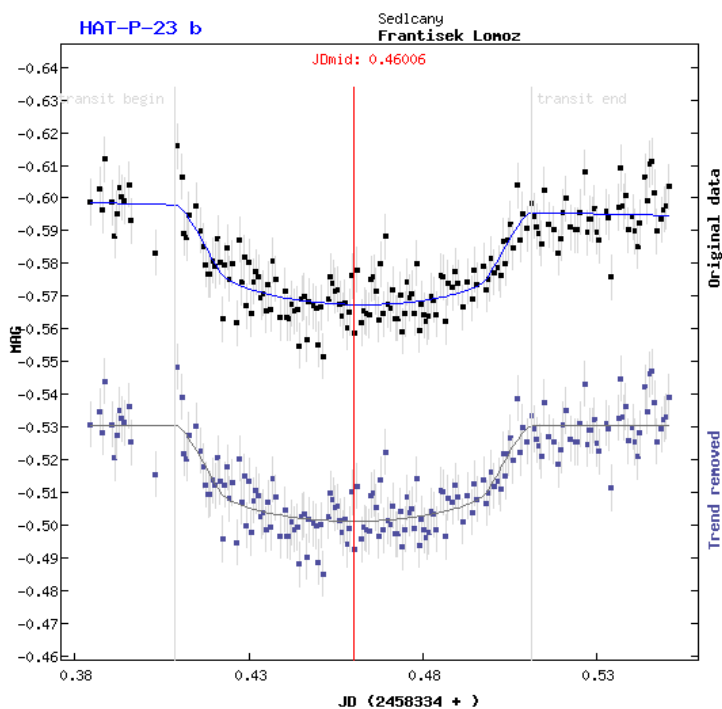


Figure 2: Example of transit observation performed by Czech amateur observer F. Lomoz. Figure is taken from the web page of VSES (<http://var2.astro.cz/tresca/transit-detail.php?id=1533369990&lang=cz>).

Transit method is the most efficient method for searching for new exoplanets because many target stars can be observed simultaneously. Exoplanetary candidates must be carefully evaluated. It can happen that the observed transit is actually shallow secondary minimum of an eclipsing binary (Fig. 3). Also, blends with background eclipsing binaries must be rejected. Blending can cause troubles in crowded fields and in large-field-of-view surveys that have broad point spread function such as SuperWASP (14''/px, Butters et al., 2010) or TESS (21''/px, Ricker et al., 2015).

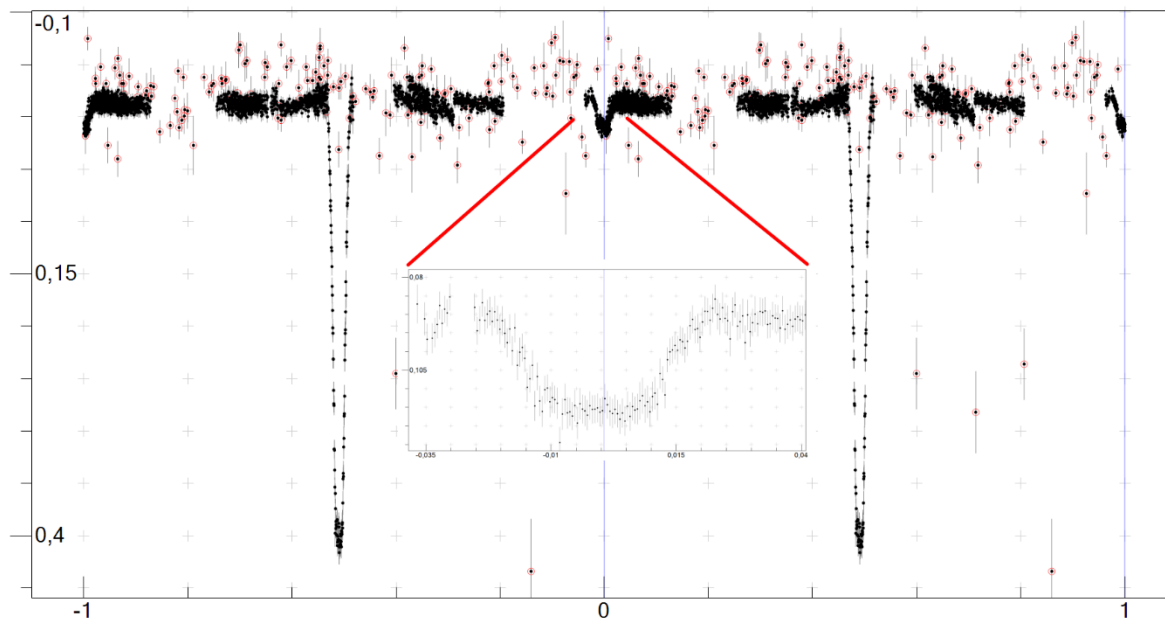


Figure 3: Example of a shallow secondary minima of an eclipsing binary that can mimic exoplanetary transit. The data were taken with a 30cm telescope from the ground (BSO, Zlín, Czech Republic).

Radial velocity measurements

The orbital movement of the exoplanet reflects in the movement of the star. The higher the mass of the exoplanet, the larger amplitude of the movement of the star. This translates in the same manner also to the velocity of the star, which can be measured unless we observe the system from pole of the orbit. Thus, measurements of radial velocities (RVs) can give us information about the minimal mass of the exoplanet. In case of transiting exoplanets, we can get the absolute mass of the exoplanet because we know the inclination from the shape of the transit.

RVs are measured from the Doppler shift of the spectral lines. The precision of the measurements increases with better signal, with the number of lines that are used for the RV estimation (the size of the used spectral region) and with resolving power of the spectrograph. Thus, larger telescopes equipped with an echelle spectrograph are advantageous. In Czech Republic, the 2-m Perek telescope in Ondřejov (the left panel of Fig. 4) can be used because it is equipped with the Ondřejov Echelle Spectrograph (OES, the right-hand panel of Fig. 4), which has broad spectral range (~360-950 nm) and high resolving power $R=50000$ (Koubský et al. 2004). Since 2017, this instrument is used by the exoplanetary group from the Astronomical Institute of CAS for monitoring of exoplanets and exoplanetary candidates.

The procedure from raw frame to RVs is very sophisticated and every step matters. First it is necessary to process the frames. Bias and flat-field corrections need to be applied, cosmic hits, bad pixels and columns need to be removed. Then, the spectrum from echelle orders is extracted, pixels are transformed to wavelengths by using Thorium-Argon lamp with well defined emission lines spread over a large spectral range. Then the spectra are normalized and stitched together to produce 1-d spectrum. However, this is still only the beginning.

The instrumental issues must be removed by shifting the spectra with respect to some stable lines. This can be, in the simplest way, done by using telluric absorption lines which are produced mainly by water vapour in the Earth's atmosphere. These lines are stable within 20 m/s. After this correction, the effect of the movement of the Earth around the Sun (30 km/s) and its rotation (465 m/s) are removed. Only then the RV measurements can be performed by comparing the shift between stellar lines.

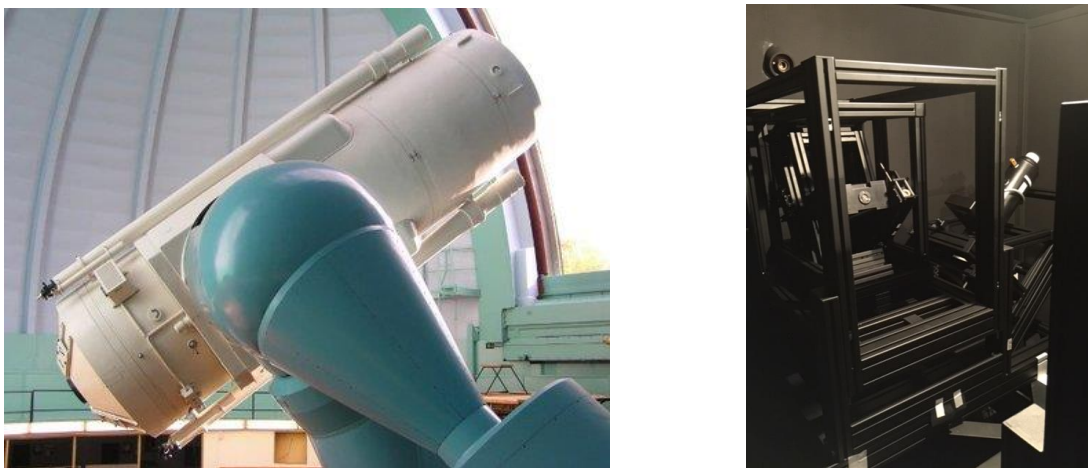


Figure 4: The Perek telescope in Onřejov (left panel) and the Ondřejov Echelle Spectrograph (right-hand panel).

From the tests performed on a bright radial velocity standard star HD 109358 (spectral type G0V, $V=4.25$ mag, exposure time 600 seconds) follows that we are able to reach stability of about 80 m/s over 8 hours, about 120 m/s over a few weeks and about 350 m/s over a year (Kabáth et al. 2019, submitted to AJ). This shows that we can monitor bright exoplanetary host stars and exoplanetary candidates hosting hot Jupiters producing RV variations with amplitudes of few hundreds of m/s. However, reasonable observations are limited to stars brighter than about 10 mag because below this limit the signal is too low even with 1-hour exposure.

Additional improvement of precision can be achieved by using iodine cell. It is a glass bulb filled with iodine vapour. During the observation, the cell is placed to the path of the light. The vapour absorbs light at precisely defined wavelengths. The disadvantage is the loss of light that can be half of the original intensity. Thus, it is usable only for bright stars. However, with this device, the stability down to about 10-20 m/s can be achieved for bright stars (tested on sig Dra and tau Cet).

In Ondřejov, we observed a few exoplanetary candidates from K2 mission (Howell et al. 2014) to evaluate their planetary nature. In three of them we found that the companions must be of stellar mass (Kabáth et al. 2019, submitted to AJ). We also discovered that one of the additional candidates is actually an Ap star showing delta Scuti pulsations which is orbited by low-mass star creating the first eclipsing binary system with Ap star (Skarka et al. 2019, submitted to MNRAS).

Other research and future prospects

Astronomers from the Astronomical Institute in Ondřejov work also on the exoplanetary atmospheres. Data from large telescopes (VLT, 3.6m telescope at La Silla) are used for this kind of investigation. However, in the brightest and largest exoplanets, the atmosphere should be theoretically detectable also in data taken with 2-m class telescopes (Kabát et al. 2019, submitted to AJ). We will monitor the candidates identified by the TESS mission (Ricker et al. 2014), which started to produce lots of new bright candidates. Perek telescope with OES can, thus, become a valuable instrument for the exoplanetary research. Identification of new bright exoplanetary candidates opens space for amateur observers to be involved. Czech astronomers plan to build a new echelle spectrograph PLATOSpec and mount it to 1.52-m telescope at La Silla in Chile. This telescope will be primarily dedicated for the spectroscopic follow-up for the PLATO mission.

Acknowledgement

MS acknowledges support from Postdoc@MUNI project CZ.02.2.69/0.0/0.0/16 027/0008360. PK acknowledges the financial support from GACR international grant 17-01752J.

References

- Butters, O. W.; West, R. G.; Anderson, D. R. et al. 2010, A&A, 520, 10, [2010A&A...520L..10B](#)
- Hebb, L.; Collier-Cameron, A., Triaud, A.H.M.J. et al. 2010, ApJ, 708, 224, [2010ApJ...708..224H](#)
- Howell, S. B.; Sobek, C.; Haas, M. et al. 2014, PASP, 126, 398, [2014PASP..126..398H](#)
- Koubský, P.; Mayer, P.; Čáp, J. et al. 2004, PAIC, 92, 37, [2004PAICz..92...37K](#)
- Marois, C.; Macintosh, B.; Barman, T. et al. 2008, Sci, 322, 1348, [2008Sci...322.1348M](#)
- Poddaný, S.; Brát, L.; Pejcha, O. 2010, NewA, 15, 297, [2010NewA...15..297P](#)
- Ricker, G. R.; Winn, J. N.; Vanderspek, R. et al. 2015, JATIS, 1a, 4003, 2015JATIS...1a4003R
- Sedaghati, E.; Boffin, H. M. J.; MacDonald, R. J. et al. 2017; Nature, 549, 238, [2017Natur.549..238S](#)
- Sobotka, P. 2008, <http://var2.astro.cz/e-perseus-detail.php?id=1218487384&parent=obcani.php&lang=cz>
- Vanderburg, A.; Johnson, J. A., Rappaport, S. et al. 2015, Nature, 526, 546, [2015Natur.526..546V](#)
- Wytttenbach, A.; Ehrenreich, D.; Lovis, C.; Udry, S. & Pepe, F. 2015, A&A, 577, 62, [2015A&A...577A..62W](#)
- Zeng, L.; Sasselov, D. D., Jacobsen, S. B. 2016, ApJ, 819, 127, [2016ApJ...819..127Z](#)

Binaries at Charles University

*In memory of RNDr. Pavel Mayer, DrSc.
(7.11.1932 - 7.11.2018)*

M. WOLF¹

(1) Astronomical Institute, Charles University, V Holešovičkách 2, CZ-180 00 Praha 8, Czech Republic

Abstract: Binaries of different types are frequent objects of long-term photometric and spectroscopic observations in the long history of the Astronomical Institute, Charles University in Prague. The overview of selected current results with significant contribution of SPHE members is briefly summarized. This research is part of an ongoing collaboration between professional astronomers and the Czech Astronomical Society, Variable Star and Exoplanet Section.

Introduction

Binaries of different types are traditionally targets of many systematic studies in history of the Astronomical Institute at Charles University in Prague for many years. In this paper we focused on the results obtained in collaboration with the Czech Astronomical Society, Variable Star and Exoplanet Section. Binaries of various types are on our current observing list: the most interesting are triple eccentric and eclipsing binaries with apsidal motion and light-time effect, multiple low-mass eclipsing binaries, cataclysmic variables, and symbiotic binaries.

Observations

There are two reflecting and computer-controlled telescopes devoted to CCD photometry of binaries at our disposal. For selected brighter systems, the photometric observations are also completed by spectroscopic measurements, mostly using the 2-m telescope in Ondřejov Observatory.

Telescope D65 at Ondřejov Observatory, Czech Republic

The 65-cm reflecting telescope located at Ondřejov Observatory near Prague is one of the most efficient telescopes used for the binary star research in our country (see Fig. 1a). It has been designed originally in 1972 by late Dr. Pavel Mayer as a Cassegrain telescope with a classical photoelectric photometer. In 1995 it was upgraded and a new CCD camera was placed to the primary focus. Nowadays there are several ongoing observing programs included photometry of near-Earth and binary asteroids (conducted by P. Pravec, AsÚ AVČR), new discoveries and follow-up of novae in M31 and M81 galaxies (K. Hornoch, H. Kučáková), flyby monitoring of the International Space Station (CIIRC ČVUT Praha), and bachelor, diploma and PhD theses of our students. The telescope has mounted a new G2-3200 CCD camera (chip KAF-3200ME, size 2184×1472, Moravian Instruments) and a set of BVRI photometric filters. The VNC/VPN connection enables a remote access to the telescope and CCD camera practically from anywhere.

Danish telescope D154 at La Silla in Chile

The 154-cm reflecting telescope located at La Silla observatory in Chile on the southern hemisphere was former ESO instrument (see Fig. 1b). Since 2012 it has a status of the Danish national telescope. The observing time is splitted between Niels Bohr Institute in Copenhagen and several groups of observers in the the Czech Republic: Ondřejov observatory, Prague and Brno universities, with different observing programs. The Large and Small Magellanic Clouds (LMC, SMC) are the main area of eclipse monitoring of several eccentric eclipsing binaries and multiple stellar systems. The binary asteroids are the subject of a study of investigators from Ondřejov led by also Petr Pravec. The VNC/VPN connection enables a remote access to the telescope and camera in Chile.



Figure 1: The 65-cm Charles University reflecting telescope at Ondřejov Observatory was built in 1972 by late Dr. Pavel Mayer (left, current photo by Kamil Hornoch). The Danish national telescope DK154 is located at La Silla observatory in Chile (right). Both telescopes are equipped with a CCD camera with a set of photometric filters and enable remote access.

Eclipsing binaries

Eclipsing binaries of various types are very frequent objects of our current detailed studies. They still represent a most general method how to derive the precise basic stellar parameters of the individual components such as radii, masses, or luminosities. With these quantities, we are able to improve and calibrate the existing stellar models (Torres et al. 2010). Moreover, the eclipsing binaries can serve as a suitable distance indicator, even for near-by galaxies in the Local Group (Hilditch et al. 2005). Monitoring of eclipses is a very simple and efficient tool especially for the period studies and enables participation of advanced amateur astronomers with small telescopes and modern detectors. Several different groups of binaries are discussed below.

Triple eccentric systems

The eccentric eclipsing binaries with an orbiting third body belong to an ideal laboratory of celestial mechanics. The study of apsidal motion in eccentric eclipsing binaries provides an important observational test of theoretical models of stellar structure and evolution (Claret & Giménez 1993). A detailed analysis of the period variations of an eccentric binary can be performed using the times of minimum light observed throughout the apsidal motion cycle, and from this, both the orbital eccentricity and the period of rotation of the periastron can be obtained with high accuracy. Rapid apsidal motion of an eccentric orbit connected with the light-time effect (LITE) presents an interesting variety of O-C diagrams with the superposition of both phenomena. The deviation of the observed values $(O-C)_{\text{obs}}$ from the linear ephemeris is given simply by

$$(O-C)_{\text{obs}} = (O-C)_{\text{aps}} + (O-C)_{\text{LITE}},$$

where $(O-C)_{\text{aps}}$ and $(O-C)_{\text{LITE}}$ are contributions from the apsidal advance of the eccentric orbit and the light-time effect caused by a third body, respectively. The theory of the third body motion and the LITE analysis was reviewed several times in the literature; see Mayer (1990), Sterken (2005), or Wolf (2014). For example, in the case of the eclipsing binary V0456 Oph the apsidal motion with short period $U = 22.6$ yr is superimposed with the light-time effect caused by the third body orbiting the eclipsing pair with the period of about 7.38 yr in a highly eccentric orbit ($e_3 = 0.8$, Fig. 2a). See more details in Wolf et al. (2017). The similar case is the well-known eccentric eclipsing binary DR Vul, where the apsidal motion with relatively short period $U = 36$ yr is modulated by the LITE with a longer period of 66.4 yr (Fig. 2b). Due to both relatively short periods (apsidal motion as well as the third-body orbit), the both systems exhibit the most interesting O-C diagrams known so far (Wolf et al. 2019). These results were published together with several active SPHE members, who contributed significantly by new CCD measurements.

Both above mentioned systems belong to the group of early-type eccentric and triple eclipsing systems with relatively short apsidal-motion and third-body orbital periods (e.g. V889 Aql, V539 Ara, GL Car, V974 Cyg, RU Mon, U Oph, AO Vel). It is highly desirable to obtain new high-dispersion spectroscopic material to obtain the radial-velocity curves and derive accurate masses of these triple systems.

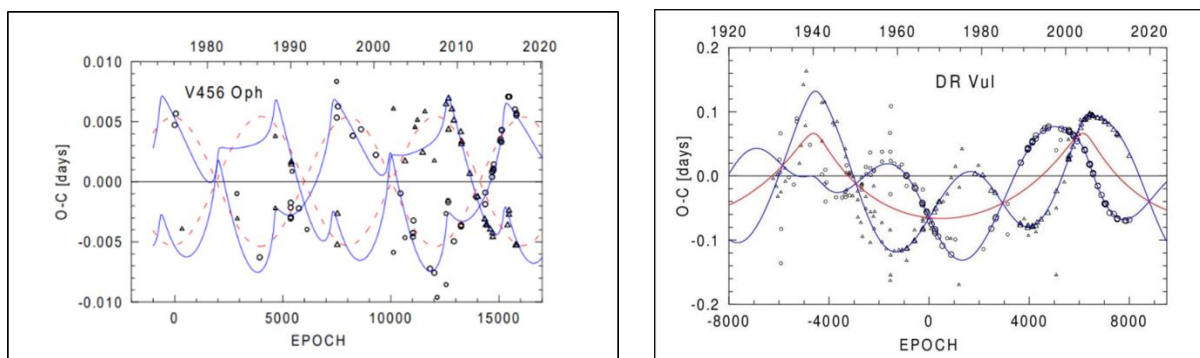


Figure 2: The historical O-C diagrams of two eccentric eclipsing binaries: V0456 Oph (left panel) and DR Vulpeculae (right). In case of V0456 Oph the rapid apsidal motion is influenced by the third body with relatively short orbital period of 7.4 years. In case of DR Vul the longer third body period (66 yr) is modulated by the apsidal motion with a short period of about 36 yr.

Table 1. Selected eccentric eclipsing binaries with third bodies studied photometrically by SPHE members in the past.

System	Sp. type	V_{\max} [mag]	P [day]	P_3 [yr]	$M_{3, \min}$ [M_{sun}]	U_{aps} [yr]
CG Aur	A7V	11.4	1.805	1.89	1.4	700
V974 Cyg	A3V	11.9	3.204	30.6	0.40	1470
V345 Lac	B5V	11.3	7.492	23.9	2.0	1580
RU Mon	B7V+B7V	10.5	3.585	59.8	1.63	361
AO Mon	B3V+B5V	9.6	1.885	3.56	2.5	33.8
V456 Oph	F1V+F2V	10.0	1.016	7.38	0.27	22.6
YY Sgr	B5V+B6V	10.2	2.628	18.6	0.81	294.7
DR Vul	B0V+B0.5V	8.64	2.251	66.4	7.15	36.1

V0361 Lyr

One of our long-term observing projects is devoted to an enigmatic eclipsing binary V0361 Lyrae. With the orbital period of roughly 7 hours creates a close near-contact binary system with a mass transfer from the evolved primary to the secondary. It was discovered as a variable star by Cuno Hoffmeister (1966). Later, Andronov & Richter (1987) noted a significant difference between heights of maxima of the light curve. The first spectroscopic and eclipse-mapping investigation was presented by Hilditch et al. (1997). They concluded, that light curve presents very probably a long-standing, elongated and shape-changing large hot structure or a hot region on the secondary component with temperature of about 10 000 K. The extraordinary brightening of 0.4 mag in V- band close to the phase 0.38 is well visible on Fig. 3a.

Regular photometric monitoring of V0361 Lyr and mid-eclipse timings since 1996 give us possibility to solve the different seasonal light curves using the well-known Phobe code (Prša & Zwitter, 2005). Up to 2016 the better results and cost function values were found for a semidetached configuration, later the light curves prefer a contact model (Fig. 3b). The corresponding changes of its orbital period are also visible on the current O-C diagram.

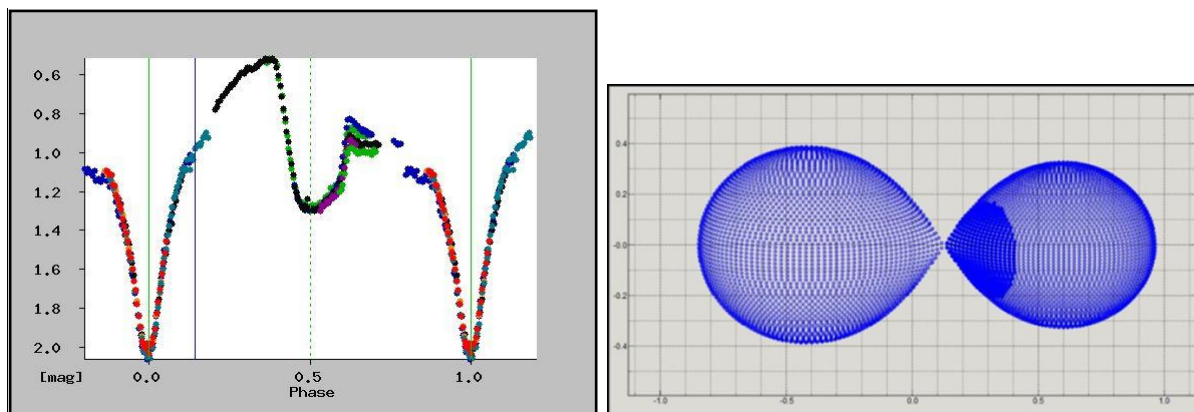


Figure 3: The light curve of V0361 Lyrae in V-band obtained during several nights in 2018. The brightening close to the phase 0.38 is clearly visible as well as variations of the light curve around phase 0.6 (left panel). The current solution of V0361 Lyr obtained in Phoebe leads to a contact binary configuration with a large hot region on the secondary component (right panel) instead of a previous semi-detached model.

Low-mas binaries

Low-mass binaries are a next interesting group of late-type main-sequence binaries, where masses of both components are usually less than 0.6 solar mass. Although M dwarfs are the most numerous stars in our Galaxy, their masses and radii are insufficiently calibrated. The origin of low-mass stars and brown dwarfs is still an unresolved question in star formation theory. Moreover, observations of low-mass stars show a discrepancy between estimated and modeled parameters, where the models give 5-10% smaller radii than observations. The identification and characterization of low-mass multiples is also highly relevant to exoplanet studies. Thus, low-mass stars and their multiple systems play an important role in stellar astrophysics.

Our long-term photometric program reveals that substantial number of these objects is in fact a multiple stellar system. In case of eclipsing binaries YY Gem (= Castor C) and GU Boo we discovered a substellar companion (probably a brown dwarf) with the mass of about 50 Jupiter mass only. Our results on five selected systems are summarized in Table 2; see also Wolf et al. (2016, 2018) for more details. These papers were published together with several advanced SPHE members, who contributed significantly by new CCD measurements.

Table 2. Low-mas eclipsing binaries with third bodies studied photometrically with contribution of SPHE members.

System	V [mag]	P [day]	P ₃ [yr]	M _{3, min} [M _{Jup}]
NSVS 01286630	13.08	0.38	3.61	108
NSVS 02502726	13.41	0.56	6.87	38
NSVS 07453183	12.50	0.37	1.14	434
GU Boo	13.11	0.49	11	54
YY Gem	9.27	0.81	54	49

Cataclysmic variables

Cataclysmic variables (CVs) are semidetached interacting binaries, consisting of a late-type star (secondary) and more massive white dwarf (primary). The secondary overfills its Roche lobe and the matter from the secondary is being transferred to the white dwarf. Around the primary with a relatively weak magnetic field is formed an accretion disc. The transferring matter hits the accretion disc and creates a shock-heating area called the bright spot. The CVs must lose their angular momentum to sustain the mass transfer process. There are two possible mechanisms of losing angular momentum: gravitational radiation (for $P_{\text{orb}} < 2$ h) and magnetic braking via the secondary star wind ($P_{\text{orb}} > 3$ h). This process of decreasing orbital period can be seen in O-C diagrams. The solution of the light curve of CVs thus belongs to rather more complicated task, including all four components: white dwarf, accretion disc with the bright spot and a late type secondary component. Four well-known systems

of similar brightness and short orbital period were studied for their possible period changes in the past: EX Dra, V2051 Oph, OY Car and Z Cha.

The dwarf nova EX Draconis is a frequently studied eclipsing binary system with an orbital period of about 5 h and deep eclipses (~1.5 mag). EX Dra was first detected in the Hamburger Quasar Survey (Bade et al. 1989) and was shown to be an eclipsing dwarf nova by Barwig et al. (1993). See also history of investigation of EX Dra in Pilarčik et al. (2012). The residuals with respect to the linear ephemeris show a cyclical behaviour. The current O–C data present a 21 yr period modulation with semi-amplitude of 2.5 min. Nevertheless, eclipse timings show significant deviations from the best sinusoidal fit, which indicates that this ephemeris is not the only and complete description of the data.

For three southern objects V2051Oph, OY Car and Z Cha we have also found cyclic period changes lasting 25, 29 and 43.5 years, respectively. Our results confirm that all three CVs below the period gap are interesting systems showing the cyclic period modulation, see Table 3 (Pilarčik et al. 2018). The most promising explanation of these cyclical changes seems to be existence of a solar-type magnetic activity in the secondary star (Applegate 1992, Lanza et al. 1998).

Our current observing list on the D65 telescope contains more than dozen of relatively well-known cataclysmic binaries for photometric monitoring: V1315 Aql, SDSS1435 Boo, AC Cnc, HT Cas, HS0455+8315 Cep, SDSS1544 CrB, Lan386 Cyg, EX Dra, newly discovered SU UMa-type CzeV404 Her (Cagaš & Cagaš, 2014), BH Lyn, SW Sex, RW Tri, TT Tri, and DW UMa.

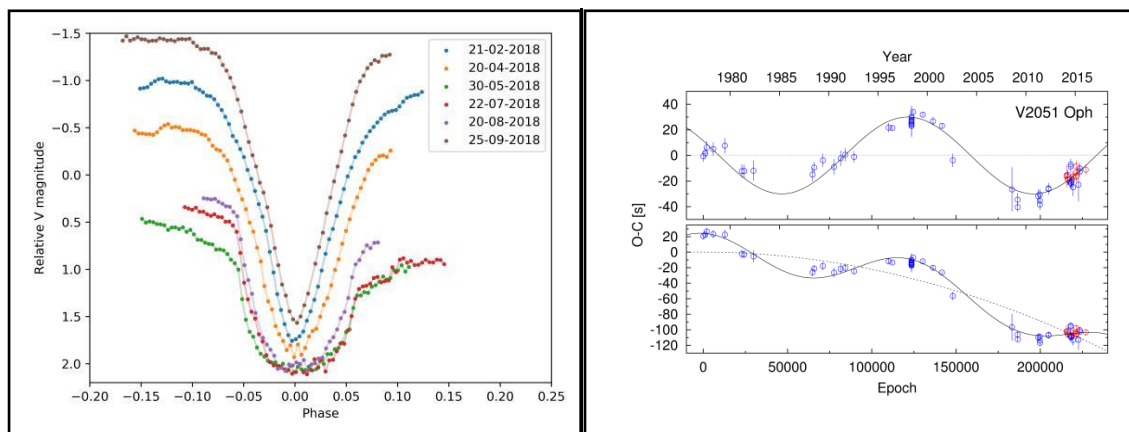


Figure 4: The differential light curves of EX Dra in V-band obtained during 2018 in Ondřejov (left). Variations in eclipse curve profile are given in different colors, the changes in brightness is about 2-3 mag (picture created by Jan Kára). The current O-C diagram for V2051 Oph shows cyclical changes with a period of about 25 years. The quadratic plus sinusoidal fitting is also suitable (bottom right panel).

Table 3. Cataclysmic binaries studied photometrically in the past.

System	Type	V [mag]	P [day]	P _{cycle} [yr]
EX Dra	dwarf nova	14.0-16.2	0.20994	21.1
V2051 Oph	SU UMa	13.5-16.5	0.06242	25.2
OY Car	SU UMa	12.4-16.3	0.06312	29.1
Z Cha	SU UMa	11.9-16.2	0.07450	43.5

Conclusions

We completed several period studies of selected eccentric eclipsing binaries, low-mass eclipsing binaries and cataclysmic variables by performing an O-C diagram analysis. In many binaries we have found an additional body (MS star or brown dwarf) orbiting the eclipsing pair and confirm the multiplicity of these systems. All our studies clearly prove that systematical monitoring of different types of short-period binaries gives us interesting results deserving regular publications. The participation of observers associated in the Variable Star and Exoplanet Section of the Czech Astronomical Society is significant.

Acknowledgements

This research was supported partially by the Czech Science Foundation, grant P209/10/0715, and in its final stage by the grant GA15-02112S. The following internet based resources were used in research for this paper: the SIMBAD database and the VizieR service operated at CDS, Strasbourg, France; the NASA's Astrophysics Data System Bibliographic Services. This investigation is part of an ongoing collaboration between professional astronomers and the Czech Astronomical Society, Variable Star and Exoplanet Section. The author would like to thank Lenka Kotková, Hana Kučáková, Kateřina Hoňková, Kamil Hornoch, Jakub Juryšek, Jan Kára, Martin Lehký, Martin Mašek, Lukáš Pilarčík, Ladislav Šmelcer, Martin Tylšar, Robert Uhlář, Marián Urbaník, Jan Vraštil, Petr Zasche, and Miloslav Zejda for participation in photometric observations and data reduction.

References

- Andronov, I.L. & Richter, G.A. 1987, *Astronomische Nachrichten*, 308, 235
- Applegate, J.H. 1992, *ApJ*, 385, 621
- Bade, N., Hagen, H.-J., Reimers, D. 1989, in 23rd ESLAB Symp ESA SP-296, 883
- Barwig, H., Fiedler, H., Reimers, D., Bade, N. 1993, in *Compact Stars in Binary Systems*, IAU Symp., 165, 89
- Cagaš, P. & Cagaš P. 2014, *IBVS No.* 6097
- Claret, A., & Giménez, A. 1993, *A&A*, 277, 487
- Hilditch, R.W., Howarth, I.D., Harries, T.J. 2005, *MNRAS*, 357, 304
- Hilditch, R.W., Cameron, A.C., Hill, G., Bell, S.A., Harries, T.J. 1997, *MNRAS*, 291, 749
- Hoffmeister, C. 1966, *Astronomische Nachrichten*, 289, 139
- Lanza, A.F., Rodono, M., Rosner, R. 1998, *MNRAS*, 296, 893
- Mayer, P. 1990, *Bull. Astron. Inst. Czech.*, 41, 231
- Pilarčík, L., Wolf, M., Dubovský, P. A., Hornoch, K., Kotková, L. 2012, *A&A*, 539, A153
- Pilarčík, L., Wolf, M., Zasche, P., Vraštil, J. 2018, *New Astronomy*, 60, 1
- Prša, A., & Zwitter, T. 2005, *ApJ*, 628, 426
- Torres, G., Andersen, J., Giménez, A. 2010, *A&A Rev.*, 18, 67
- Sterken, Ch. 2005, *The light-time effect in astrophysics*, ASP Conf. Series No. 335
- Wolf, M. 2014, *Contrib. Astron. Obs. Skalnaté Pleso*, 43, 493
- Wolf, M., Kučáková, H., Hynek, T., Šmelcer, L. 2010, *A&A*, 514, A75
- Wolf, M., Zasche, P., Kučáková, H., Vraštil, J., Hornoch, K., Šmelcer, L., Bílek, F. et al. 2016, *A&A*, 587, A82
- Wolf, M., Zasche, P., Kučáková, H., Hoňková, K., Juryšek, K., Mašek, M., et al. 2017, *AcA*, 67, 257
- Wolf, M., Kučáková, H., Zasche, P., Vraštil, J., Hoňková, K., Hornoch, K., et al. 2018, *A&A*, 620, A72
- Wolf, M., Zasche, P., Kučáková, H., Mašek, M., Hoňková, K., Juryšek, K., Paschke, A. et al. 2019, *AcA*, 69

Double eclipsing systems: from observer's perspective

P. ZASCHE¹

(1) Astronomical Institute, Charles University, Faculty of Mathematics and Physics, CZ-180 00, Praha 8, V Holešovičkách 2, Czech Republic, email: zasche@sirrah.troja.mff.cuni.cz

Abstract: Double eclipsing systems are still rather rare objects. Due to this reason their observations are still very welcome. However, how to observe them? How to choose which one to observe? Or even, how to discover some new ones in the star field?

Introduction – what are the double eclipsing binaries?

Double eclipsing systems (sometimes also called doubly eclipsing systems) are those ones showing two sets of eclipses with different periods. It means one can only need photometry to detect any such star. This double eclipsing behaviour necessarily means that there are two independent eclipsing binaries orbiting with different periods, but one do not know whether these two binaries are bound to each other and constituting a 2+2 quadruple system. In general, both these binaries can also be very distant from each other, only projected into the same position on the sky.

During the last ten years there were discovered several such systems, some of them are quite well-known nowadays. This is for example the case of V994 Her, which was discovered in 2008 by Lee et al. (2008). Much later (Zasche & Uhlař 2016) it was proved that the two binaries orbit around each other on their mutual orbit with the period of about 2.9 years only, hence constitute a multiple system. Another quite well-known and often observed double eclipsing system is the one called 1SWASP J093010.78+533859.5 (see e.g. Lohr et al. 2015), containing one contact and one detached binary.

However, these two systems (plus V482 Per) are the exceptions from the rule. Huge majority of the known double eclipsing systems were discovered thanks to the large photometric surveys monitoring the southern fields, the Magellanic Clouds and the Galactic center. Due to this reason, we have quite unfavourable statistics, see Fig. 1. As one can see on this picture, the large majority of systems is located in the south, hence quite unreachable for the northern-hemisphere observers.

Observations – what can observer do?

Altogether we know nowadays more than 140 such systems, but only for several of them their mutual motion (hence also the quadruple nature) was proved up to date. Hence, any new observation for these interesting objects is very welcome and can lead to new proof that also another system is in fact a quadruple.

Observing the double eclipsing system can be quite tricky. The main problem is that there exist two periods, which entangle to each other and our task is to disentangle the complete photometry into two separate binaries. The main advantage is a fact that the two periods are known. Hence, we can plan our observation according to the predictions of particular phase to be observed and also to calculate the phase of the second binary. Here comes the main aspect of the whole issue – please be aware of the pair which you are observing! Sometimes the contribution of the other pair can be neglected (in case of “flat” part of the light curve outside of minima), but sometimes it is not possible. This is the case of the already mentioned system 1SWASP J093010.78+533859.5, where one of the pairs is contact and its magnitude is steadily changing over the whole phase. It means, this contribution easily cannot be ignored and has to be subtracted somehow. This is usually not a task for observer, but for some professional astronomer to do so. Hence, a tight collaboration between the two is usually necessary.

Another quite important aspect is a fact that due to large fraction of the third light, the individual eclipses can be quite shallow. This is particularly important when considering the way how to observe such a target. It means that sometimes the two binaries have quite similar eclipse depths (in the case where the binaries are similar to each other also in masses and luminosities), but sometimes the two binaries have very different photometric amplitudes. The first (similar) case is e.g. 1SWASP J093010.78+533859.5, while the second (very different) case should be e.g. KIC 4247791. In some special cases when the second binary has its eclipses only very shallow, one can ignore them. But more secure is to obtain the photometry in that part of the light curve, when the second pair is outside of its minimum, has flat parts outside of eclipses and we are also sure about its ephemerides. However, this can be quite tricky - to plan proper observations according to both of these ephemerides. See our Fig. 2, where an attempt to plot this was done. The system V994 Her was used to construct the diagram showing the two sets of eclipses

and how they interfere with each other. The observer should take care of it and observe only proper eclipses, or be aware of it and subtract the contribution of the other pair.

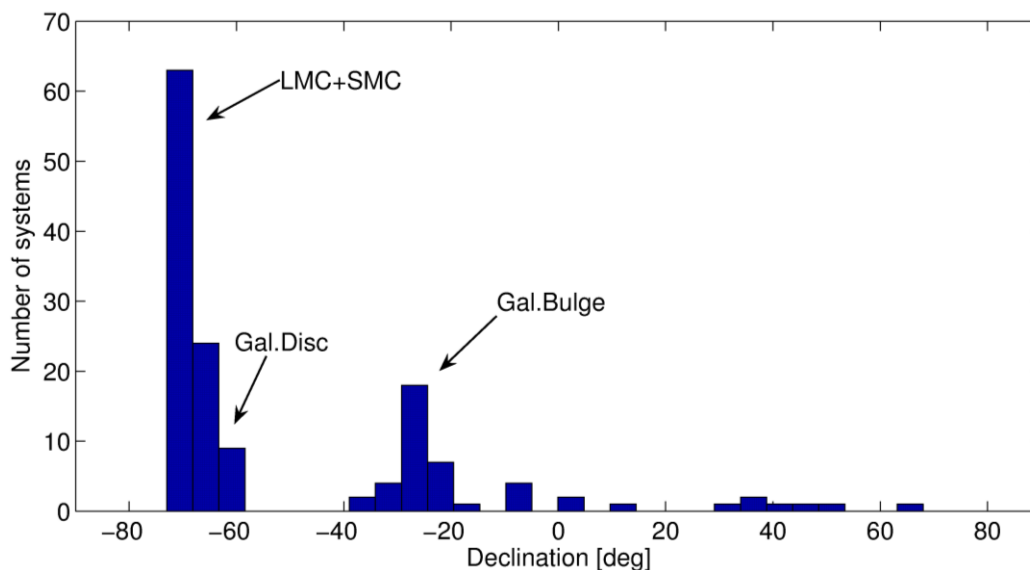


Figure 1: Plot of the distribution of double eclipsing systems known yet. The huge majority of the targets on the southern sky is evident, mainly due to large surveys.

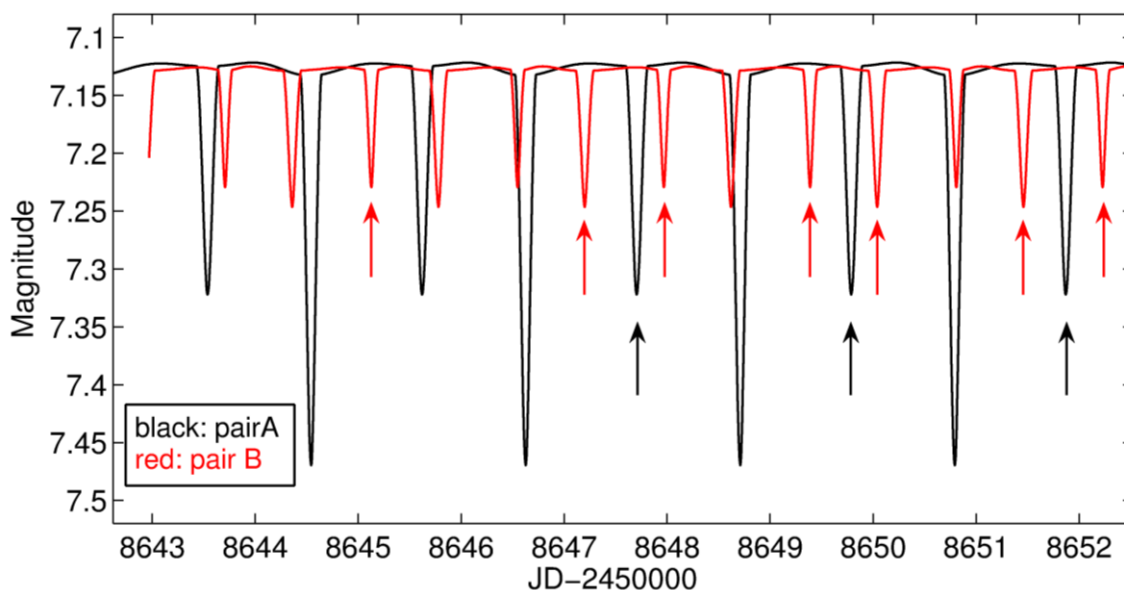


Figure 2: Plot of the combined light curve of V994 Her according to the ephemerides of both pairs. The contributions of both pairs are being combined in every time of observation. But as one can see, only some of the eclipses of the particular pair can be observed with no disturbance of the other pair with also a short part of the constant phase (good ones indicated by arrows).

List of potential targets for courageous observers

The list of potential targets for observations is nowadays more extensive, but still has several limitations. Besides the fact of position on the sky as mentioned above (Fig.1), also other limitations can play a role. One important fact is the magnitude of the target. There are not so many brighter systems, most of them is fainter than 12 mag, which makes them more difficult to observe by amateur observers with their medium-size telescopes. Another limiting factor is also the value of period – sometimes we deal with quite long orbital periods. And in some cases the period is shorter, but the light curve is of W UMa or Beta Lyr type, hence is changing over the whole phase. Therefore, it is necessary to subtract this contribution.

In Table 1 there are given the targets satisfying the criteria ($\text{DEC} \geq -10$ deg), which can be observed with smaller telescopes. Their position, periods, magnitude ranges of both pairs, as well as their GCVS classification types are given. For more detailed information about the shape of the light curve, a reference for particular system is given. Sometimes the estimation of “D” or “d” (duration of the eclipse or length of totality) is a crucial factor for particular system and observatory whether to observe the target or not. One has to be very careful when observing and during subsequent interpretation (time of eclipse of particular pair, when the eclipses are similar and one can easily interchange them).

Name	Position	Pair A		Pair B		Type	Reference
	[RA DE]	PeriodA [d]	Mag.range	PeriodB [d]	Mag.range		
EPIC 220204960	00 48 32.65 +00 10 18.5	13.2735	17.1-17.104	14.4158	17.1-17.104	EA + EA	2017MNRAS.467.2160R
V482 Per	04 15 41.33 +47 25 19.9	2.44675265	10.25-10.55	6.001749	10.25-10.27	EA + EA	2017ApJ...846..115T
CzeV343	05 48 24.01 +30 57 03.6	1.209364	13.68-12.86	0.806869	13.68-13.83	EA + EA	2012A&A...544L...3C
CoRoT 223993566	06 41 49.17 +10 07 19.4	1.18067	14.14-14.20	0.934856	14.14-14.15	EA + EA	2017MNRAS.471.1230H
CoRoT 110829335	06 49 04.86 -05 51 31.3	8.9304	13.65-13.70	50.3075	13.65-13.66	EA + EA	2017MNRAS.471.1230H
ISWASP J093010.78+533859.5	09 30 10.75 +53 38 59.8	0.2277142	9.54-9.72	1.3055472	9.54-9.82	EW + EA	2015A&A...578A.103L
EPIC 212651213	13 55 43.46 -09 25 05.9	5.07655	10.98-11.09	13.1947	10.98-11.00	EA + EA	2016MNRAS.462.1812R
V994 Her	18 27 45.90 +24 41 51.0	2.083265783	7.14-7.46	1.42003948	7.14-7.25	EA + EA	2016A&A...588A.121Z
CoRoT 310266512	18 31 19.74 -05 49 54.6	7.421	14.23-14.42	3.266	14.23-14.24	EA + EA	2015PASP..127..421F
CoRoT 310284765	18 33 51.26 -05 39 23.5	2.371125	14.79-15.01	1.8754	14.79-14.85	EA + EA	2017MNRAS.471.1230H
KIC 3832716	19 01 34.60 +38 54 17.7	1.14187687	13.34-13.74	2.1702736	13.34-13.47	EA + EA	2018Ap&SS.363..267F
CoRoT 211659387	19 04 00.93 +03 30 32.2	0.393957	15.42-15.60	4.00	15.42-15.57	EW + EA	2017MNRAS.471.1230H
KIC 4247791	19 08 39.56 +39 22 36.9	4.100871	11.58-11.78	4.049732	11.58-11.58	EA + EA	2012A&A...541A.105L
TYC 2693-926-1	20 26 43.83 +35 20 30.0	1.350447	12.08-12.28	1.099203	12.08-12.28	EA + EW	2018PZ.....38....3K
NSVS 154567	22 31 41.96 +68 46 22.3	11.4838	13.29-13.54	2.93956	13.29-13.47	EW +	2018PZ.....38....3K

Table 1: List of targets visible from the northern observatories. Their position, designation and periods are given together with the approximate magnitude ranges (in V filter) for both pairs. The reference in the last column is given for closer look to the shape of the light curve of both pairs to estimate the duration of the eclipses, etc.

How to discover new systems

As was already plotted above in Figure 1, the number of systems on the northern and southern part of the sky is very different. Hence, one can expect that much more systems are still waiting to be discovered also on the northern part of the sky. Maybe some of these targets are already located in the observed fields in the vicinity of some well-known variable star. Hence, one has to pay attention on some unexpected behaviour of our photometric data for particular system. Sometimes there appear special humps, dips, or asymmetries of the light curves (see the Fig 3 below). However, it is also advisable to observe the whole curve near eclipses, not only the central part – but also the constant phase outside of minimum itself.

Also when uploading the observation of minimum into the databases like e.g. <http://var2.astro.cz/> one has to be very careful and not to delete every data point which is somehow deviating or not following the assumed trend. Any such distortion can be caused by the other pair, and the two eclipses can interfere with each other (as schematically plotted in Fig. 2).

Discussion and Conclusion

Recent discoveries of new double eclipsing binaries brought to us an important finding – a huge majority of these systems are really bound to each other and constitute rare quadruple systems. Such systems are of large importance in the stellar structure and evolution theories. However, their mutual orbits (of both pairs around a common barycenter) can be rather short sometimes – only a few dozens of the orbital periods of the inner pairs. Hence, periods of about 50-200 days can only hardly be detected when observing the particular target only once per a year. Therefore, a much more dense photometry (e.g. one minimum every other week?) would be needed to detect the outer period of both pairs more conclusively.

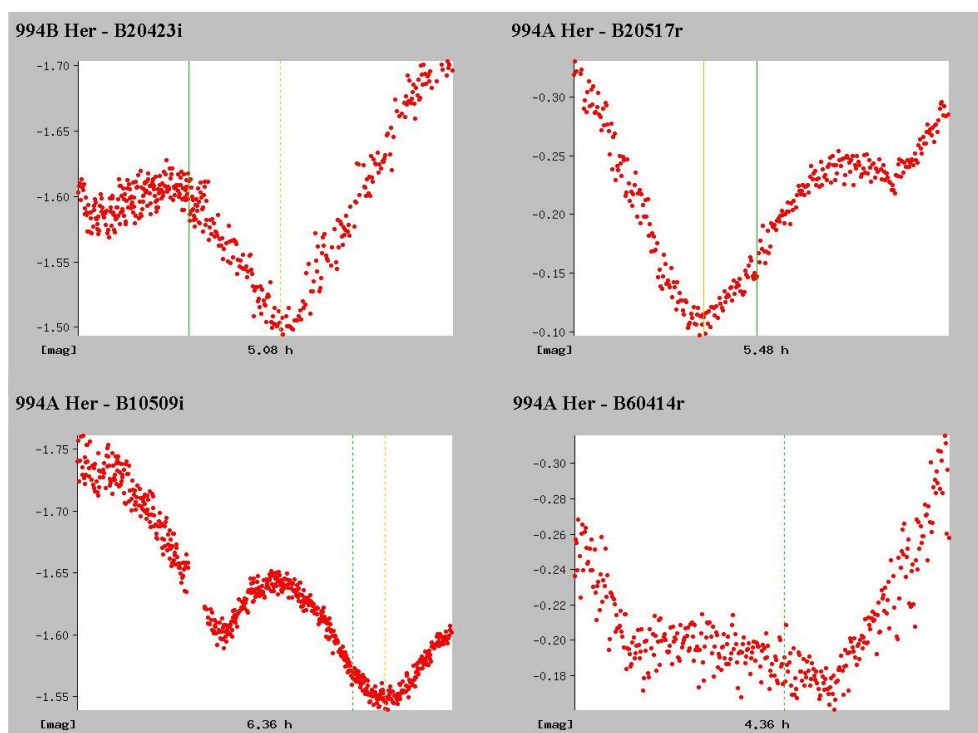


Figure 3: An example of different shapes of eclipses of V994 Her as observed during our photometric campaign. As the two pairs interfere with each other, the normal symmetric shapes of the eclipses became very distorted due to the presence of the second pair during one particular observing run.

Acknowledgement

This research has made use of the SIMBAD and VIZIER databases, operated at CDS, Strasbourg, France and also of NASA's Astrophysics Data System Bibliographic Services.

References

- Cagaš, P., Pejcha, O., 2012, A&A, 544, L3, [2012A&A...544L...3C](#)
- Fedurco, M., Parimucha, Š., 2018, Ap&SS, 363, 267, [2018Ap&SS.363..267F](#)
- Fernández Fernández, J., Chou, D.-Y., 2015, PASP, 127, 421, [2015PASP..127..421F](#)
- Hajdu, T., Borkovits, T., Forgács-Dajka, E., et al., 2017, MNRAS, 471, 1230, [2017MNRAS.471.1230H](#)
- Khruslov, A.V., 2018, Peremennye Zvezdy, 38, 3, [2018PZ.....38....3K](#)
- Lee, C.-U., Kim, S.-L., Lee, J.W., et al., 2008, MNRAS, 389, 1630, [2008MNRAS.389.1630L](#)
- Lehmann, H., Zechmeister, M., Dreizler, et al., 2012, A&A, 541, A105, [2012A&A...541A.105L](#)
- Lohr, M.E., Norton, A.J., Gillen, E., et al., 2015, A&A, 578, A103, [2015A&A...578A.103L](#)
- Rappaport, S., Lehmann, H., Kalomeni, B., et al., 2016, MNRAS, 462, 1812, [2016MNRAS.462.1812R](#)
- Rappaport, S., Vanderburg, A., Borkovits, T., et al., 2017, MNRAS, 467, 2160, [2017MNRAS.467.2160R](#)
- Torres, G., Sandberg Lacy, C.H., Fekel, F.C., et al., 2017, ApJ, 846, 115, [2017ApJ...846..115T](#)
- Zasche, P., Uhlař, R., 2016, A&A, 588, A121, [2016A&A...588A.121Z](#)

The Next 50 Years of Variable Star and Exoplanet Section

O. PEJCHA¹

(1) Institute of Theoretical Physics, Faculty of Mathematics and Physics, Charles University, Prague, Czech Republic

Abstract: I give a personal account of some of the discoveries involving citizen astronomers and the lessons they teach us on how to best adapt to the changing landscape of astronomy in the future.

Introduction

We are now experiencing revolution in time-domain astronomy. The amount of available data in the time domain has been growing exponentially owing to the projects like Sloan Digital Sky Survey (York et al. 2000), All-Sky Automated Survey (Pojmanski 2002), Catalina Real-Time Transient Survey (Drake et al. 2009), Palomar Transient Factory (Law et al. 2009), Zwicky Transient Factory (Bellm 2014), Asteroid Terrestrial-impact Last Alert System (Tonry et al. 2018), Pan-STARRS (Kaiser et al. 2002), All-Sky Automated Survey for Supernovae (Shappee et al. 2014, Kochanek et al. 2017) and many others. These efforts will culminate with the Large Synoptic Survey Telescope (Ivezic et al. 2008), which will begin discovering tens of millions of variable stars and millions of transients starting in 2023. Given this progress, it is imperative to ask how will the members of our Section – citizen astronomers with small optical telescopes and CCD cameras – maintain contact with the forefront of astronomical research?

The first answer to this question is rather trivial: citizen astronomers, whose time on the sky is not paid by public funds, are not required to be involved in any research at all and can devote their time to whatever enterprise they find intriguing. Nonetheless, our Section has for a long time maintained a very close contact with astronomical research and many members find this involvement very attractive. For this audience and to celebrate our long and esteemed history, exemplified by the 50th anniversary Conference on Variable Star Research in 2018, I provide an outlook to the future.

The title of this paper refers to the distant future 50 years from now. It is impossible to know what exciting discoveries are awaiting and how will astronomy and society look like at that time; even the largest infrastructure projects are planned on 20- to 30-year timescale. But we can use our past to guide us in the future. In this paper, I review few discoveries, where citizen astronomers played an important part and which were important for me personally. For each discovery, I try to come up with skills or technological advancements that made them possible and generalize them for the future. Obviously, this is a very personal account and the views expressed are only of my own.

Lessons from past discoveries

The first discovery happened before my time in astronomy, but I heard about it from those involved as well as other contemporaries. In April 1993, Kamil Hornoch and Jan Kyselý were visually recording brightness of supernova SN1993J and each of them independently noticed that one of the stars in the vicinity of the supernova (actually one of the recommended comparison stars) was changing brightness. Hornoch alerted nearby observatory, where their discovery was quickly confirmed with photoelectric photometer. The result was published soon afterward (Hanžl et al. 1993). Their discovery must have influenced on some level many optical observations of SN1993J, which turned out to be one of the most studied supernovae with unusual spectral evolution (spectral type IIb) and with its progenitor detected in pre-explosion images (e.g., Schmidt et al. 1993). The primary lesson I take from this discovery is that *in addition to our primary goal we must be aware of our surroundings and notice what is happening elsewhere*. Such an auxiliary discovery might be even more important than our primary goal.

The second event is an independent discovery of the main outburst of V838 Mon made by Ladislav Šmelcer on February 2, 2002. On that night I was being trained how to use 40cm telescope at Brno observatory by Petr Sobotka. We received a phone call from Šmelcer and immediately altered our program to continuously monitor this object. The observations were published (Sobotka et al. 2002). Later, this outburst of V838 Mon gave rise to prominent light echoes, which were recorded in some of the most spectacular images from the Hubble Space Telescope. The nature of V838 Mon outburst has been debated, but the prevailing opinion attributes the brightening to the merger of two stars, making V838 Mon a prototype of “luminous red novae” (e.g., Soker & Tytenda 2006). Observations of transients were not systematically organized by our Section in those days and Šmelcer’s discovery therefore illustrates that it is important to *try new things and the luck might follow*.

The third lesson is based on the work of Kamil Hornoch summarized in his paper (Hornoch et al. 2008). Hornoch made an industry out of discovering classical novae in nearby galaxies such as M81 and M31. He has done this with a large variety of telescopes, some of them similar to what citizen astronomers have access to. Although I have never followed this field closely, I learned that professional astronomers hold respect for Hornoch and his work. I think the reason for this success is the combination of *intuition for identifying a subfield not entirely cornered by professional astronomers* due to lack of resources or interest and the *diligence and persistence in painstakingly taking observations, comparing them to archives, finding collaborators, and reporting on the findings. Doing things better than everybody else* is a good path to success.

The fourth lesson is the discovery of double eclipsing binary CzeV343 by Pavel Cagaš in 2012 (Cagaš & Pejcha 2012). While few double eclipsing binaries were known before, and many more were identified afterward, CzeV343 is special by having the orbital periods of the two binaries close to 3:2 resonance. The result is a complex light curve that slowly changes as the signatures of the two binaries shift with respect to each other. What enabled this discovery? Even when professional astronomers aggressively pursue time-domain surveys, *there are still combinations of cadence, depth, field of view, and wavelength that have not been fully explored. One should identify these areas, even if intuitively, and go all in.* In this case, Cagaš used large field-of-view telescope and camera to image a single field few hundred times every night in many consecutive nights. The transient-oriented surveys would likely have missed this object, because the usual pattern of revisiting a field every day or every few days combined with the near-resonance of periods and with the long-term changes in the system parameters would scramble the light curve beyond recognition. On a personal note, this discovery inspired me to pursue more deeply issues related to stellar dynamics and collisions of stars.

Conclusions

An important question concerns with the fundamental difference between time-domain surveys and citizen scientists, who often use similar hardware. It is the software that transforms raw images into human-readable data and ultimately science. Although software is a challenge for professional astronomers as well, I worry that citizen astronomers might be falling behind and that this lag is starting to restrict the variety of projects that could be executed with the existing hardware. To give an example, image subtraction and machine learning would greatly simplify many of the menial tasks faced by citizen astronomers in the time domain. Developing or adapting existing software is conceptually similar to building a small observatory in the sense of starting with the design, continuing with the assembly from existing and perhaps modified components, and finally debugging. Both take a lot of time, effort, and there is a learning curve. Yet, there seems to be a barrier to software development among citizen astronomers, which might be connected to wider societal issues. I do not have a magic solution, but I feel that everybody should try to get involved. Since much of the software developed by professional astronomers is now open source and publicly available, there is a great underutilized potential of reusing the available tools.

I think our Section and our members are uniquely positioned to continue making impact on astronomical research. Of course, there are challenges, primarily related to software, but these are not show-stoppers. In fact, the Section leadership has been continuously working on the software issues. More participation from the membership at large would of course be very beneficial.

To conclude, I would like to recommend that all of our members follow new developments in astronomy and actively try to observe the same or similar phenomena to stay in contact with the forefront of the astronomical research. I also suggest that everybody devotes ~10% of their observing time to try new things to actively nurture discovery. This is such a small amount of time that the primary goal will not be significantly affected: 90 or 100 minima timings do not make that big of a difference. I also suggest to report on these experiments at our annual conference to get feedback, inspiration, and to continuously enhance the intellectual environment of our Section.

Acknowledgement

I thank all citizen astronomers who I have interacted with over the years for the many things I have learned and for the continuous inspiration. I am privileged to have my research funded from public sources (currently Horizon 2020 ERC Starting Grant #803158, MSMT-39022/2018-1 from the Czech Ministry of Education, Youth, and Sports, PRIMUS/SCI/17 from Charles University, and US Embassy in Prague Small Grants Program).

References

- Bellm, E., 2014, The Third Hot-wiring the Transient Universe Workshop, [2014htu.conf...27B](#)
- Cagaš P., Pejcha O., 2012, A&A, 544L, 3, [2012A&A...544L...3C](#)
- Drake A. J., et al., 2009, ApJ, 696, 870, [2009ApJ...696..870D](#)
- Hanžl D., Kyselý J., Hornoch K., 1993, IBVS 3879, [1993IBVS.3879....1H](#)
- Hornoch K., et al., 2008, A&A, 492, 301, [2008A&A...492..301H](#)
- Ivezic Z., et al., 2008, arXiv e-print, [2008arXiv0805.2366I](#)
- Kaiser N., et al., 2002, Proceedings of the SPIE, [2002SPIE.4836..154K](#)
- Kochanek C. S., et al., 2017, PASP, 129, 104502, [2017PASP..129j4502K](#)
- Law N. M., et al., 2009, PASP, 121, 1395, [2009PASP..121.1395L](#)
- Pojmanski G., AcA, 52, 397, [2002AcA....52..397P](#)
- Schmidt B. P., et al., 1993, Nature, 364, 600, [1993Natur.364..600S](#)
- Shappee B. J., et al., 2014, ApJ, 788, 48, [2014ApJ...788...48S](#)
- Sobotka P., et al., 2002, IBVS 5336, [2002IBVS.5336....1S](#)
- Soker N., Tylenda R., 2006, A&A, 451, 223, [2006A&A...451..223T](#)
- Tonry J. L., et al., 2018, PASP, 130, 64505, [2018PASP..130f4505T](#)
- York D. G., et al., 2000, AJ, 120, 1579, [2000AJ....120.1579Y](#)